Effects of Proton Radiation on InGaAs Photodiodes and Laserdiodes

[ESTEC Working Paper EWP-2117]

Claire Garden

April 1999-May 2000

QCA / ESTEC / ESA

ACKNOWLEDGMENTS

I would like to thank my supervisor Ali Mohammadzadeh for his help, his guidance and his real support during this one-year trainee program.

I would like to thank Ralf de Marino, Head of the Radiation Effects and Analysis Techniques Section (QCA, ESTEC) for giving me the opportunity of working in the section.

I would like to thank Martin Endemann (APP-PPI) and Igor Zayer (TOS-EEO) for providing me with the samples for this study, Wojtek Hadjas from the Paul Scherrer Institute (CH) and Guy Berger from the University of Louvain-La-Neuve (B) for their help and kindness during the irradiation runs.

For his help and collaboration during this work, I would like to thank Dominic Doyle (TOS-MMO).

I would like to thank as well all members of the Components Division for their kindness and pleasant atmosphere during these 14 months.

Finally, I would like to thank all the people I met at ESTEC that helped me to get through this project by their support and kindness.

Abstract

This report presents the results of a study investigating the effects of proton radiation on InGaAs photodiodes and laserdiodes used in space application. The work was carried out in the frame of a Young Graduate Trainee programme in the Radiation Effects & Component Analysis Techniques Section, Components Division, ESTEC (ESA).

During 14 months, the following tasks were performed:

- preparatory investigation to study proton displacement damage for InGaAs photodiodes and laserdiodes (literature study)
- design and production of test boards employed during irradiation tests and measurements
- configuration of an optical test bench suitable to support all necessary measurements
- development of HP-VEE programmes for measurement system control
- test plan development
- pre-irradiation characterisation of all tested devices
- irradiation of test devices plus post-irradiation measurements
- pre- and post-irradiation data analysis
- interpretation of the results

In brief, the study shows that InGaAs laserdiode and photodiode devices tested here degrade after exposure to proton irradiation.
In parallel, heavy ion irradiation testing was also performed on some InGaAs photodiodes. Results of the measurements show that the level of degradation of the photodiode parameters depends on the atomic weight.

TABLE OF CONTENTS

I. INTRODUCTION

Electronic components used in space applications must be reliable and withstand the harsh environment encountered in outer space (i.e. temperature, radiation, etc). It is therefore necessary to evaluate a component's suitability for use in space applications by performing ground based environmental tests.
Radiation effects (ionising and displacement damage) on Si devices have been extensively studied. However, less research has been undertaken to map the effects of displacement damage due to energetic particles (heavy ions and protons) on InGaAs devices.

The Radiation Effects and Components Analysis Techniques Section (QCA) at ESTEC / ESA is responsible for the assessment and control of the effects of space radiation on components and for the development and provision of component analysis techniques. One specific responsibility of this section is the definition, the implementation and supervision of study and research activities regarding the simulation of space radiation, the understanding of its effects on components and to propose measures to reduce it.
In April 1999, a study was initiated at QCA to evaluate the effects of displacement damage caused by energetic particles (mainly protons, but also heavy ions) on InGaAs photodiodes and laserdiodes. During 14 months, a complete measurement system was implemented to perform pre- and post-irradiation characterisation of photodiodes and laserdiodes (dark current, photocurrent, I-V characteristic, optical power and threshold current). The results of these measurements are presented in this report.

After briefly describing the space radiation environment and its effects on laserdiodes and photodiodes, the implemented measurement system is presented. Test device specifications are then presented, followed by a description of the radiation test plan. Finally, measurement data and an interpretation of the results are given.

II. RADIATION IN SPACE AND ITS EFFECTS ON LASERDIODES AND PHOTODIODES

A. Introduction of space radiation

1. Radiation in space environment

The space radiation is composed of a wide spectrum of particles with different energies. There are three main sources of radiation: particles found in the radiation belts, cosmic rays and solar flares [1,2].

a. Radiation belts

Before describing the radiation belts, a brief overview of the region known as magnetosphere is given.

The Earth can be considered as a magnetic dipole, its shape distorted by the solar wind. The pressure of the solar wind is responsible for the elongated shape of the magnetosphere. As illustrated in figure 1, the dayside magnetic field is compressed by the solar wind while the night side magnetic field is stretched out to a long distance.

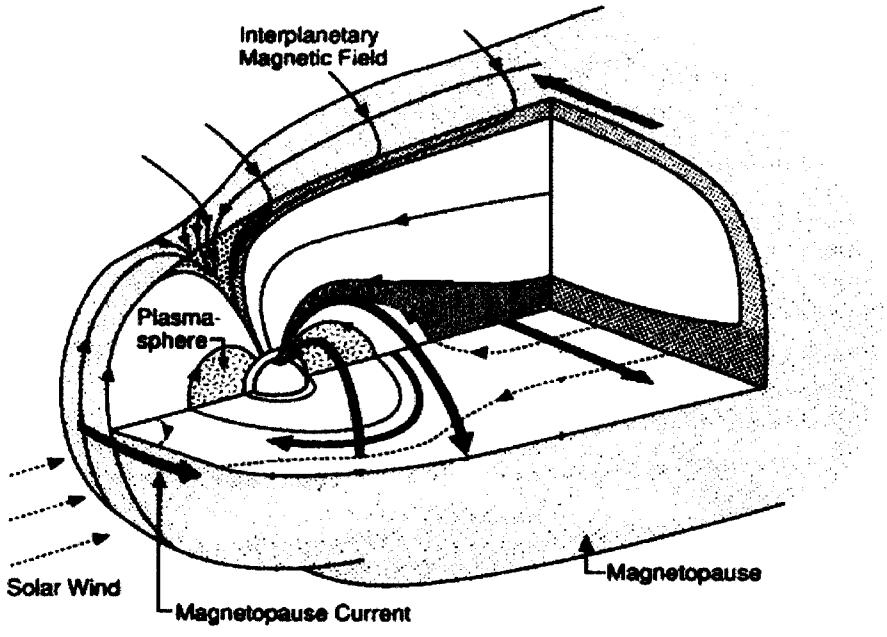

Figure 1: Magnetosphere

The trapping of energetic particles in the Earth's magnetic field composes what is called the Earth's radiation belt (Van Allen belts). Depending on regions, the number of electron and proton particles trapped in the magnetic field varies. Figures 2 and 3 show the trapped electron and proton radiation belts in the Earth's magnetic field respectively.

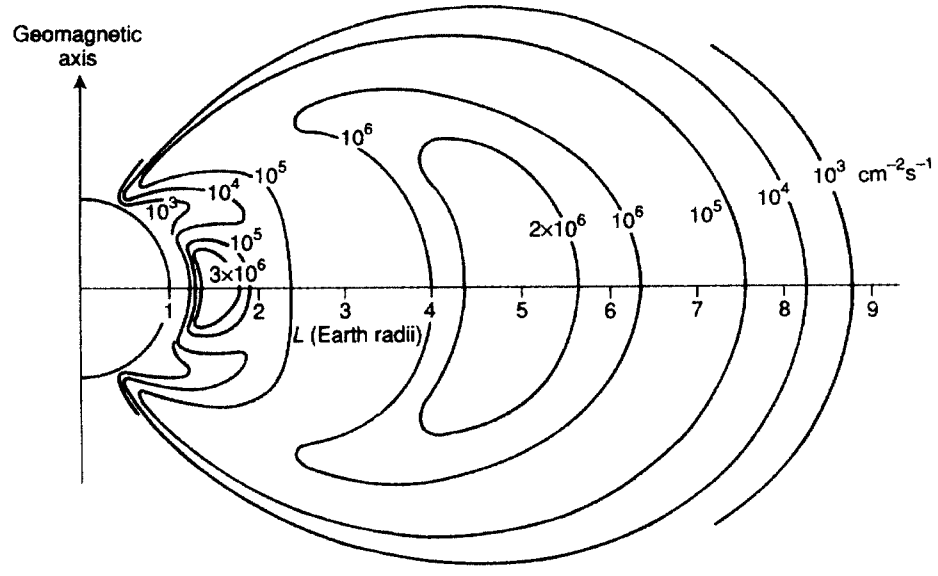

Figure 2: Isoflux map of electron radiation belts

(The radius of the Earth is 6371 km)

The electron belts consist of two distinct zones with high fluxes. The inner zone is centred at approximately 1.4 earth radii and extends to approximately 2.4 earth radii whereas the outer zone is centred at around 5 earth radii and extends to about 12 earth radii. In the first zone, electron energies are less than 5 MeV whereas in the second they are more intense and can be as high as 7 MeV [1,2].

Only one zone may be defined for proton particles (see figure 3 next page). The flux varies monotonically with energy and distance with a maximum at around 2 Earth radii. The energy of the trapped protons may vary from ~ 1 MeV to 400 MeV.

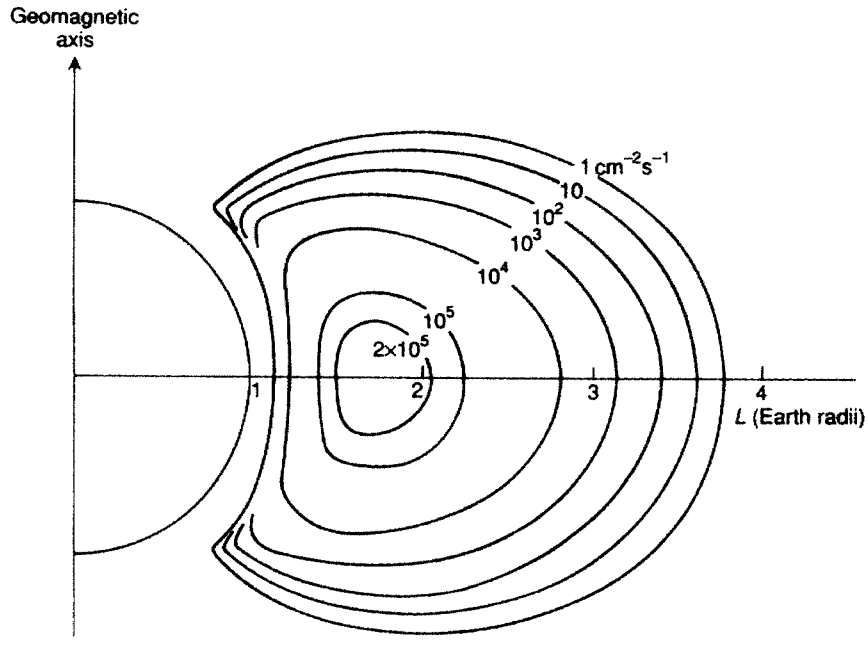

Figure 3: Isoflux map of proton radiation belt

(The radius of the Earth is 6371 km)

b. Cosmic rays

Cosmic rays are composed of protons (83%), helium nuclei (13%), electrons (3%) and highly energetic heavy ion nuclei (1%). They originate from the sun and sources external to our solar system. Ion energies can be high: the most energetic ion ever detected had an energy of 3 10^{20} eV. Cosmic rays may create in electronic devices Single Event Effects (SEE), i.e. the change of state of a bistable element.

c. Solar flares

The sun is a constant source of particles. However, the radiation from the sun increases at periods of high activity, known as solar storms. During these events mainly high-energy protons (up to several hundred MeV) are emitted with electron and alpha particles at lower fluxes. Although the produced protons are less energetic than those trapped in the Earth's magnetic field, spacecrafts may be exposed to considerable total dose levels.

2. Radiation damages in materials

Displacement damage and ionisation are the two main interactions caused by energetic particles traversing the material [1,2,3].

a. Displacement damage

When energetic particles pass through matter, they can "knock out" an atom and remove it from its equilibrium position. The space remaining from the displaced atom is called a vacancy. The resulting mobile atom is called an interstitial. The ejected atom may have enough energy to knock out a second atom creating a second vacancy. This may happen several times, producing a cascade of displaced atoms. Each removed atom can either recombine with a vacancy or lodge in an interstitial position in the lattice.

Vacancies can combine with impurities in the crystal or with other vacancies creating stable defect centres. Generally, the mobility of the vacancies is very high. The defect centres are electronically active and can act as traps for electrons and holes reducing their lifetime in the material, and consequently modifying the device behaviour.

b. Ionisation

The main energy loss mechanism of a particle in a semiconductor is via ionisation by the generation of electron hole pairs. Many electrons will be in an excited state in the conduction band and will become highly mobile under the application of an electric field. Any solid -even an insulator- thus conducts for a time at a level higher than is normal.

B. Radiation effects on photodiode and laserdiode components

1. Radiation damage in photodiodes

Studies presented in the literature showed that proton-irradiating photodiodes lead to an increase of dark current and a decrease of the photocurrent. However, before describing these effects, a brief overview of the photodiode mechanism is given.

a. General overview of photodiode mechanism

A photodiode works by generating current from photons absorbed in its active area [4,5]. In a semiconductor material, a region depleted of mobile charge carriers is formed near the P-N junction. This zone is called depletion region. Incident radiation within this region will create electron-hole pairs, immediately separated by the internal field (see figure 4).

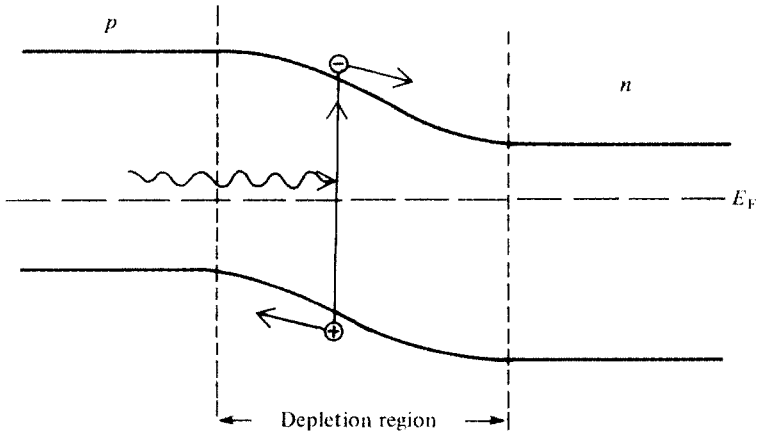

Figure 4: Diagram illustrating the generation and separation
of an electron-hole pair within the depletion region of a P-N junction

With no external voltage applied, this internal field will prevent the majority carriers to cross the junction. Minority carriers however are still capable of reaching the junction by diffusion and give rise to leakage current. Electron-hole pairs generated outside the depletion region will most likely recombine, consequently not contributing to the photocurrent.

Then, two different modes of operation can be defined for the photodiode [4,5].

In a photovoltaic mode, the separation of the electron-hole pairs gives rise to the creation of an externally measurable potential called open circuit voltage.

When a reverse bias voltage is applied to the device, the field is strong enough to accelerate the mobile carriers resulting in a current flowing through the diode (see figure 5). This mode is called photoconductive mode.

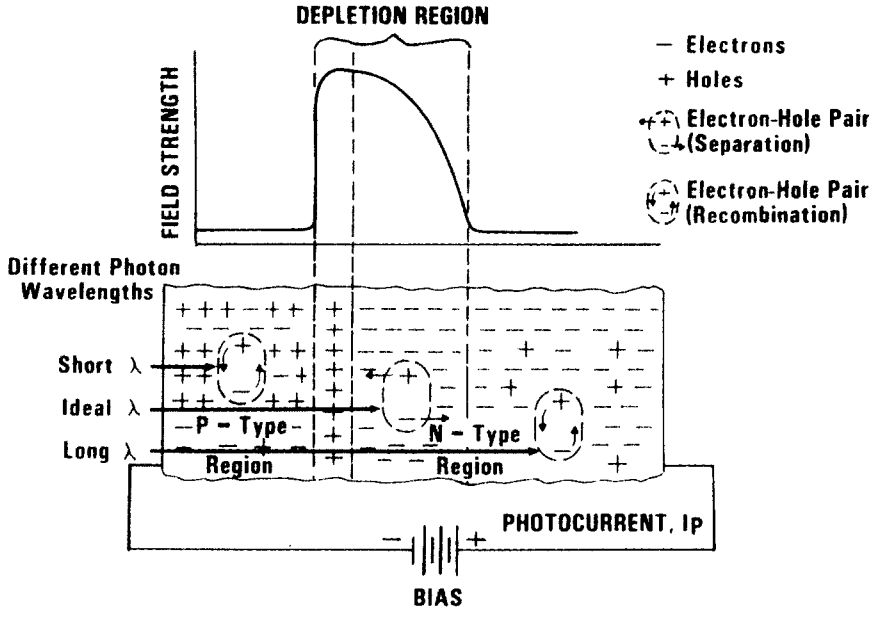

Figure 5: Creation of photocurrent through a junction P-N

The following figure summarises the two-operation modes of a photodiode.

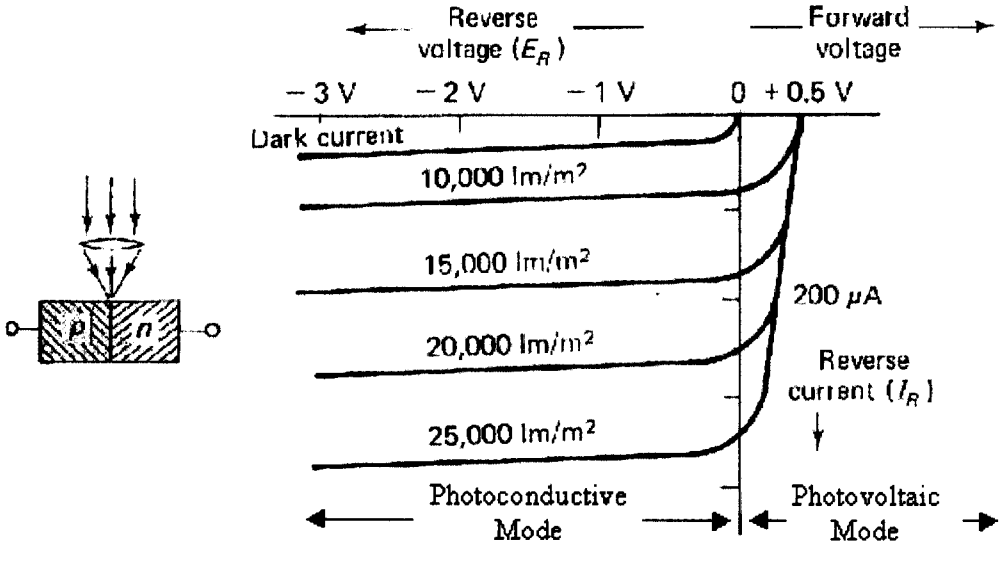

Figure 6: Illumination characteristics of photodiode

b. Decrease of photocurrent

One effect of the radiation on photodiode is the decrease of the photocurrent. As previously described in this chapter, radiation may create defects in the material such as lattice imperfections. These defects are associated with energy levels situated in the forbidden band gap acting as recombination centers: they will trap electrons and holes (that would otherwise contribute to the photocurrent) which recombine and consequently reduce their lifetime in the depletion region [6,7]. Due to the increase of traps, fewer carriers will contribute to the generation of current, leading to a decrease of the photocurrent.

c. Increase of dark current

Another effect of radiation on photodiodes is the increase of the dark current. Dark current is defined as the current that flows when the photodiode is not illuminated by a light source.

Radiation results in the creation of stable states in the forbidden band-gap. Electrons trapped in those states require less energy to jump to the conduction band than electrons situated in the valence band. Irradiating a device increases the number of states in the band gap, enabling more electrons to jump to the conduction band, thus increasing the device dark current.

2. Radiation damage in laserdiode

Before describing the two main effects of radiation on laserdiode (increase of the threshold current and decrease of the optical output), a description of how a laserdiode works is given.

a. General overview of laserdiode mechanism

A laser operates by emitting a coherent light, i.e. radiation of essentially one wavelength, through a process called "stimulated emission". To better understand the mechanism of a laser, first of all, the three basic transition processes, -absorption, spontaneous emission and stimulated emission- will be described.

The absorption process corresponds to the transition of an electron from the ground state to the excited state through the absorption of a photon (see figure 7 (a) next page) [7,8].

After a short time and because the excited state of the atom is unstable, the excited atom will decay to the ground state with the emission of a photon. This process is called spontaneous emission and is illustrated in figure 7 (b). This mechanism is also called radiative recombination. If no photon is emitted during the recombination of an electron in the conduction band with a hole in the valence band, then the process is called non-radiative recombination.

In the case of stimulated emission, a photon impinges an electron still situated in the excited state. This causes the emission of photons with the same energy as the incident photon and the transition of the electron from the excited state to the ground state. The stimulated emission is illustrated in figure 7 (c).

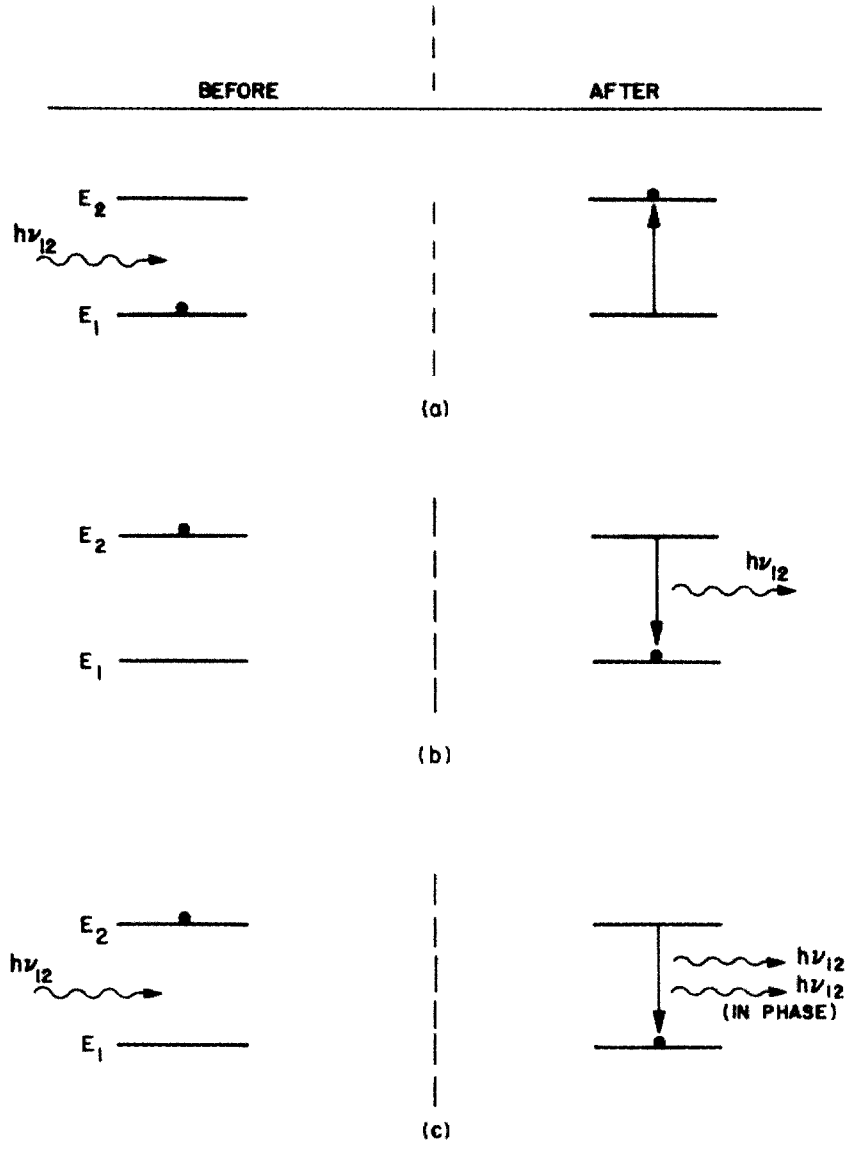

Figure 7: The three transition processes between two energy levels E1 and E2.
The black dot represents the state of the atom.
(a) Absorption; (b) Spontaneous emission; (c) Stimulated emission

To enhance the stimulated emission in a laserdiode, a population inversion must be created within the semiconductor.

A population inversion occurs when a larger number of electrons are in an excited state than in the ground state. Generally, this is created in the area of the laserdiode called active region. To obtain a population inversion, two conditions should be full-filled. First, the diode must be forward biased. Secondly, the two sides of the junction must be heavily doped.

A population inversion in a laserdiode will lead to spontaneous emission, which again results in stimulated emission. With higher current injected into the laserdiode, the stimulated emission rate will increase. As the emission rate exceeds the absorption rate, laser action occurs and the laserdiode starts emitting light.

b. Increase of threshold current

Radiation is known to increase the threshold current of a laserdiode [6,7]. The threshold current (I_{th}) defines the minimum driving current where the laser diode starts to emit laser light.

Radiation induced defects may act as recombination and trap centers increasing the non-radiative recombination rate by capturing excited electrons. Either the electron returns to the excited state or it decays to the ground state with no production of a photon, as illustrated in figure 8.

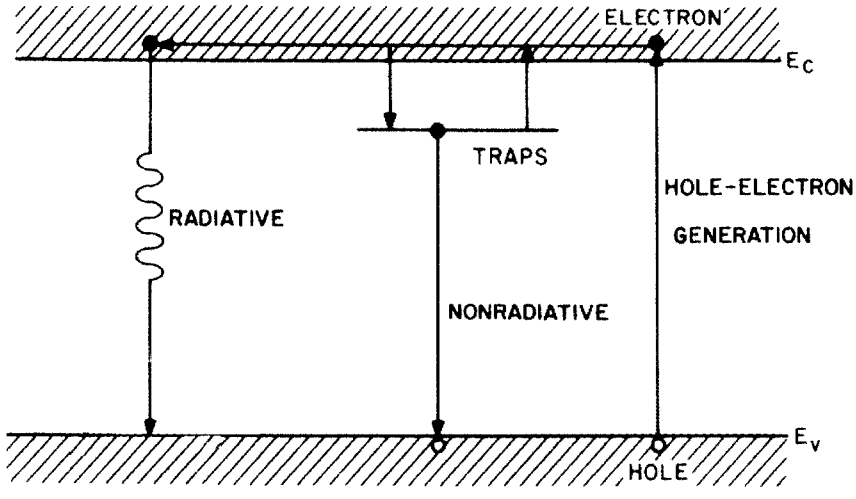

Figure 8: Competition between radiative and non-radiative processes

The creation of non-radiative centers decreases the carrier lifetime competing with the radiative process. Due to the increase of the non-radiative centers, a higher current must be injected to compensate for the reduction of photon emission and for reaching lasing conditions.

c. Degradation of optical power

The degradation of the optical power with radiation is mainly due to the increase of the threshold current [9]. As the injected current must be higher to compensate for the loss of carriers, the optical output of an irradiated laserdiode decreases with respect to a non-irradiated laserdiode for the same current value.

III. EXPERIMENTAL PART

In this section, a description of the electronic components tested during the study will be given. Then, the next chapter will describe the test set-up used during the measurements, followed by the presentation of the irradiation test plan.

A. Device descriptions

In total, two InGaAs laserdiodes and 51 InGaAs photodiodes were tested during this study. Two laser modules and four photodiodes were provided by the MIPAS ODS project (an ESA project) and the remaining photodiodes were manufactured by THOMSON-CSF. The following paragraphs give the device specifications.

1. InGaAs MIPAS ODS components

The laser modules were manufactured by ORTEL and the photodiodes by GMMT.

a. Laser module specifications

The following specification details the sub-assembly of InGaAs MIPAS laser module, 1610A-E15.

Note: this specification applies for a bias current of I_{th} + 40mA.

- **Part type number of samples**

NFT 680 24447-00 S/N 27

NFT 680 24447-00 S/N 36

- **Optical parameters**

Table 1 lists the optical parameters of the laserdiodes.

Characteristics	Rating
Wavelength	1310 ± 20 nm
Optical output power	> 3 mW
Optical reverse isolation	> 30 dB
Side mode suppression ratio	>30 dB

Table 1: Optical parameters

- **DC parameters**

Table 2 lists the DC parameters of the laserdiodes.

Characteristics	Rating
Laser bias threshold	< 40 mA
Operating current	65 mA (typ.) 100 mA(max.) @2V
Laser breakdown voltage	> 2 V
Monitor photodiode dark current	< 200 nA
Monitor photodiode operating current	0.2 mA (min) 2.0 mA max
Monitor photodiode breakdown voltage	> 15 V
Operating temperature range	-20 to +60°C

Table 2: DC parameters

- **Maximum ratings**

Table 3 lists the maximum ratings.

Characteristics	Maximum Rating
DC forward current	150 mA (Duration 60sec)
Storage temperature	-40 to +70°C
Solder temperature *	265°C

Table 3: Maximum Ratings

* Duration 10 seconds maximum at distance of not less than 1.5mm from the body

- **Fibre**

The fibre is a polarising single mode fibre.

- **Physical dimension**

Figure 9 shows the physical dimensions of the laser modules.

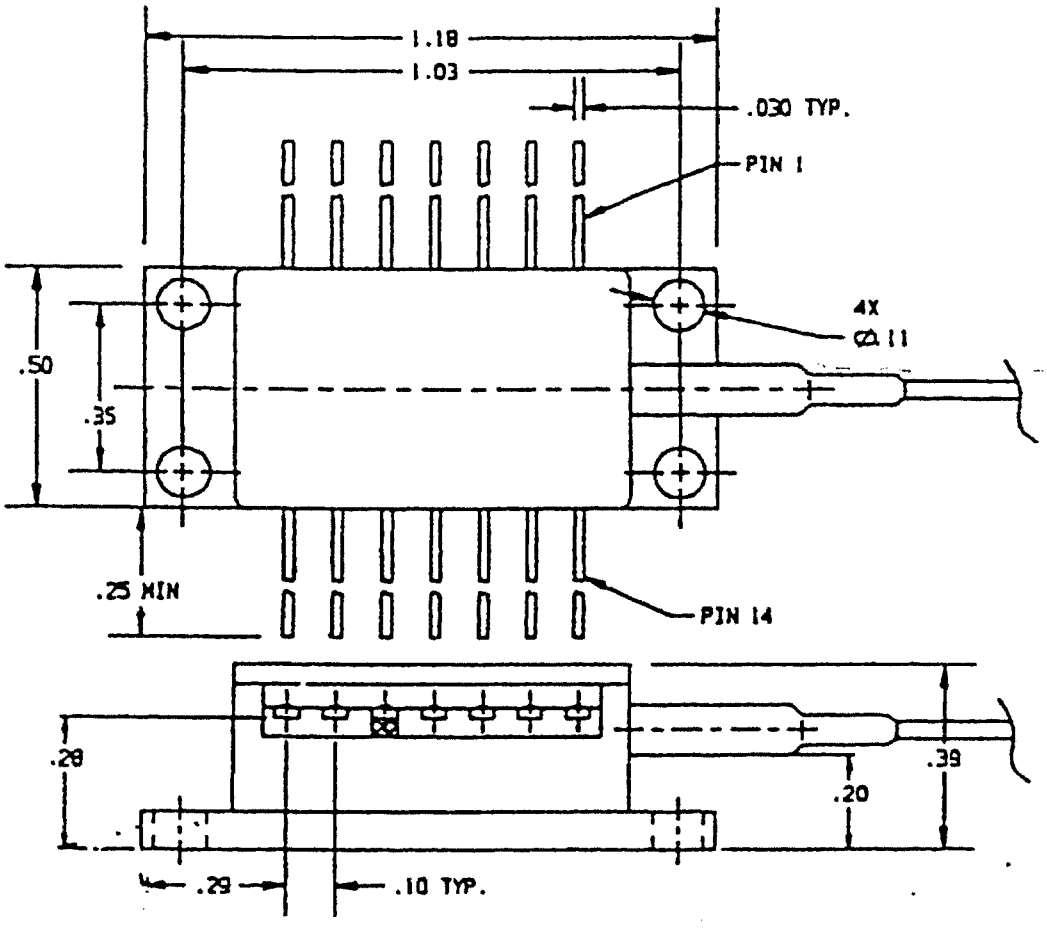

Figure 9: Physical dimensions of the laser modules

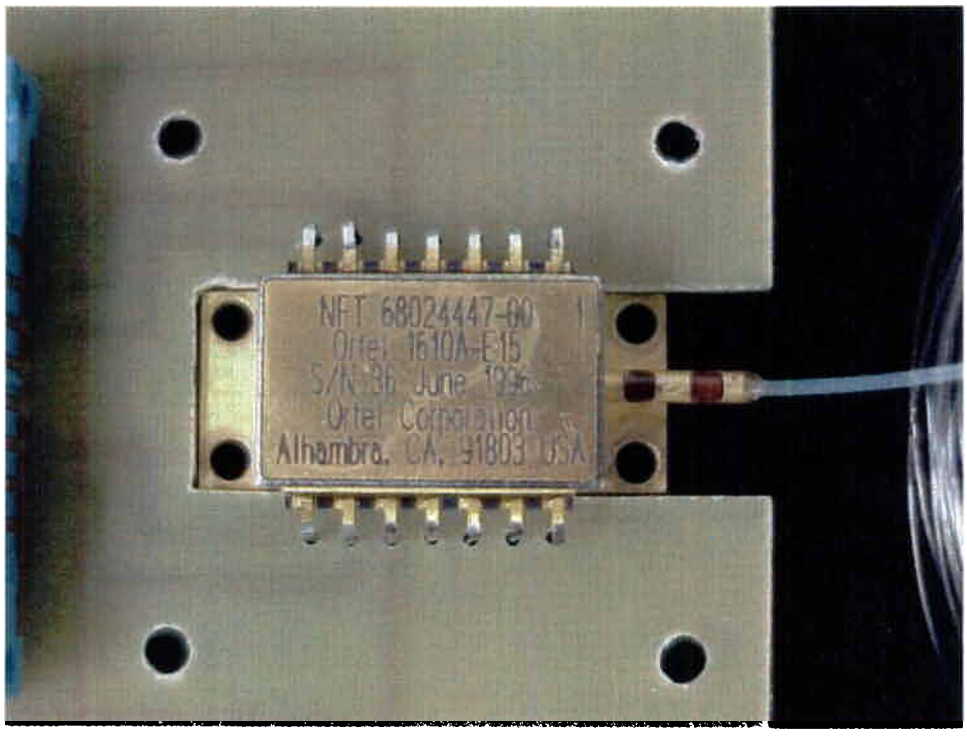

Figure 10: A close view of SN 36 MIPAS laserdiode mounted on a test PCB

Note:

The laserdiodes were provided:

- with broken fibres
- end-connectors not compatible with measurement instrument

Modifications and repairs were made by the Swiss Company Diamond. The laser modules were supplied with 5.5m fibres and D-6106 DIN connectors. However after repair, the cable length was reduced to approximately 7 cm. The original connector was replaced with a FC type connector.

b. Photodiode specifications

The following details the ratings, physical and electrical characteristics of the InGaAs/InP photodetectors type 68031954-yy supplied by MIPAS ODS project.

- **Part type number of samples**

SCD 68031954-01-161-9536F (SN 161)

SCD 68031954-01-163-9536F (SN 163)

SCD 68031954-01-243-9536F (SN 243)

SCD 68031954-01-249-9536F (SN 249)

Note: Photodiode SN 161 was damaged during pre-irradiation characterisation and was not used for the irradiation tests.

- **Maximum ratings**

Table 4 lists photodiodes maximum ratings.

Characteristics	Maximum Rating
Maximum short time storage temperature *	+ 125 °C
Minimum short time storage temperature *	- 103 °C
Maximum operating temperature	+ 125 °C
Minimum operating temperature	- 103 °C
Maximum reverse voltage	20 V
Maximum forward current	20 mA
Solder temperature **	260 °C

Table 4: Maximum Ratings

* Recommended storage conditions are between 0 and + 30 °C.

** Duration 10 seconds maximum at distance of not less than 1.5mm from the body and the termination shall not be resoldered until 3 minutes have elapsed.

- **Photodetector parameters**

Table 5 lists photodetector parameters.

Characteristics	Rating	Unit	Condition
Dark Current	10	nA	@ V_R 5V
Photo sensitivity (responsivity)	800	mA/W	@ V_R 5V λ = 1300nm
Minimum electrical Resistance diode Chip to case	1	10^{10} Ohm	
Shunt resistance	1	G Ohm	@ V_R 10mV
Cut off frequency (With ring contact)	200	MHz	@ V_R 5V and R50 Ohm
NEP at λp	5.7×10^{-14}	$\frac{W}{\sqrt{Hz}}$	@ 0V bias
D* (λp)	7.7×10^{11}	$\frac{cm\sqrt{Hz}}{W}$	@ 0V bias
Capacitance	10	pF	
Rise and fall time	2.0 / 2.0	nsec	@ 50 Ohm
Spectral response	1.0 – 1.7	µm	

Table 5: Photodetector parameters

- **Mechanical parameters**

Table 6 lists mechanical parameters.

Characteristics	Rating	Unit	Condition
Centering of detector chip	≤50	µm	Radius. Related to flange
Active area	∅500	µm	

Table 6: Mechanical parameters

- **Physical dimension**

The physical dimensions of the photodiode are illustrated figure 11.

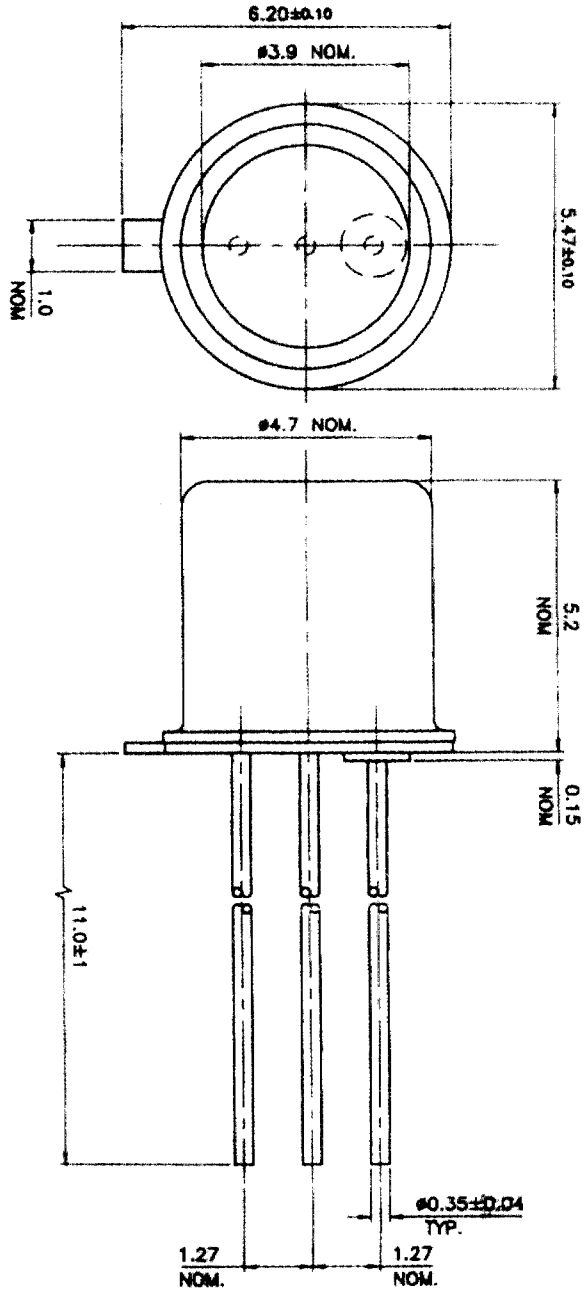

Figure 11: Physical dimension of the MIPAS photodiodes.

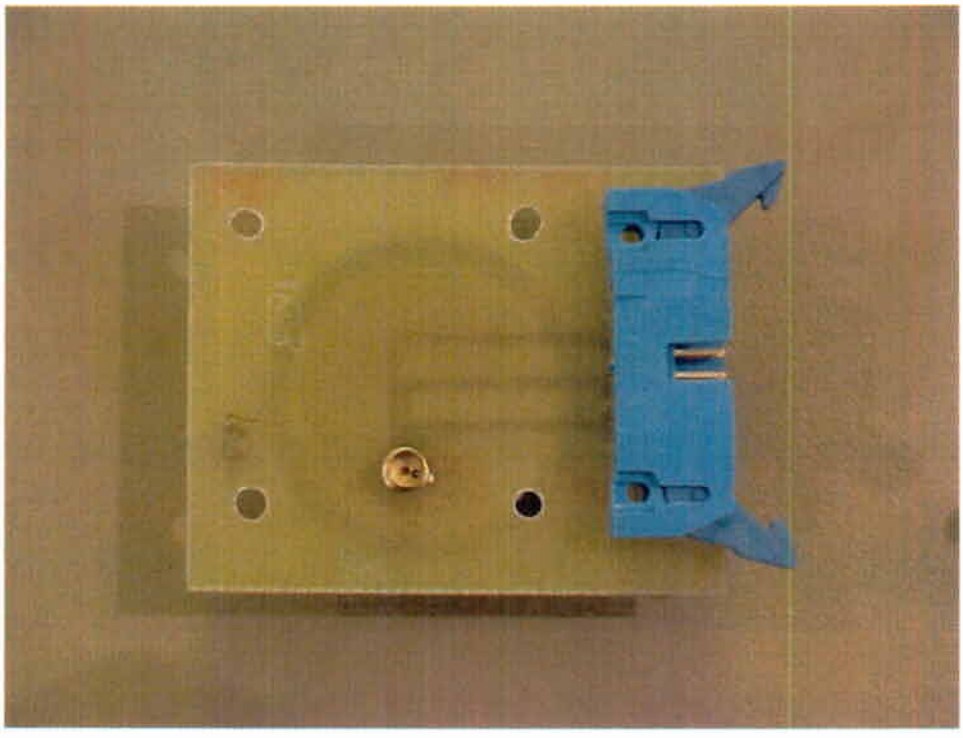

Figure 12: General overview of the MIPAS SN 163 photodiode mounted on its test PCB

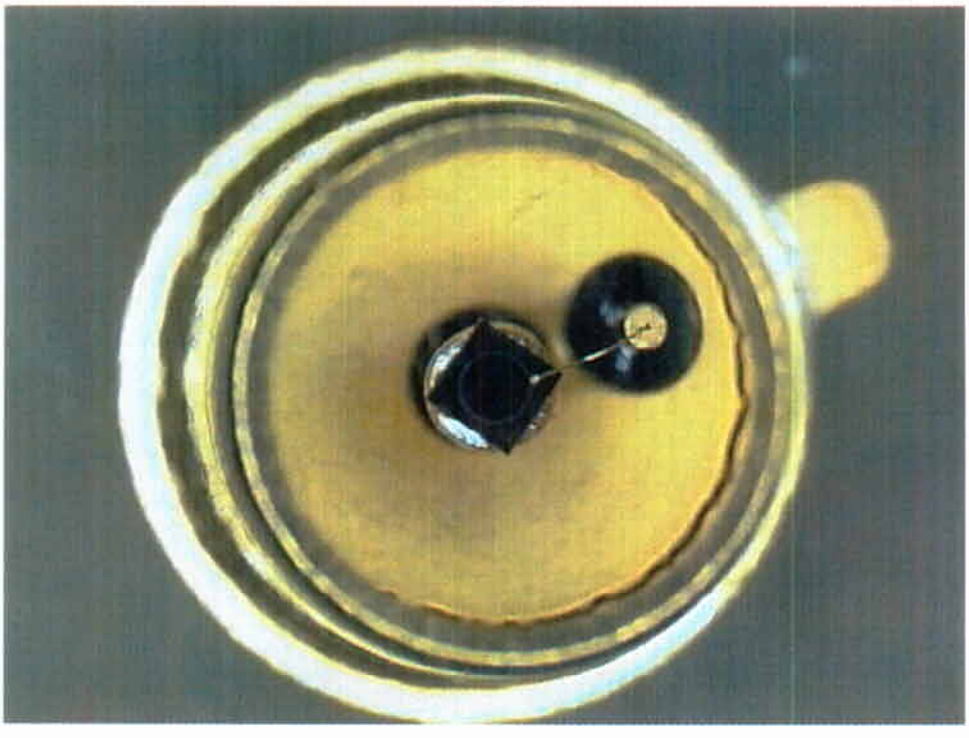

Figure 13: Close up view of the MIPAS SN 163 photodiode

2. THOMSON-CSF components

Seven 3 µm epitaxy layer, seven 6 µm epitaxy layer and two MSG SEVIRI InGaAs devices were provided by THOMSON-CSF (F). Each device is composed of three photodiodes. In total, 48 photodiodes from THOMSON were tested during this study.

- **Part name of test samples**

InGaAs technology with 3 µm epitaxy layer	InGaAs technology with 6 µm epitaxy layer	MSG InGaAs technology
110B506-L3B5	111B611-L3B7	
110B506-L3B6	111B611-L5B7	
110B506-L3B7	111B611-L5B8	972-952-L6B5
110B506-L5B6	111B611-L6B6	972-952-L7B4
110B506-L6B10	111B611-L6B7	
110B506-L6B11	111B611-L6B8	
110B506-L6B12	111B611-L6B9	

Table 7: Part numbers of THOMSON photodiodes

- **Structure of the devices**

The following figure presents the structure of THOMSON photodiodes and table 8 lists the thickness of each layer.

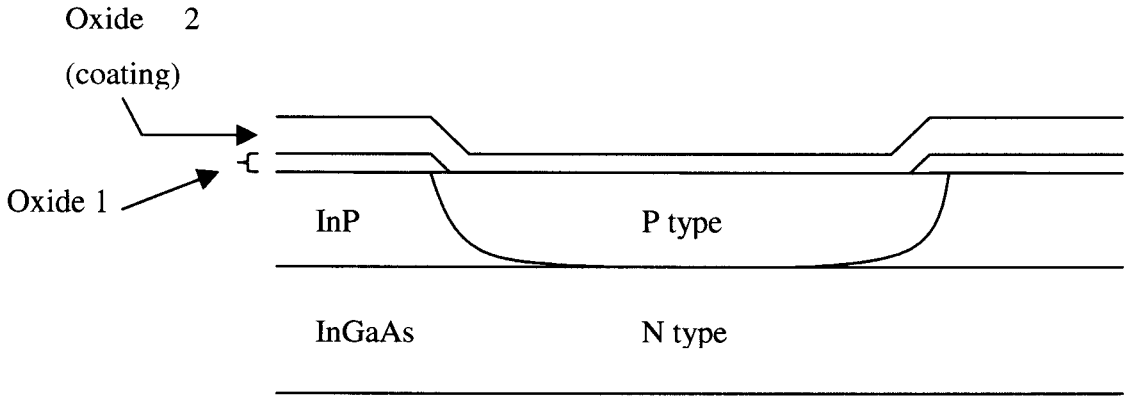

Figure 14: Structure of the photodiode

Thickness / Doping levels	MSG InGaAs Technology	3 µm thick InGaAs Technology	6 µm thick InGaAs Technology
N type InGaAs	4 µm- 2 10^{15} at/cm^3	3 µm-10^{16} at/cm^3	6 µm-10^{16} at/cm^3
InP	1.2 µm	1.2 µm	1.2 µm
Oxide 1	750 nm	340 nm	340 nm
Oxide 2	350 nm	350 nm	350 nm

Table 8: Thickness of the different layers in THOMSON photodiode structure

- **Maximum ratings**

Table 9 lists the maximum ratings for the photodiodes.

Characteristics	Maximum Rating
InGaAs forward current	2 mA
InGaAs reverse voltage	12 V
Illumination level	2 mW
Operating temperature range	0 / 70 °C
Storage temperature range	- 40 to +85 °C
Solder temperature	260 °C

Table 9: Maximum Ratings

- **Physical dimension**

Figure 15 shows the physical dimensions of the photodiodes.

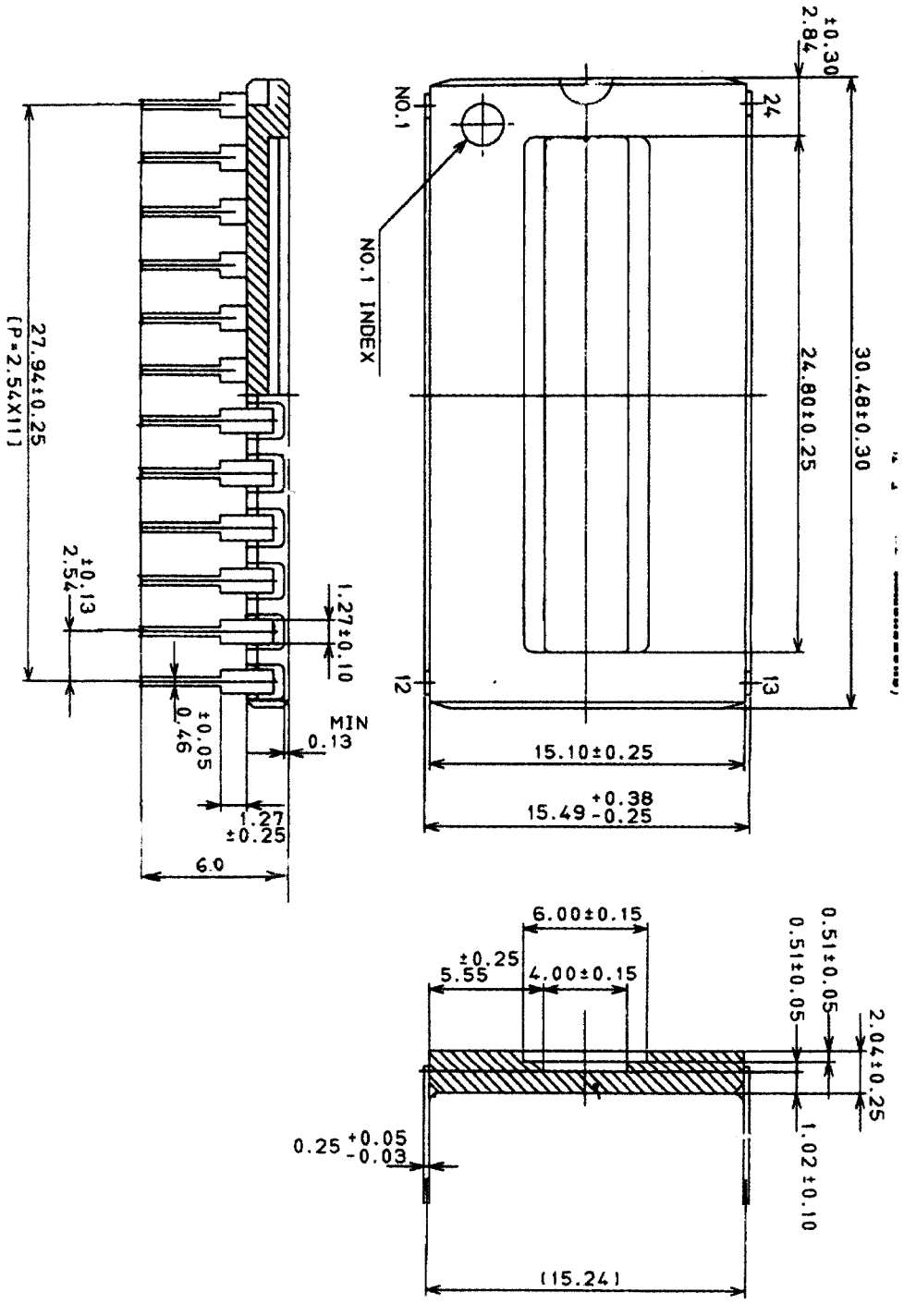

Figure 15: Physical dimensions of the photodiodes

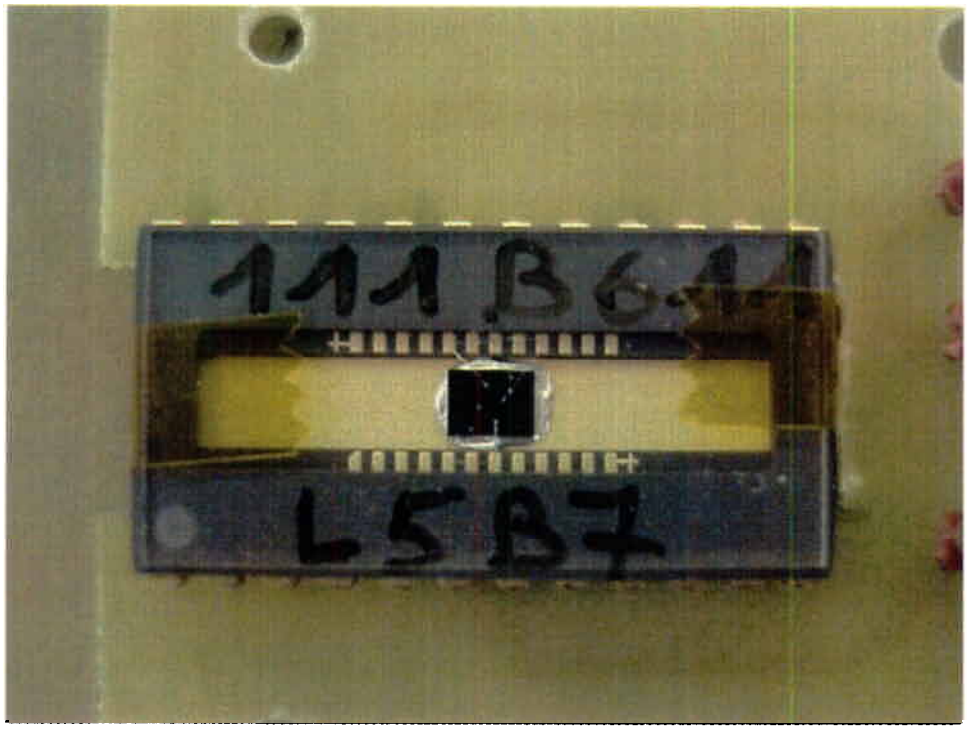

Figure 16: An image of the 111B611-L5B7 component from THOMSON. All the photodetectors were supplied with a protective glass window.

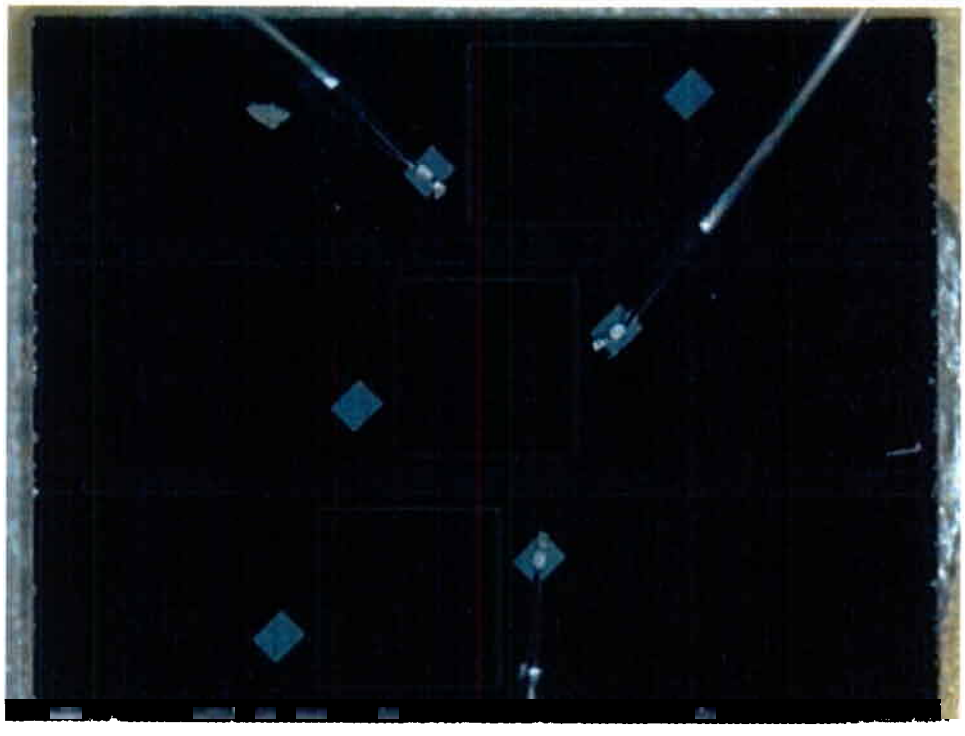

Figure 17: Close view of three diodes inside 110B506-L6B12 Thomson device

B. Test set-up

This chapter describes the configuration of an optical test-bench to perform all the necessary pre- and post-irradiation characterisations of the InGaAs photodiodes and laserdiodes.

1. PC boards

To perform the measurements and for ease of handling the devices during irradiation campaigns, a PCB was made for each component.

The PCBs were made so that the device package was in direct contact with a Peltier cooler. The PCBs were produced in the Components Laboratory at ESTEC.

Figure 10 (previously presented page 21) shows the MIPAS photodiode PCB. Figure 18 and 19 show MIPAS laserdiode and THOMSON PCB's.

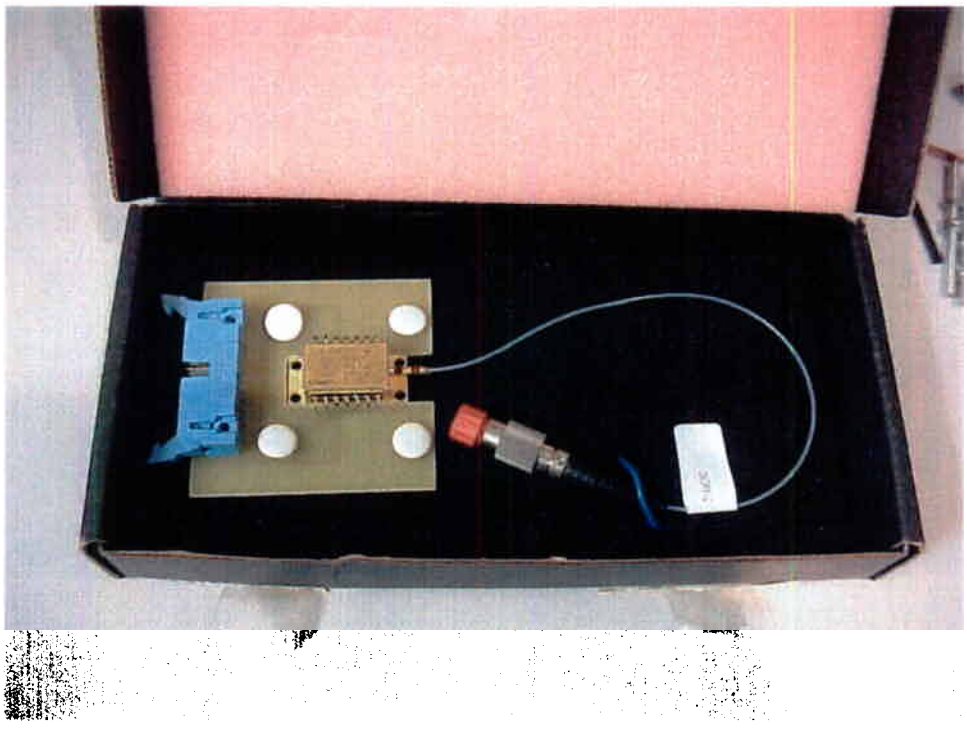

Figure 18: Image showing the SN36 MIPAS laserdiode mounted on its PCB

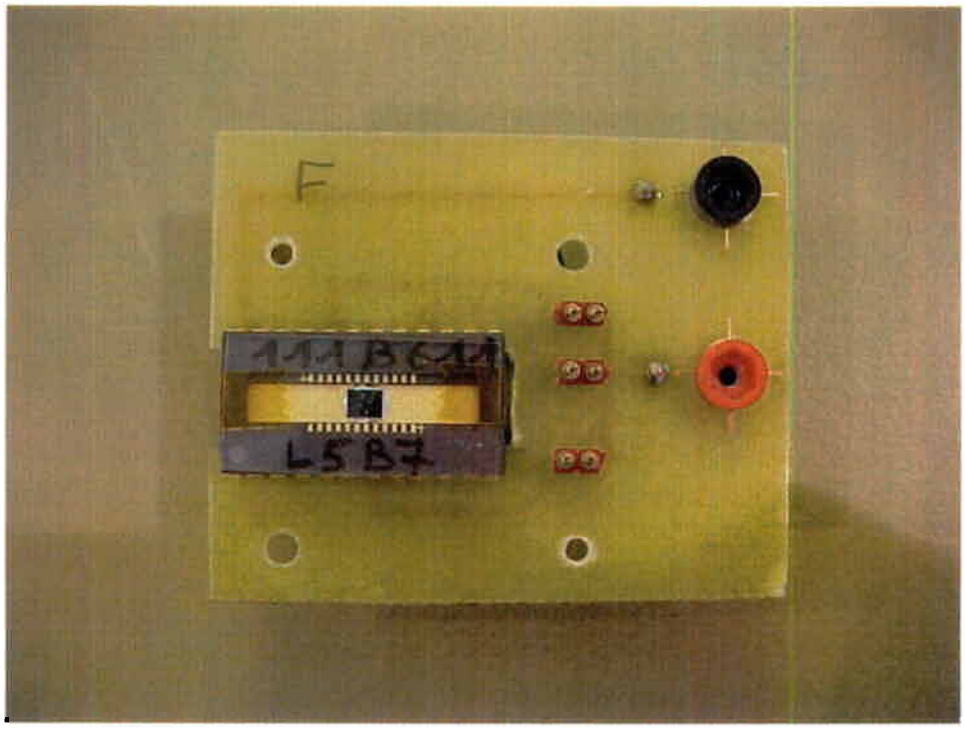

Figure 19: Image of 111B611-L5B7 THOMSON device mounted on its PCB

2. HP-VEE programs

To assure the repeatability and the automation of the measurements, programs in HP-VEE language were written.

HP-VEE is a visual programming language, enabling users:

- to control instruments through a GPIB card
- to process measurements (acquisition and display of data)
- to record results.

According to the type of characterisation and equipment used, several programs were written to facilitate the system control and the repeatability of measurements.

As an example, figure 20 shows the HP-VEE program interface for performing dark current measurements.

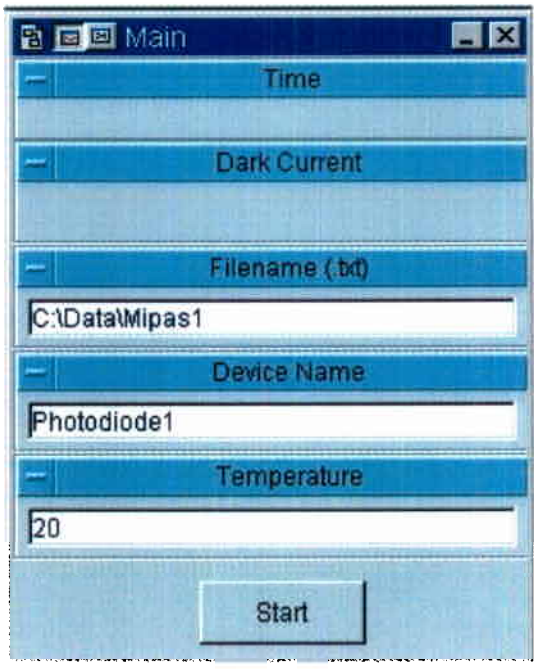

Figure 20: Example of the "Dark_Current" program HP-VEE interface system

As it can be seen in figure 20, the user is required to enter some distinct parameters such as device name, temperature and filename (here "Mipas1"). Then during measurements, this interface will show the time and the date of measurements and of course the value of the dark current. However, the main program behind this interface (not accessible by the user) is composed of an interconnected set of HP-VEE library modules as illustrated in figure 21 next page.

This program can be divided into 5 parts. The first part commands the number of times the program will be executed. The second part switches "on" the power supply, providing a pre-set voltage level. The third part commands the Picoammeter to measure the dark current and to save this value. The fourth part commands the program to store parameters entered by the user (i.e. filename, temperature, and device name) and of the measured dark current value on a data file on the PC hard disk (the filename being chosen by the user). Finally, the fifth part commands the switching "off" of the power supply. The output of this program is a file containing the data and the user defined parameters in a spread sheet compatible format.

The other HP-VEE programs employed during the measurements will not be detailed in this report, but are described in the supporting documentation.

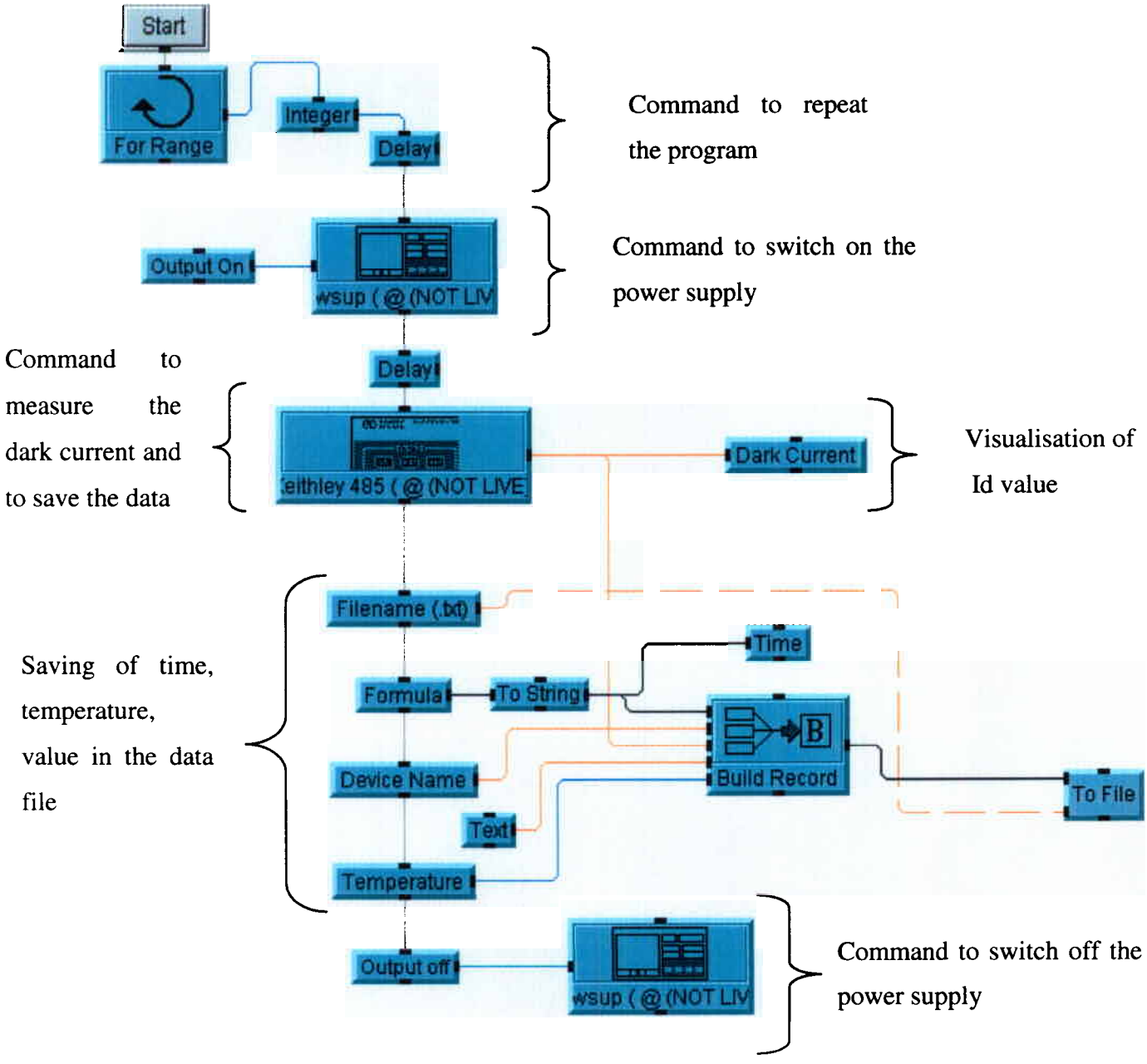

Figure 21: Visualisation of "Dark_Current" main program

3. Excel programs

The data saved during experiments were sorted and analysed with Microsoft Excel using macros written in Visual Basic. For each set of data -dark current, photocurrent, I-V, optical power- visual basic programs were written. As an example, the source code of the visual basic program for sorting the measured dark current data is listed in Annex 1. The program extracted measured dark current values, averaged these values and then provided the value in nA.

4. Laserdiode experimental bench set-up

The following paragraphs present the set-up implemented for measuring the pre- and post-irradiation characteristics (optical power and threshold current) of the laserdiodes.

a. Optical power measurement

Output power (in dB) as a function of wavelength for different injected currents was measured for each laser module before and after irradiation.

Figure 22 illustrates the measurement set-up for laserdiode characterisation.

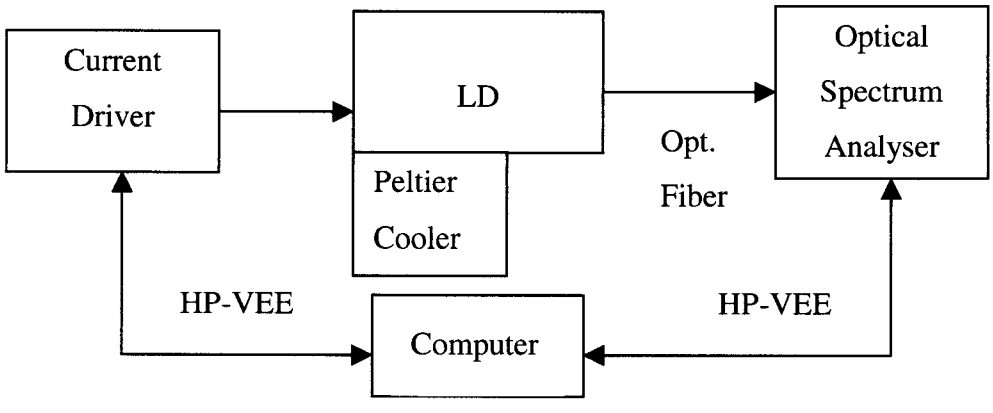

Figure 22: Measurement set-up for electrical characterisation for laserdiodes

The laserdiode package was mounted directly in contact with a Peltier cooler to obtain a fixed temperature of 20°C. The diode current driver ILX-3900 controlled the values of the current injected into the laserdiode. The output of the laserdiode was connected to the optical spectrum analyser Ando AQ-6310 measuring output power (in dB) versus the wavelength for each value of the laserdiode drive current. Then the maximum of the output power was deduced from the previous curve. Finally, the characteristic of the laserdiode (output power (W) as a function of the injected currents) was plotted.

Table 10 shows the 13 current steps applied during laserdiode output power measurements.

Step	1	2	3	4	5	6	7	8	9	10	11	12	13
I (mA)	10	20	25	27	30	35	40	45	50	60	70	80	90

Table 10: Test conditions for the laserdiodes

b. Threshold current

Threshold current (minimum-driving current needed for the laserdiode to emit laser light) was calculated by plotting the driver current to output power curve and calculating the linear fit. The point at which a straight-line-fit to the linear portion of the curve intercepts the x-axis corresponding to the zero optical power define the threshold current, as illustrated in figure 23.

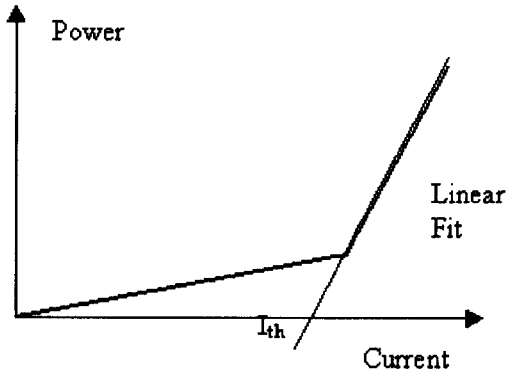

Figure 23: Determination of the threshold current

5. Photodiode experimental bench set-up

The following paragraphs describe the test set-ups implemented to measure the photodiode characteristics (i.e. dark current, I-V curve and photocurrent).

a. I-V characterisation

The I-V characteristic was recorded for each device.

Figure 24 shows the I-V characteristic test bench set-up.

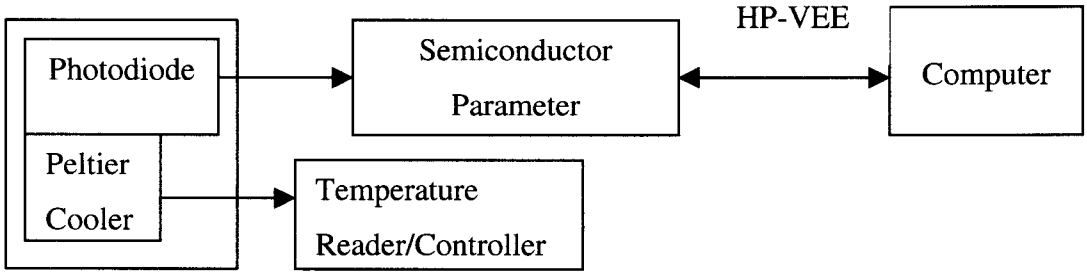

Figure 24: I-V test bench set-up

The photodiode was mounted on a PC board directly in contact with a Peltier cooler to obtain a fixed temperature. The system was placed in a closed box to avoid stray light from external sources effecting the measurements. The I-V characteristics were measured by a Semiconductor Parameter Analyser.

The test conditions are listed below:

- Measured values: Current
  Voltage
- Fixed values: No source light
  Temperature of the system fixed at 20°C

The following table lists the parameters used during the measurements.

Manufacturer	Voltage Variation	Compliance	Step
THOMSON	-1V to 0.49 V	1.7 mA	10 mV
MIPAS	-1V to 0.63 V	10 mA	10 mV

Table 11: Parameters used during the measurements

b. Photocurrent

Figure 25 illustrates the test set-up for photocurrent measurement.

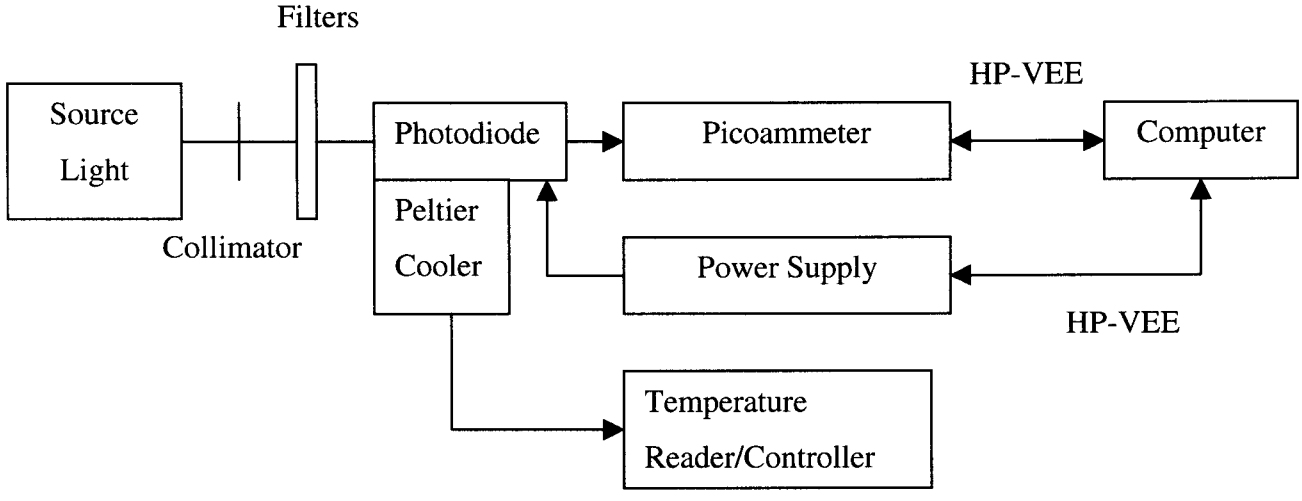

Figure 25: Test set-up for photocurrent characterisation

Four optical bandpass filters were employed in the photocurrent as a function of wavelength measurements. Two reference photodiodes were used to calibrate the light beam (for each wavelength) as a function of X, Y and Z positions with reference to the light source.

Each reference photodiode is optimised for one wavelength. These are 850 and 1300 nm. The light power, in table 12, thus reflects the Quantum Efficiency (QE) of the two reference photodiodes.

Photocurrent of the tested photodiodes when illuminated by monochromatic light (as defined in table 12) was measured employing a Keithley 485 Picoammeter. The reverse voltage was set by a HP 6634A Power Supply.

The test conditions are the following:

- Measured values: Photocurrent
- Fixed values: Reverse voltage fixed at – 5V
  Temperature of the system regulated at 20°C

Step	1	2	3	4
Bandpass Filters (nm)	700	900	1100	1300
Light Input ($\mu W/mm^2$)	1.9607	0.9048	0.3646	0.6671

Table 12: Value of the light inputs for the different optical bandpass filters

c. Dark current

Figure 26 illustrates the test set-up for measuring dark current.

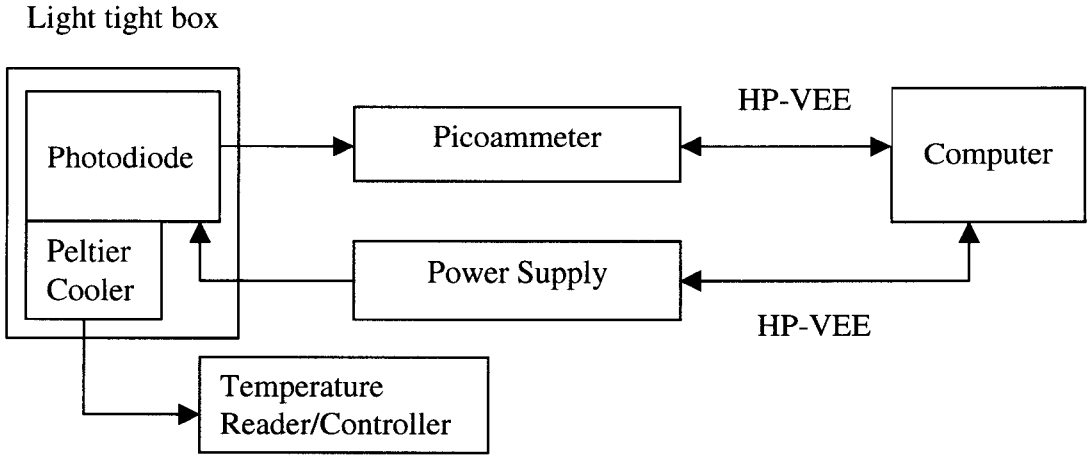

Figure 26: Dark current test bench set-up

During measurements, the photodiode was isolated in a dark box to avoid stray light effecting the measurements. The reverse voltage was set by the HP 6634A power supply and the dark current was measured employing a Keithley 485 Picoammeter.

The test conditions are listed below.

- Measured values: Dark current
- Fixed values: Reverse voltage fixed at –5V
  Temperature of the photodiode at 20°C
  No light

C. Irradiation test plan

The samples were submitted to two irradiation runs. The proton irradiation was performed at Paul Scherrer Institute (PSI) in Switzerland using the Proton Irradiation Facility (PIF), whereas for the heavy ions, the radiation were performed at the Cyclotron Research Centre at Louvain-La-Neuve (Belgium).
The two proton irradiation runs were performed during calendar weeks 5 and 15 of 2000 and the two heavy ion irradiation runs were performed during calendar weeks 7 and 11 of 2000. The study schedule is provided in Annex 2.

The following tables 13, 14, 15 and 16 show the energies and the fluences used during the two proton and heavy ion irradiation runs.

- **THOMSON devices:**

THOMSON Photodiodes	Fluence (p/cm^2)		3 µm 110B506-	6 µm 111B611-	MSG devices 972-952-
	1^{rst} run	2nd run			
30 MeV	10^8	10^{10}		L3B7	
	10^9	10^{11}	L3B5		L6B5
	10^{11}	10^{12}	L3B6	L5B7	
6 MeV	10^{12}		L6B10	L6B7	
	10^8	10^{12}			L7B4
	10^8	10^9		L5B8	
	10^9	10^{11}	L3B7		
	10^{10}	10^{12}	L5B6	L6B6	

Table 13: Fluences and energies used during the proton irradiation runs

THOMSON Photodiodes	Fluence (ions/cm^2)		3 µm 110B506-	6 µm 111B611-
	1^{rst} run	2nd run		
Argon	10^5	10^7		L6B8
Neon	10^5	10^7	L6B11	

Table 14: Fluences and energies used during the heavy ion irradiation runs

Note 1: Devices 110B506-L6B12 and 111B611-L6B9 were kept as references.

- **MIPAS Devices:**

MIPAS Photodiodes	Fluence (p/cm^2)		Serial Number
	1^{rst} run	2^{nd} run	
30 MeV	10^8	10^9	SN 243
	10^{10}	10^{12}	SN 249

Table 15: Fluences and energies used during the proton irradiation run for MIPAS photodiodes

Note 2: Device SN 163 was kept as reference.

MIPAS Laser diode	Fluence (p/cm^2)			Serial Number
	1^{st}	2^{nd} run	3^{rd} run	
30 MeV	10^{10}	10^{10}	10^{12}	SN 36

Table 16: Fluences used during the proton irradiation run for MIPAS laserdiode

Note 3: SN 27 laserdiode was kept as a reference for the two first irradiation runs.

IV. RESULTS

This chapter presents the results of this study. Analyses of the pre-and post-irradiation measurements were performed in order to determine the effects of proton radiation on InGaAs components.

A. MIPAS devices

1. Laserdiodes

Only two laserdiodes were available for irradiation tests, these were serialised as SN36 and SN27. In total three proton irradiation runs were performed at Paul Scherrer Institut (PSI, CH). Table 17 lists the irradiation history of both devices.

Devices	First run	Second run	Third run
SN36	10^{8} p/cm^{2} 30 MeV proton.	10^{10} p/cm^{2} 30 MeV proton.	10^{12} p/cm^{2} 30 MeV proton.
SN27	Not irradiated	Not irradiated	10^{11} p/cm^{2} 6 MeV proton. (results not available)

Table 17: Laserdiodes irradiation history

For the two first runs only SN36 was irradiated, SN27 was assigned as the reference device. Post second run irradiation measurement showed some ambiguous results, thus a third irradiation run was initiated where SN36 was irradiated to 10^{12} p/cm^{2} 30 MeV protons.

Pre / post-irradiation measurements of the reference diode were performed to ensure optical test-bench stability and measurement repeatability. System stability is illustrated in figure 27 where pre- and post-irradiation measurements of the reference laserdiode, are depicted.

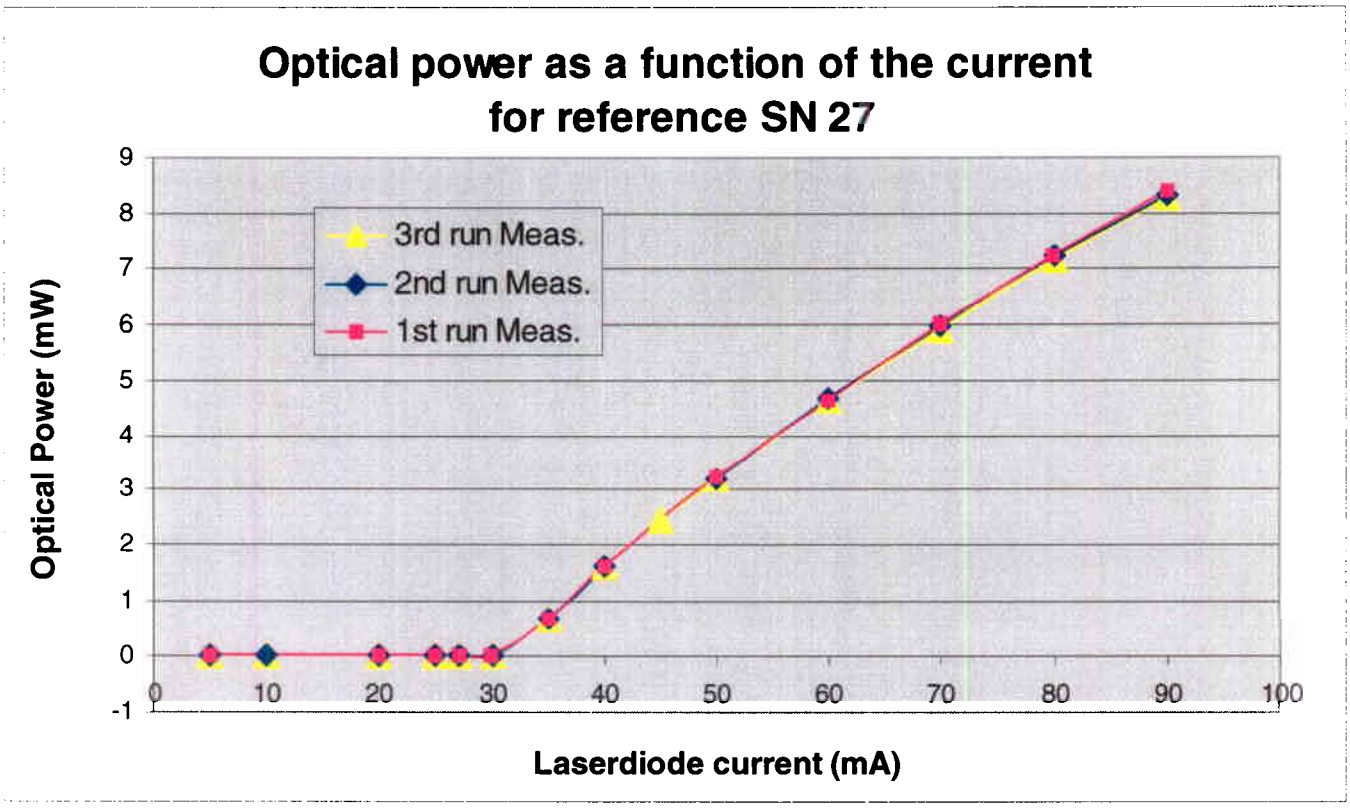

Figure 27: Optical power as a function of input current for the reference laserdiode (SN27).

In figure 27, the label assigned 1st run identifies pre irradiation reference measurements while labels assigned 2nd and 3rd run identify the post first and second irradiation reference measurements, respectively. Maximum difference between the three measurements is in the order of 1.7%. Pre / post-irradiation optical power measurement results for SN36 are illustrated in figure 28. Note that the pre-irradiation optical power of device SN27 (figure 27) is approximately twice that of device SN36 (figure 28).

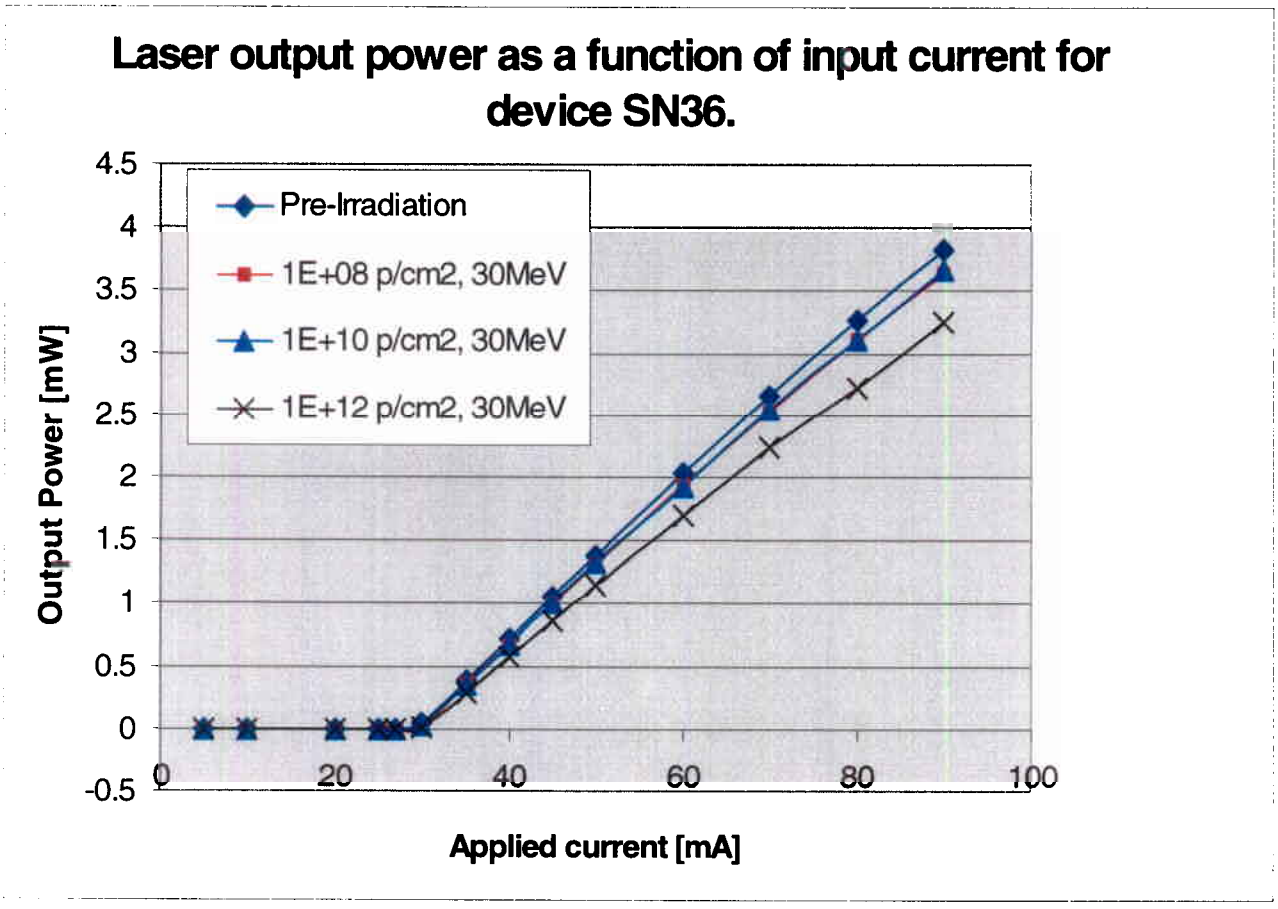

Figure 28: Optical power as a function of input current for SN36

Figure 28 illustrates that the optical power degrades with increasing proton fluence. Surprisingly, output power degraded only marginally after the second irradiation run (10^{10} p/cm^2) compared to the first irradiation run results (10^8 p/cm^2). Initially it was thought that a saturation level was reached. However, post third irradiation run (10^{12} p/cm^2) measurements showed a continuous degradation of the optical power. This is illustrated more clearly in figure 29 where the percentage degradation of output power with respect to pre-irradiation measurements as a function of fluence is depicted (for three different laser input currents).

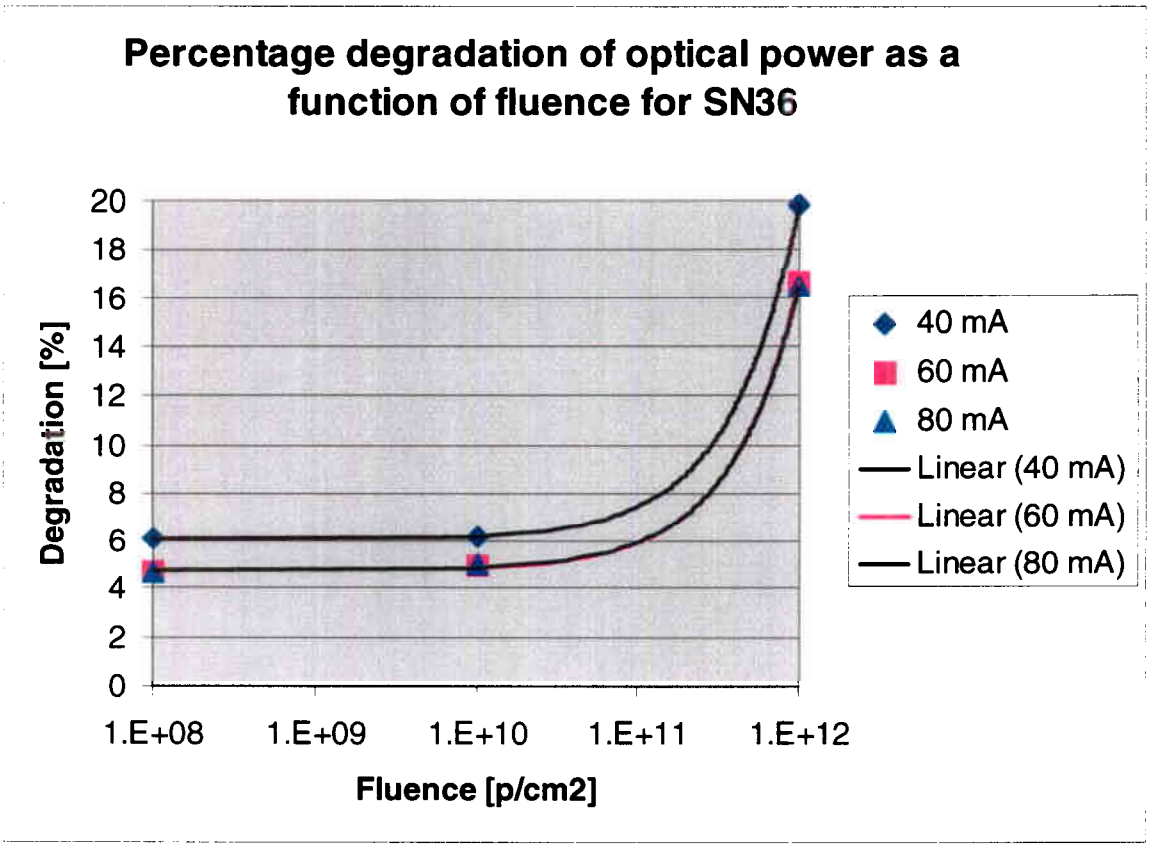

Figure 29: Percentage degradation of laser optical power as a function of fluence for three different input current values.

The laser optical power degraded by approximately 5 to 6% after the first and second irradiation run. It is noticed that the optical power degradation between the first and second irradiation run is marginal. However, the degradation increased to between 16 and 20% after the third irradiation run. Post-irradiation measurements showed only negligible threshold current shift (threshold current value < 40mA).

It is believed that the degradation mechanism observed results from a combination of radiation induced degradation on the different components comprising the laserdiode module. Thus, the optical power degradation may be attributed to displacement damage effects in the laserdiode, creation of colour centres in the lens or a combination of both.

Coarse prediction (not including shielding considerations) of the radiation environment experienced by these devices suggest a MSG EOL integral proton fluence (protons > 10 MeV) of 1 to 4 10^{10} p/cm^2. Figure 3 illustrates that the laserdiode optical power is degraded by approximately 5 to 6% after only 4 10^{8} p/cm^2. However, the optical power degradation changes only marginally for fluences 1 to 4 10^{10} p/cm^2. The following equations are obtained from linear fits to the curves in figure 29:

$Op_{dp} = 6.1 + 1.4\ 10^{-11}F$ for 40 mA laserdiode input current

$Op_{dp} = 4.8 + 1.2\ 10^{-11}F$ for 60 and 80 mA laserdiode input current

Op_{dp} = the optical power degradation in percentage.

F = Proton fluence in p/cm^2 30 MeV protons.

It has to be emphasised that the above analysis is based on one test sample only providing poor statistical data. However, the results give an indication of how the laserdiode operation is affected by the proton environment.

Conclusion:

The above analysis shows that the MIPAS laserdiode module optical power degrades when exposed to protons. Expected end of life proton (> 10 MeV protons) fluence is in the order of 1 to 4 10^{10} p/cm^2 resulting in an optical power degradation of approximately 5 to 6%. Predicted end of life fluence is a coarse value not taking into account device / spacecraft shielding.

Unfortunately, irradiation data at different proton energies is not available. However, low energy protons are thought to be more damaging than higher energy protons.

The laser diode was not continuously powered during measurements. Future investigations will focus on annealing effects due to continuous laser operation (increased laserdiode junction temperature).

2. Photodiodes

Two photodiodes from the MIPAS instrument were submitted to two irradiation runs with a proton energy of 30 MeV. Comparison of the pre- and post-irradiation results (dark current, I-V characteristic and photocurrent) are presented in the following pages.

The third photodiode was keep as a reference.

a. Dark current results

The reference SN 163 was characterised before each set of measurements in order to verify proper conditions of the test bench set-up. Variation between measurements was approximately 2%.

Table 18 presents the results of the dark current values before and after irradiations for the two photodetectors.

MIPAS Dark Current (nA) $T = 20^{\circ}C$, $V_R = -5$ V						
MIPAS Serial number	Fluence (p/cm^2), 30 MeV					
	Pre-irrad.	10^8	10^9	10^{10}	10^{11}	10^{12}
SN 243	-0.12	-0.21	-1.44			
SN 249	-11.06			-24.32		-1 657

Table 18: Dark current values for the two irradiated photodiodes from MIPAS

The dark current of SN243 was observed to increase by 63% and a factor of 12 for fluences of 10^8 and 10^9 p/cm^2 respectively. Sample 249 was irradiated to higher fluences than SN243, consequently higher dark current values were observed: ~118% and a factor of 148 for fluences of 10^{10} and 10^{12} p/cm^2 respectively.

b. I-V characteristic results

Figure 30 shows the pre- and post-irradiation I-V characteristics for sample SN 243.

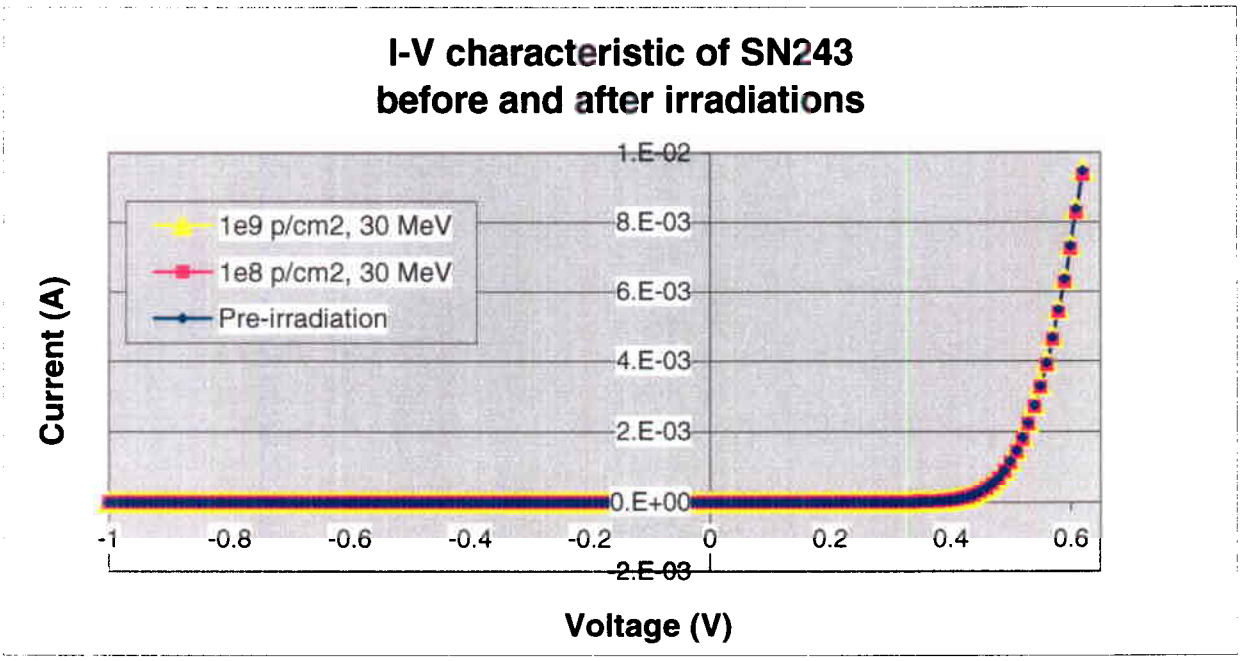

Figure 30: I-V plot of SN243 before and after proton irradiation

The I-V characteristic of sample SN243 did not change with radiation.

However, in figure 31 (see next page), I-V curves for SN249 changed after being irradiated to a fluence of 10^{12} p/cm^2. Figure 32 shows the same graph but for a different current and voltage resolution.

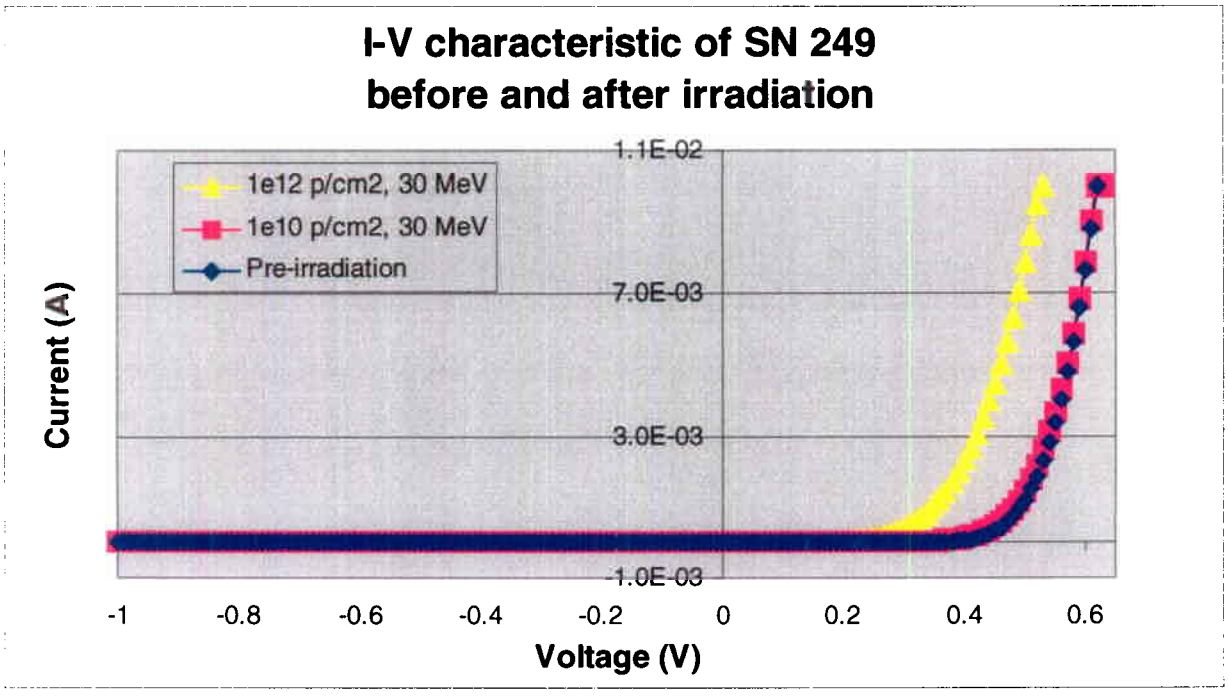

Figure 31: I-V plot for SN249 before and after irradiation

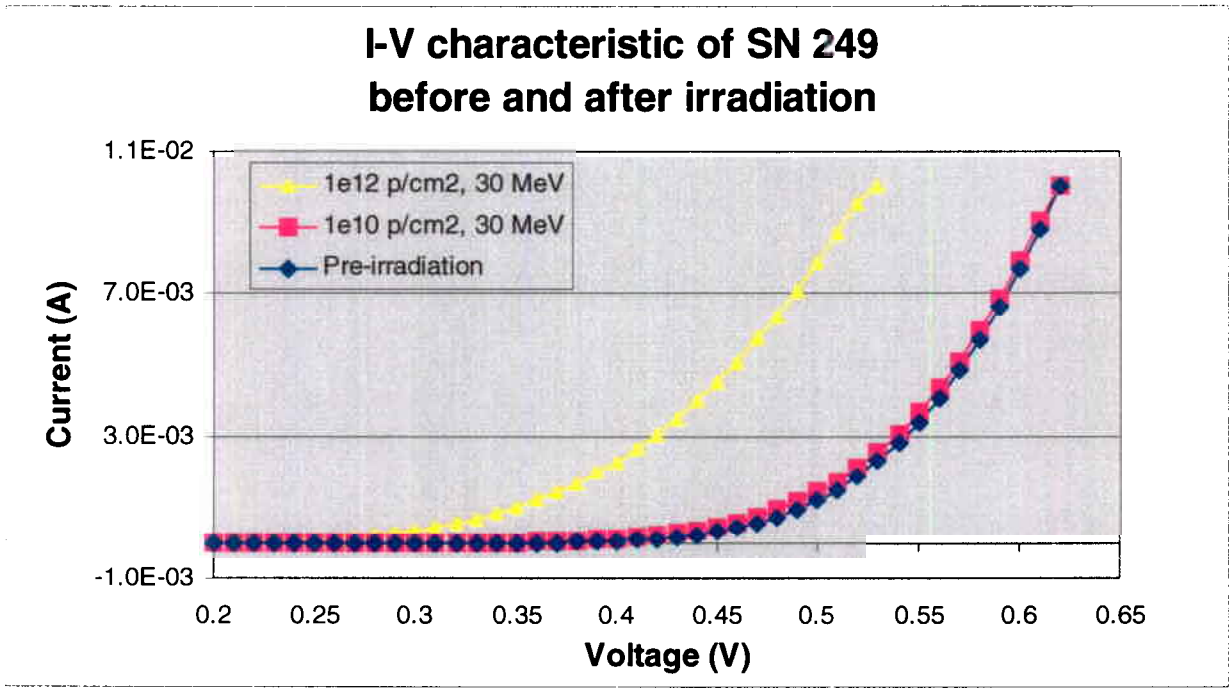

Figure 32: Detailed view of figure 31 for voltage > 0.2V

As illustrated in figure 32, a small reduction of the voltage is visible for fluence of 10^{10} p/cm^2. At a fluence of 10^{12} p/cm^2, this decrease becomes more pronounced.

The reverse biased part of the I-V curve was also effected by the proton irradiation, as illustrated in figure 33. The dark current increased significantly for fluence of 10^{12} p/cm^2. A dark current increase was also observed after a fluence of 10^{10} p/cm^2, however not as much as for a fluence of 10^{12} p/cm^2.

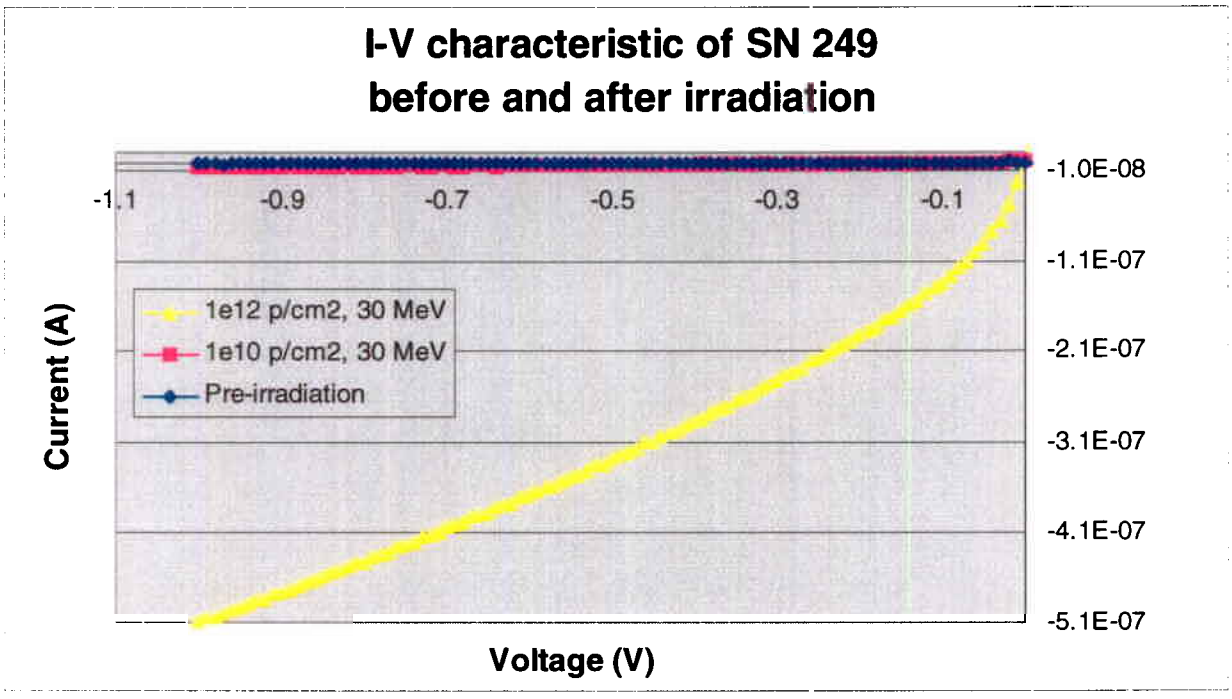

Figure 33: Detailed view of figure 30 for voltage < 0V

Conclusion:

Changes in the I-V curves were observed when the samples were irradiated at fluence higher that 10^9 p/cm^2 at 30 MeV. The following effects were observed:

- decrease of the threshold voltage in the forward bias part of the characteristic
- increase of the dark current at low voltages.

c. Photocurrent results

Photocurrent measurements were performed for four different wavelengths (700, 900, 1100 and 1300 nm). The post-irradiation dark current values were significant compared to the photocurrent values. However, the dark current value is only an offset and was subtracted from the photocurrent measurements.

Results of the offset corrected photocurrent measurements for the two samples are plotted in figures 34 and 35.

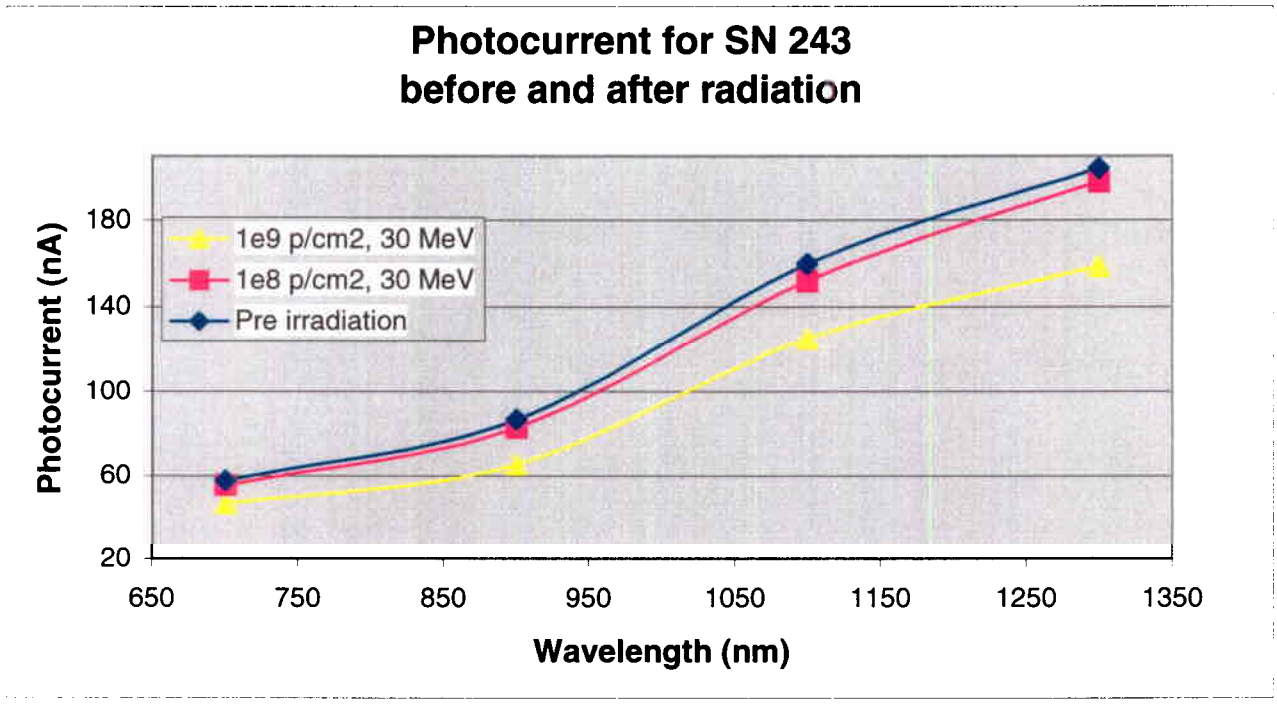

Figure 34: Photocurrent (corrected for dark current)
as a function of the wavelength for SN243

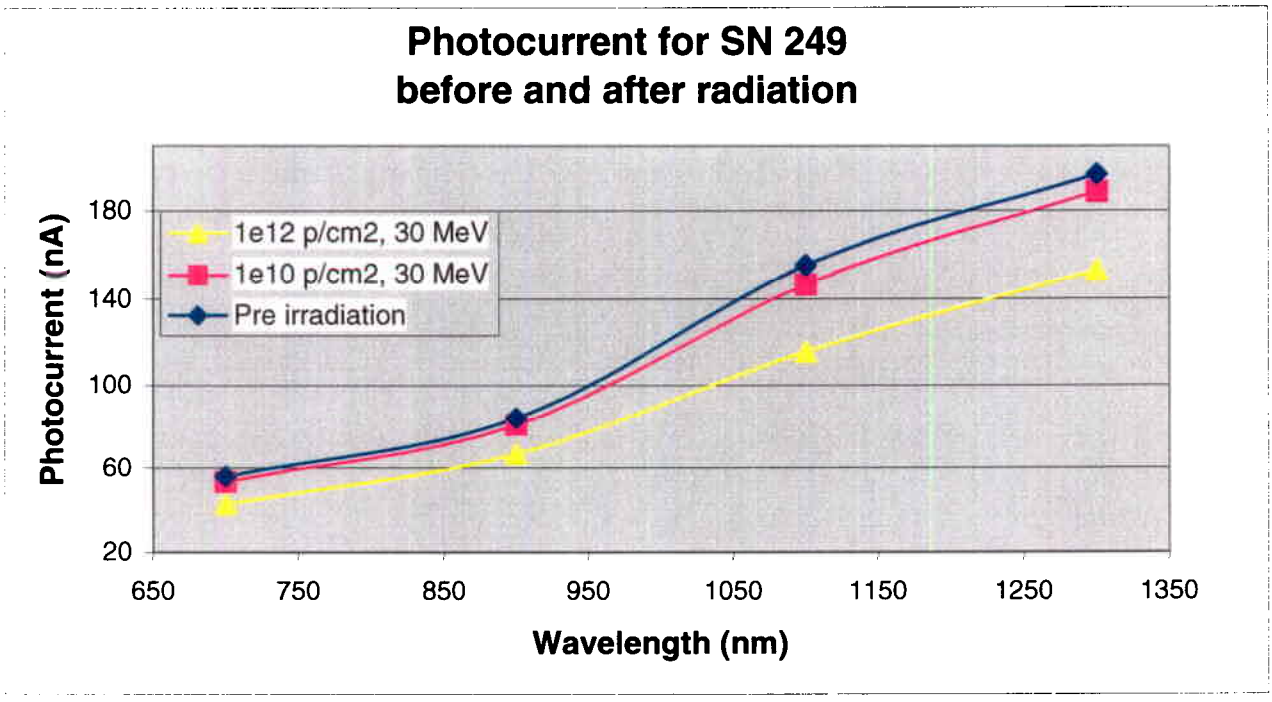

Figure 35: Photocurrent (corrected for dark current)
as a function of the wavelength for SN249

Sample SN243 show a ~20% photocurrent degradation at 10^9 p/cm^2 while SN249 show this degradation after 10^{12} p/cm^2 a considerable spread in results between the two devices.

d. Conclusion

The following effects of radiation on the MIPAS InGaAs photodiodes were observed in agreement with results reported in the literature.

- Increase of the dark current
- Decrease of the threshold voltage in the forward part of the I-V characteristic
- Increase of the current in the reverse part of the I-V characteristic
- Decrease of the photocurrent

These effects are due to the creation of traps in the forbidden bandgap. Indeed, this defects:

- Increase the probability of transition of electrons from the valence band to the conduction band, thus increasing the leakage current.

- Trap electrons and holes, permitting their recombination with no contribution to the photocurrent, thus decreasing the value of the current.

B. THOMSON devices

1. Dark current results

a. MSG devices

The following table shows the results of the dark current measurements for the two MSG photodiodes after proton irradiation. Variation between measurements for the reference is about 10%.

MSG Dark Current (nA) $T = 20^{\circ}C$, $V_R = -5$ V								
MSG 972-952-	Energy	Diode Ref.	Fluence (p/cm^2)					
			Pre-irrad.	10^8	10^9	10^{10}	10^{11}	10^{12}
L6B5	30 MeV	d1	-17.68		-17.03		-471.84	
		d2	Note 1		-		-	
		d3	Note 1		-		-	
L7B4	6 MeV	d1	-10.52	-11.09				-65 308
		d2	-11.64	-12.35				-65 832
		d3	-10.38	-11.06				-66 472

Table 19: Pre-and post-irradiation dark current for MSG photodiodes

Note 1: The sample 972-952-L6B5 was provided with diodes d2 and d3 damaged

Considering the variation between measurements, the dark current values of both devices did not change after the first irradiation run. However, increase of the leakage current was observed after the second proton exposure. To better understand these results, the dark current increase in relation to the pre-irradiation values were plotted as a function of fluences for both devices in figure 36.

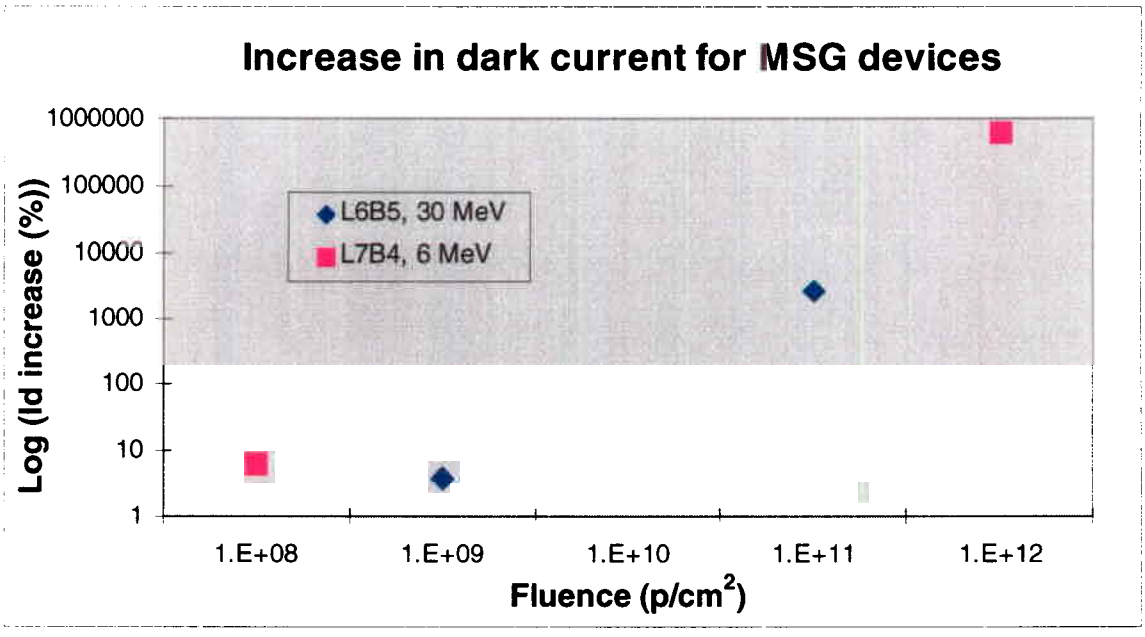

Figure 36: Increase of the dark current as a function of fluences for MSG photodiodes

No dark current increase is observed at fluences lower than 10^{10} p/cm^2 (it is considered being in the measurement variation). However, the dark current increases significantly when the two photodiodes were irradiated to fluences of 10^{11} and 10^{12} p/cm^2. Due to insufficient data, the difference between 6 and 30 MeV data can not be explained.

b. THOMSON 6 µm and 3 µm InGaAs layer devices

Results of dark current measurements are presented in tables 20 and 21.

3 µm layer thickness (110-B506-)	Energy	Diode Ref.	Value of dark current (nA) for different fluence (p/cm^2) at –5V					
			Pre-irrad.	10^8	10^9	10^{10}	10^{11}	10^{12}
L3B5	30 MeV	d1	-0.072		-5.97		-665.76	
		d2	-0.072		-5.15		-641.88	
		d3	-0.071		-6.72		-646.74	
L3B6		d1	-0.064				-570	-7 663
		d2	-0.063				-557	-7 536
		d3	-0.068				-532	-7 459
L3B7	6 MeV	d1	-0.098		-6.15		-3 809.8	
		d2	-0.095		-4.51		-3 797.8	
		d3	-0.091		-5.76		-3 796	
L5B6		d1	-0.075			-62.9		-53 876
		d2	-0.072			-62.8		-53 862
		d3	-0.076			-60.9		-53 830
L6B10		d1	-0.070					-6 990
		d2	-0.073					-6 912
		d3	-0.076					-6 888

Table 20: Pre- and post-irradiation dark current values
for the 3 µm thick InGaAs layer devices

6 µm layer thickness (111-B611-)	Energy	Diode Ref.	Value of dark current (nA) for different fluence (p/cm^2) at –5V					
			Pre-irrad.	10^8	10^9	10^{10}	10^{11}	10^{12}
L3B7	30 MeV	d1	-0.072	-1.59		-102.66		
		d2	-0.095	-0.66		-87.57		
		d3	-0.093	-0.82		-101.97		
L5B7		d1	-0.020				-773	-9 747
		d2	-0.094				-776	-9 756
		d3	-0.097				-781	-9 567
L5B8	6 MeV	d1	out	out	out			
		d2	-0.17	-1.46	-27.27			
		d3	-0.18	-1.76	-28.40			
L6B6		d1	-0.094			-63.47		-53 366
		d2	-0.12			-66.36		-53 762
		d3	-0.11			-70.5		-54 224
L6B7		d1	-0.10					-7 780
		d2	-0.12					-7 740
		d3	-0.16					-7 706

Table 21: Pre- and post-irradiation dark current values
for the 6 µm thick InGaAs layer devices

To better understand these results, plots showing the dark current increase (in relation to the pre-irradiation values) were plotted. Figures 37 and 38 show these graphs for 6 and 3 µm thick InGaAs devices respectively.

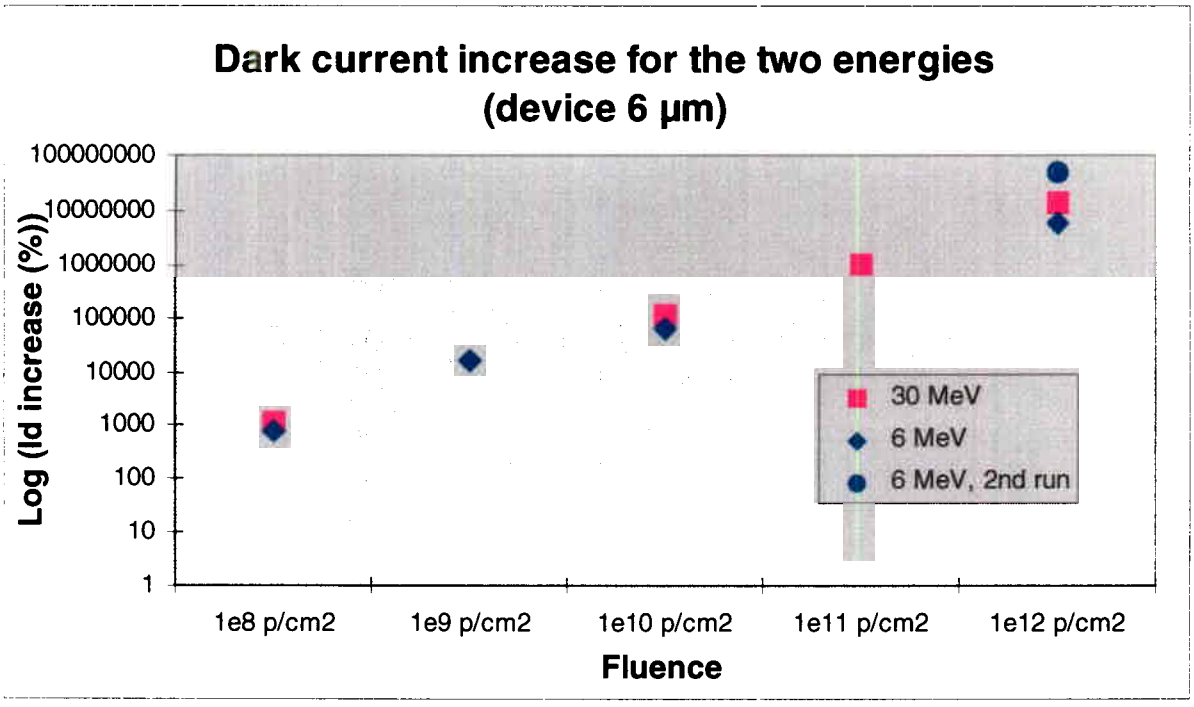

Figure 37: Dark current increase as a function of fluences for both energies (6 and 30 MeV) and for the 6 µm thick InGaAs layer photodiodes

Figure 37 shows that the increase of the dark current is linear with the fluences. Sample L6B6 shows a larger than expected dark current increase after the second 6 MeV proton exposure. This is most probably due to the beam quality of the second irradiation run (further explained in the conclusion page 57).

Same remarks can be made for figure 38 (see next page) showing the dark current increase for the 3 µm thick layer photodiodes. Indeed, the increase is linear with the fluences, no difference between the two energies is observed and the last irradiation of sample L5B6 irradiated with an energy of 6 MeV shows a larger than average dark current increase.

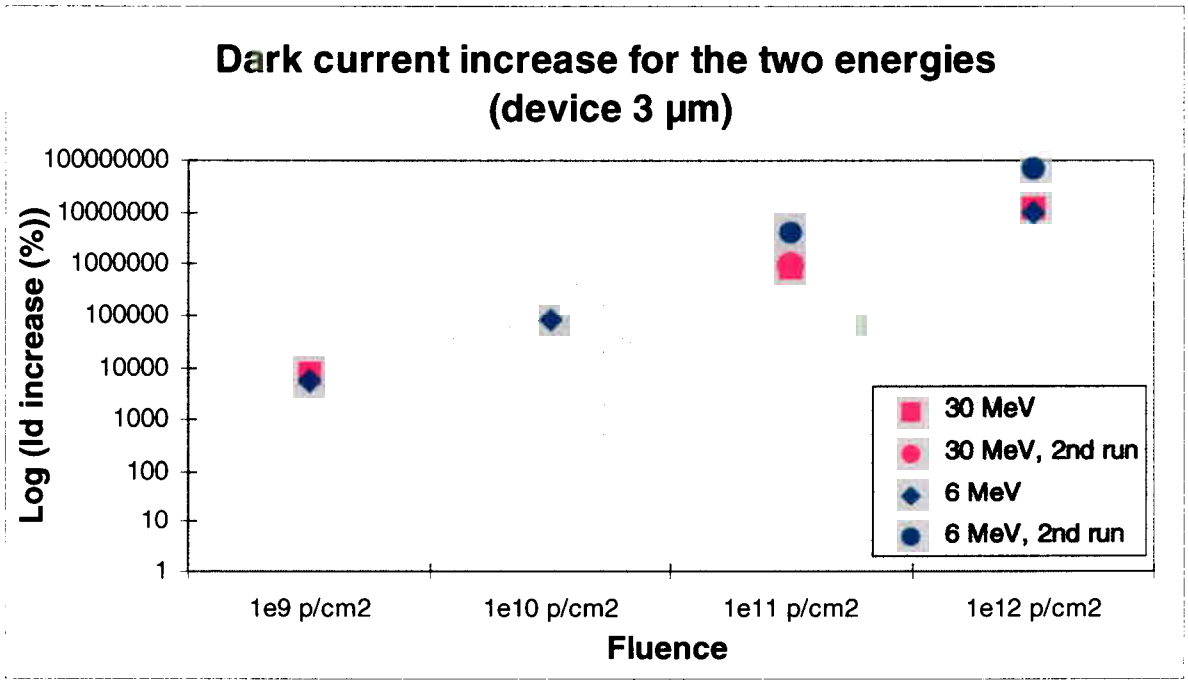

Figure 38: Dark current increase as a function of the fluences for both energies (6 and 30 MeV) for the 3 µm thick InGaAs layer photodiodes

Figure 39 illustrates the dark current increase for both InGaAs thickness and both proton energies.

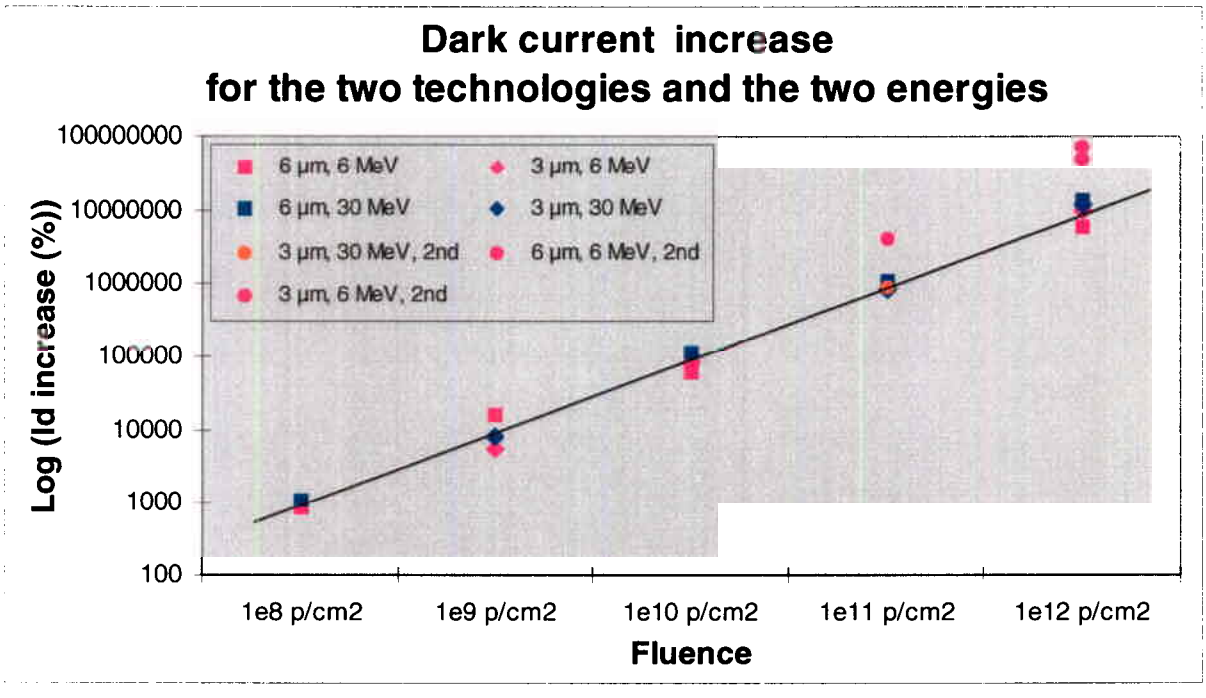

Figure 39: Dark current increase as a function of the fluences for both energies (6 and 30 MeV) for both layers (3 and 6 µm)

As illustrated in figure 39, the increase of the dark current is linear with the fluence. A fit curve was added to the plot to show the linearity. Some of the post second 6 MeV irradiation dark current data show higher dark current increase than expected.

Conclusion:

The dark current increases linearly with fluence and is seemingly the same for the two active layers and proton energies. However, a second 6 MeV proton irradiation run resulted in a higher dark current value than expected. This may be explained by the fact that contrary to the first low energy (6.7 MeV) proton run, the actual peak energy of the second proton run was 4.7 MeV, as appropriate beam energy degraders were not available at the time of irradiation. The energy spectrum of the second irradiation run showed a broad tail in the low energy region. Thus, the large number of low energy protons resulted in the increased damage to the test sample. In future irradiation runs, it is desired to extend the proton energy range to obtain a better understanding of the NIEL mechanism.

2. I-V characteristic results

I-V measurements (current as a function of the voltage) were performed for all THOMSON photodiodes.

a. MSG technology

Figures 40 and 41 present the I-V plots for the MSG photodiodes.

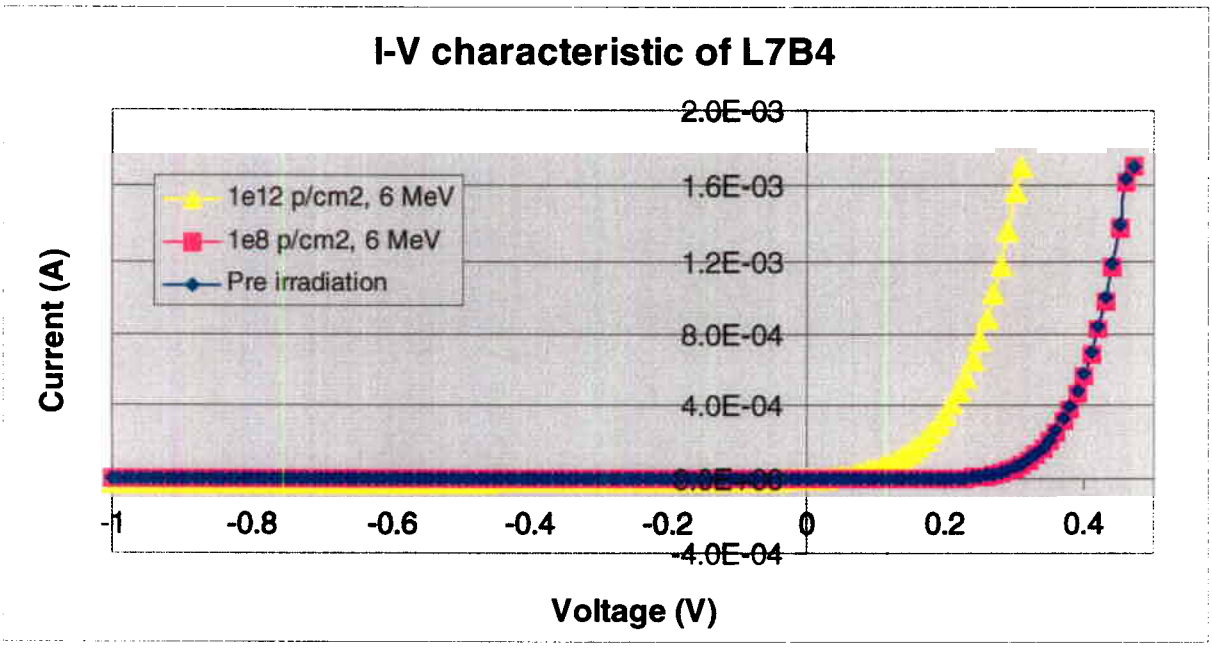

Figure 40: I-V plot of device L7B4 (MSG device)

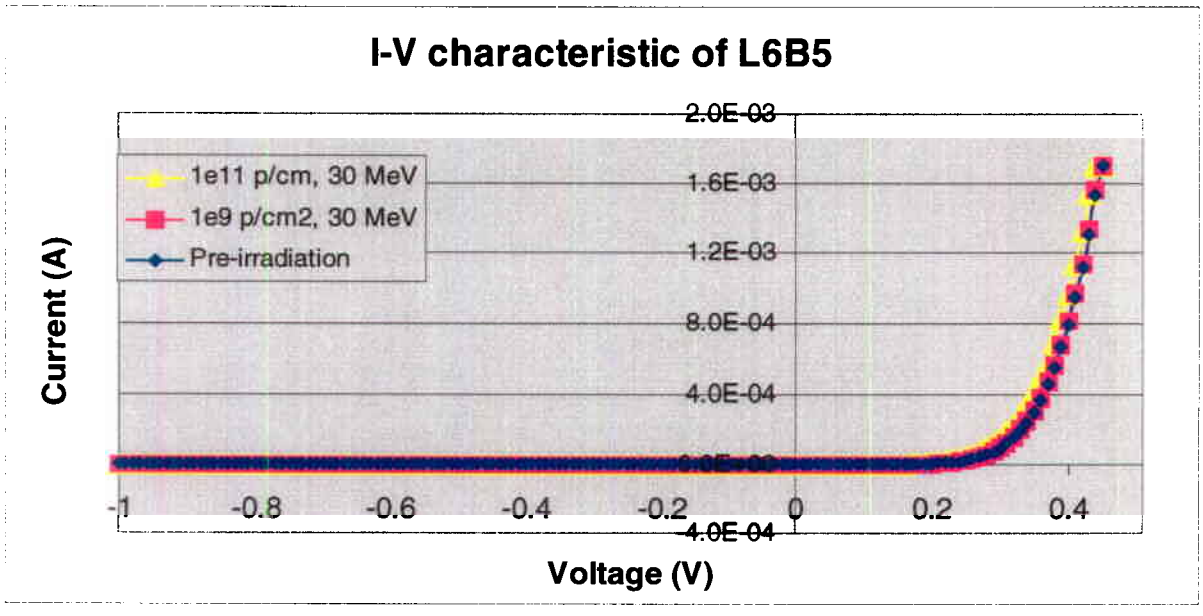

Figure 41: I-V plot of device L6B5 (MSG device)

The I-V plot of sample L7B4 shows that the threshold voltage decreases when the photodiode is irradiated to a fluence of 10^{12} p/cm^2. However, no changes are observed for lower fluence. Similarly, an increase of the current at reverse voltage was observed only for a fluence of 10^{12} p/cm^2.

No change between the pre- and post-irradiation I-V curve values for sample L6B5 is observed. However, a closer examination of the data, figures 42 and 43, indicate the following:

- A threshold voltage decrease is observed when the sample is irradiated to a fluence of 10^{11} p/cm^2.
- An increase of the reverse current is observed for a fluence of 10^{11} p/cm^2.

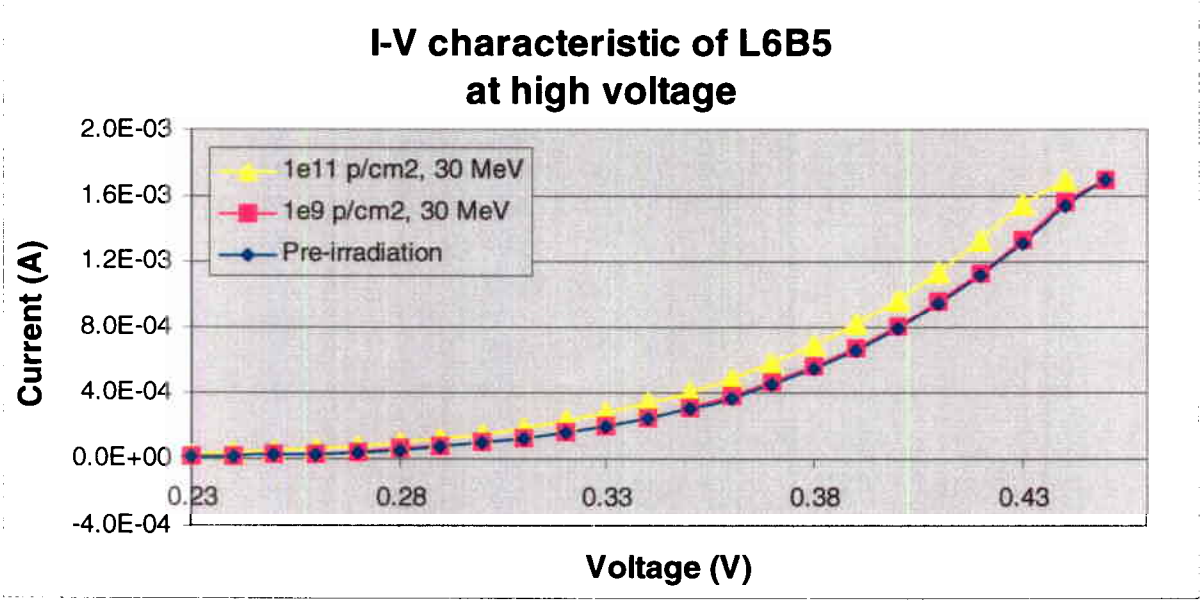

Figure 42: Detailed view of figure 7 for voltage > 0.23 V

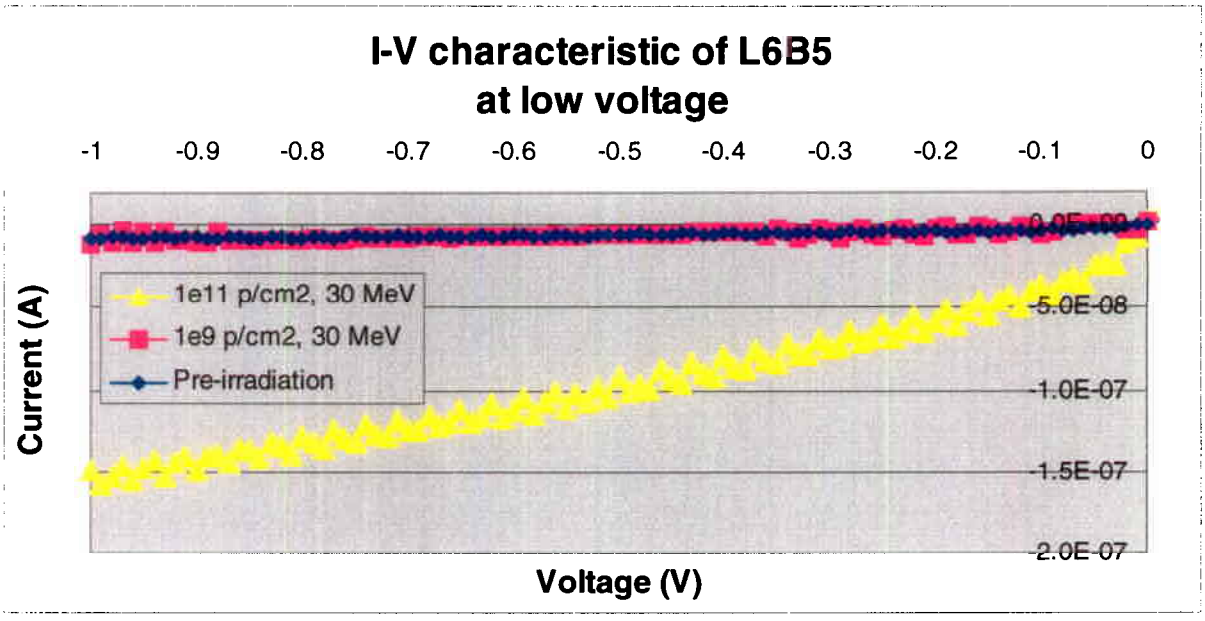

Figure 43: Detailed view of figure 7 for voltage <0 V

Conclusion:

The following effects of radiation were observed on the I-V characteristic of the MSG photodiodes at a high fluence (10^{11} p/cm^2):

- Decrease of the threshold voltage
- Increase of the reverse current

b. 3 and 6 µm thick InGaAs layer devices

Pre- and post-irradiation I-V measurements were performed on Thomson photodiodes. The complete I-V curves will not be presented in this report. However, typical examples are given.

Tables 22 and 23 present a summary of the different changes that can be observed on the I-V plots after irradiation.

R indicates increased reverse current.

F indicates decreased threshold voltage.

No R and No F indicate no change in the reverse or forward region of the I-V plot, respectively.

3 μm layer thickness (110-B506-)	Energy	I-V changes at different fluence (p/cm^2)				
		10^8	10^9	10^{10}	10^{11}	10^{12}
L3B5	30 MeV		F No R		F R	
L3B6					F R	F R
L3B7	6 MeV		No F No R		F R	
L5B6				F R		F R
L6B10						F R

Table 22: Changes observed on I-V curves after irradiation for 3 μm thick devices

6 μm layer thickness (111-B611-)	Energy	I-V changes at different fluence (p/cm^2)				
		10^8	10^9	10^{10}	10^{11}	10^{12}
L3B7	30 MeV		F No R		F R	
L5B7					F R	F R
L5B8	6 MeV		No F No R		F R	
L6B6				F R		F R
L6B7						F R

Table 23: Changes observed on I-V curves after irradiation for 6 μm thick devices

These tables show that differences between pre- and post-irradiation I-V measurements were observed when the devices were irradiated at fluences higher than 10^9 p/cm^2.

Figures 44, 45, 46 and 47 present typical I-V curves.

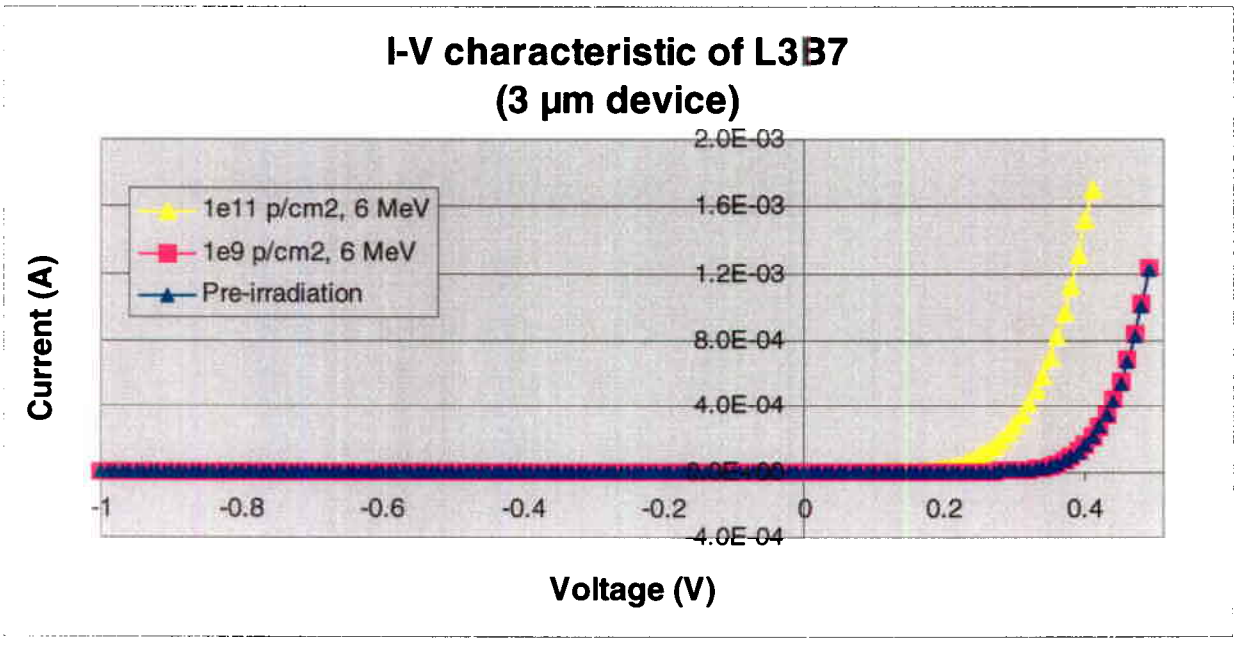

Figure 44: IV plot for device L3B7 (3 µm thick layer device)

The following figure illustrates the reverse bias region of the I-V curve for device L3B7.

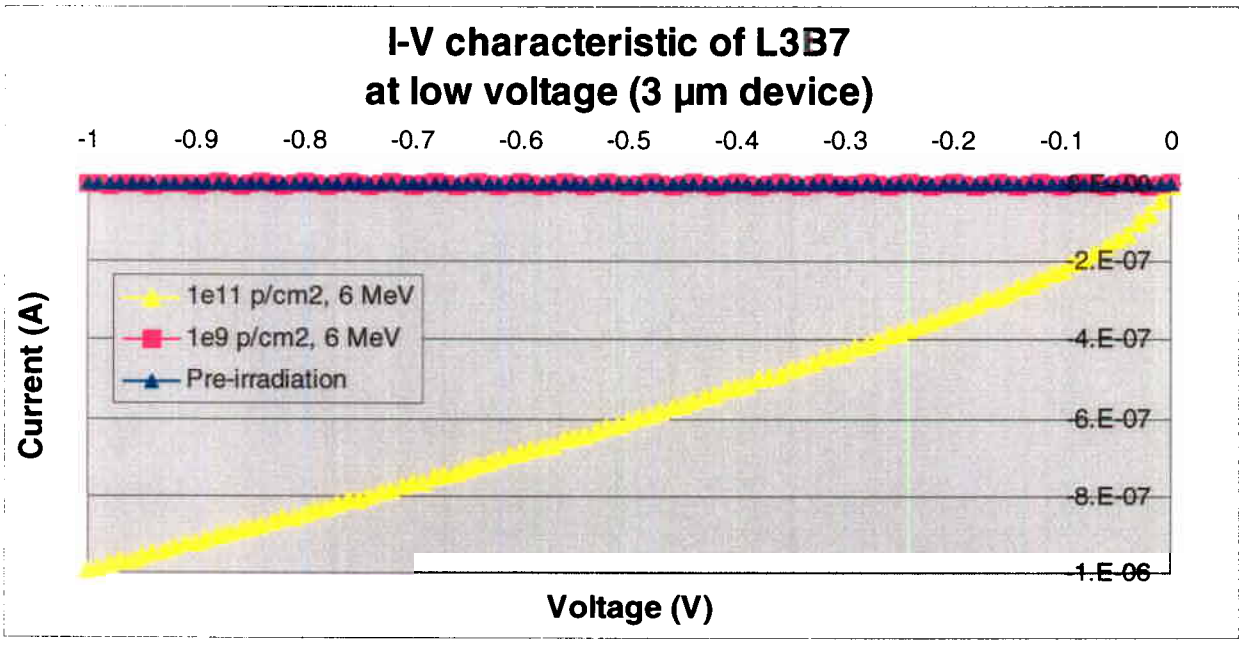

Figure 45: Detailed view of figure 44 for voltage < 0V

The two next figures show the I-V curves after irradiation to high fluences. A decrease of threshold voltage an increase of the dark current (in the reverse biased region of the curve) is observed.

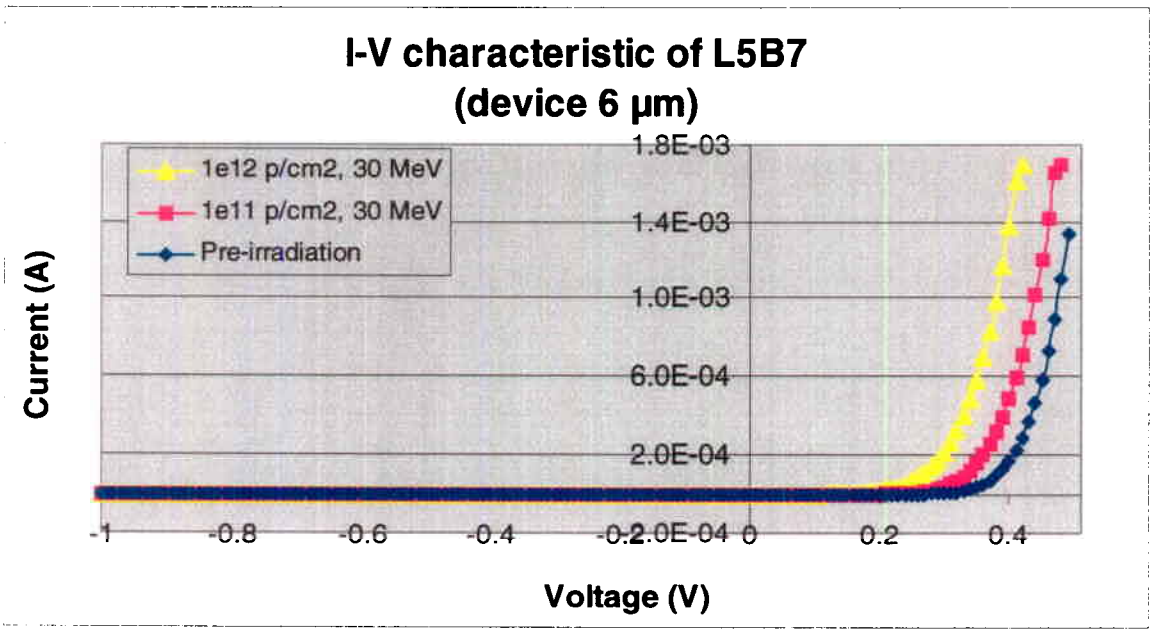

Figure 46: I-V plot for device L5B7 (6 µm thick layer device)

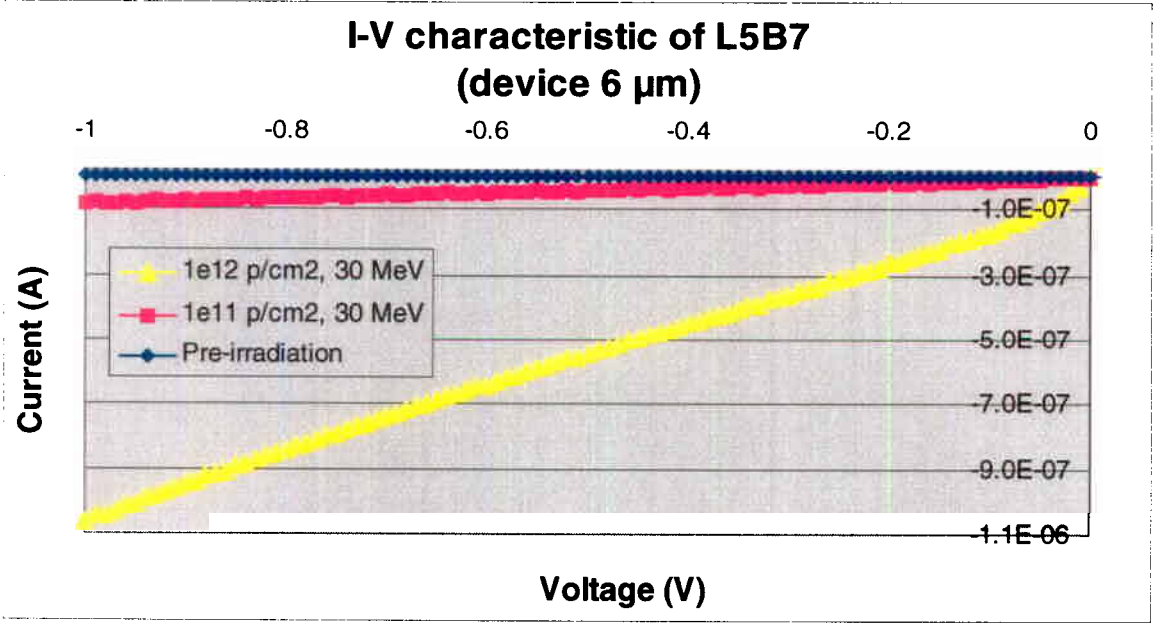

Figure 47: Detailed view of figure 45 for voltage < 0V

Conclusion:

The I-V measurements show a decrease of the threshold voltage and an increase of the reverse current when the photodiodes were irradiated to fluences higher than 10^9 p/cm^2.

3. Photocurrent results

As previously described, the dark current increased up to 3 orders of magnitude for the high fluences. These values were so high that they affected the photocurrent measurements. To avoid this, dark current values were subtracted from photocurrent measurements.

Dark current related problem may have been avoided by cooling of the samples during test or by the use of a stronger source light. Unfortunately, these improvements were not possible due to the availability of equipment.

Measurement results of photocurrent as a function of wavelength (corrected for dark current values) are presented in the following pages.

Measurement variation is about 5 %.

a. MSG Technology

Table 24 presents the pre- and post-irradiation photocurrent values for the two MSG devices.

MSG number	Energy	λ (nm)	Value of photocurrent (nA) for different fluence (p/cm^2) at –5V					
			Pre-irrad.	10^8	10^9	10^{10}	10^{11}	10^{12}
972-952-L6B5	30 MeV	700	137		132		124	
		900	146		144		122	
		1100	295		287		268	
		1300	409		400		332	
972-952-L7B4	6 MeV	700	140	132				
		900	147	144				
		1100	301	291				Note 1
		1300	417	407				

Table 24: Pre- and post-irradiation photocurrent values for the two MSG devices.

Note1: The dark current values were so high that measurements of the photocurrent were not accurate enough to give reasonable photocurrent values.

For both devices, the photocurrent values did not change after the first irradiation run (values are in the measurement variation). However, a decrease is observed for device L6B5 at a fluence of 10^{11} p/cm^2. Figure 48 illustrate a plot of the photocurrent as a function of fluences for device L6B5.

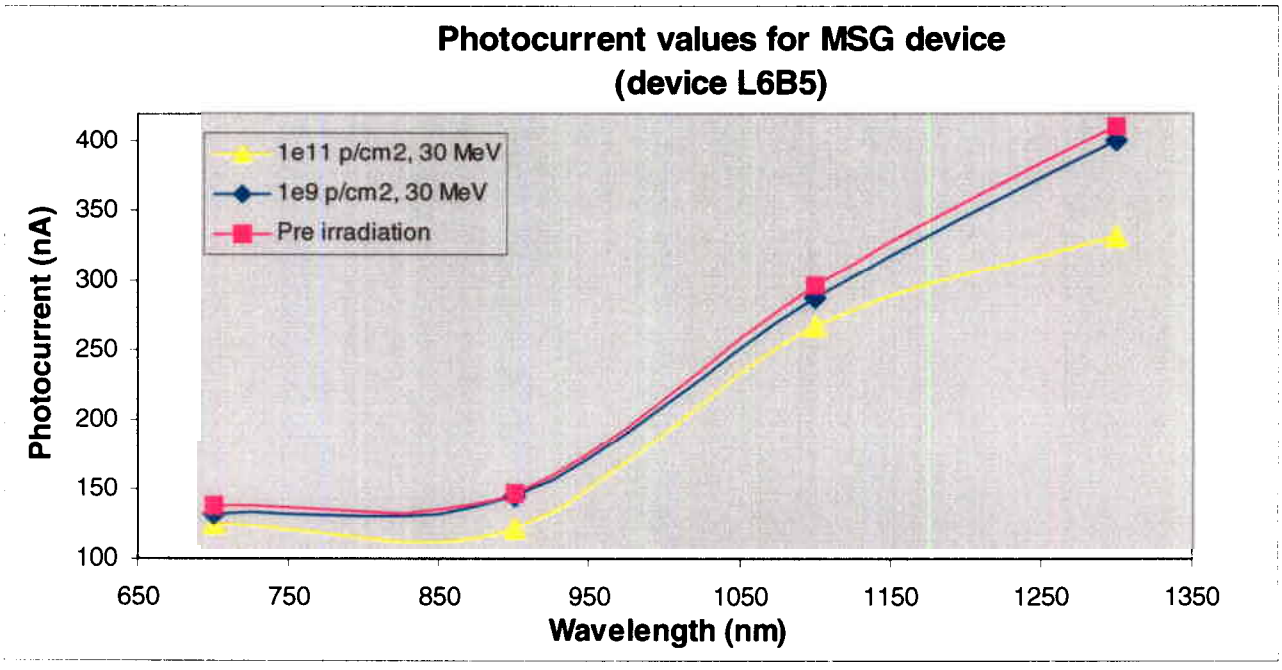

Figure 48: Photocurrent as a function of wavelength for device L6B5

Conclusion:

The photocurrent value decreases when the MSG devices are irradiated to fluences higher than 10^9 p/cm^2.

b. 3 and 6 µm thick layer devices

Tables 25 and 26 present the results of the photocurrent measurements for 3 and 6 µm thick InGaAs layer THOMSON photodiodes.

3 µm layer thickness (110-B506-)	Energy	λ (nm)	Value of photocurrent (nA) for different fluence (p/cm^2) at –5V					
			Pre-irrad.	10^8	10^9	10^{10}	10^{11}	10^{12}
L3B5	30 MeV	700	192		175		124	
		900	177		167		109	
		1100	314		289		210	
		1300	440		412		294	
L3B6		700	188				150	125
		900	176				149	109
		1100	313				260	205
		1300	442				368	292
L3B7	6 MeV	700	189		173		48	
		900	176		166		12	
		1100	307		282		108	
		1300	434		406		186	
L5B6		700	180			146		45
		900	167			143		14
		1100	304			258		101
		1300	442			378		279
L6B10		700	174					17
		900	167					56
		1100	299					160
		1300	437					258

Table 25: Photocurrent results for 3 µm thick layer devices

6 μm layer thickness (111-B611-)	Energy	λ (nm)	Value of photocurrent (nA) for different fluence (p/cm^2) at –5V					
			Pre-irrad.	10^8	10^9	10^{10}	10^{11}	10^{12}
L3B7	30 MeV	700	166	156		121		
		900	164	158		114		
		1100	269	253		232		
		1300	403	385		297		
L5B7		700	164				115	104
		900	159				119	92
		1100	263				213	204
		1300	427				336	274
L5B8	6 MeV	700	163	153	132			
		900	159	155	115			
		1100	261	248	230			
		1300	395	379	295			
L6B6		700	164			138		53
		900	157			142		27
		1100	260			237		70
		1300	396			365		201
L6B7		700	157					3
		900	155					27
		1100	262					127
		1300	400					235

Table 26: Photocurrent results for 6 μm thick layer devices

Figures 49 and 50 show the photocurrent values for each wavelength as a function of the fluence for the two proton energies. As illustrated in these figures, the photocurrent decreases with increasing proton fluence. However, the decrease is in some instances slightly higher for 6 MeV proton exposure.

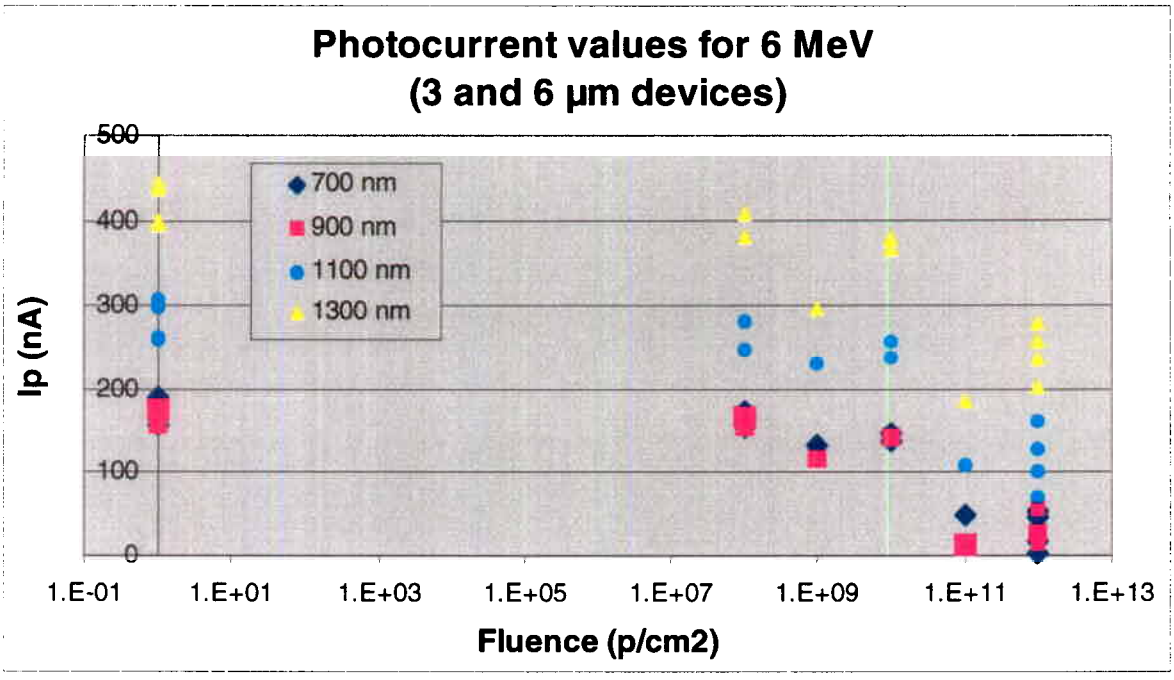

Figure 49: Photocurrent values for each wavelength as a function of the fluence for both InGaAs thickneses for an energy of 6 MeV.

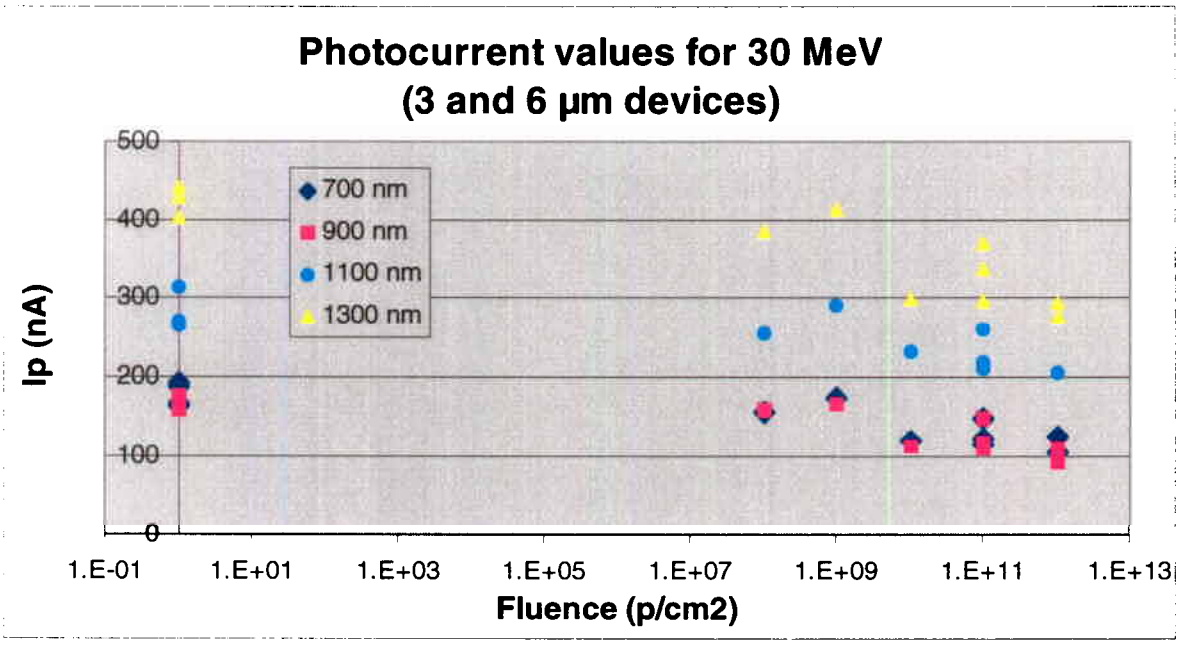

Figure 50: Photocurrent values for each wavelength as a function of the fluence for both InGaAs thickneses for an energy of 30 MeV.

Figures 51 and 52 show the photocurrent decrease as a function of fluence for a wavelength of 1300 nm. The photocurrent is observed to decrease linearly with the

fluence when the photodiodes are irradiated with 30 MeV or 6 MeV protons. No conclusive evidence for a difference between the two device types can be found.

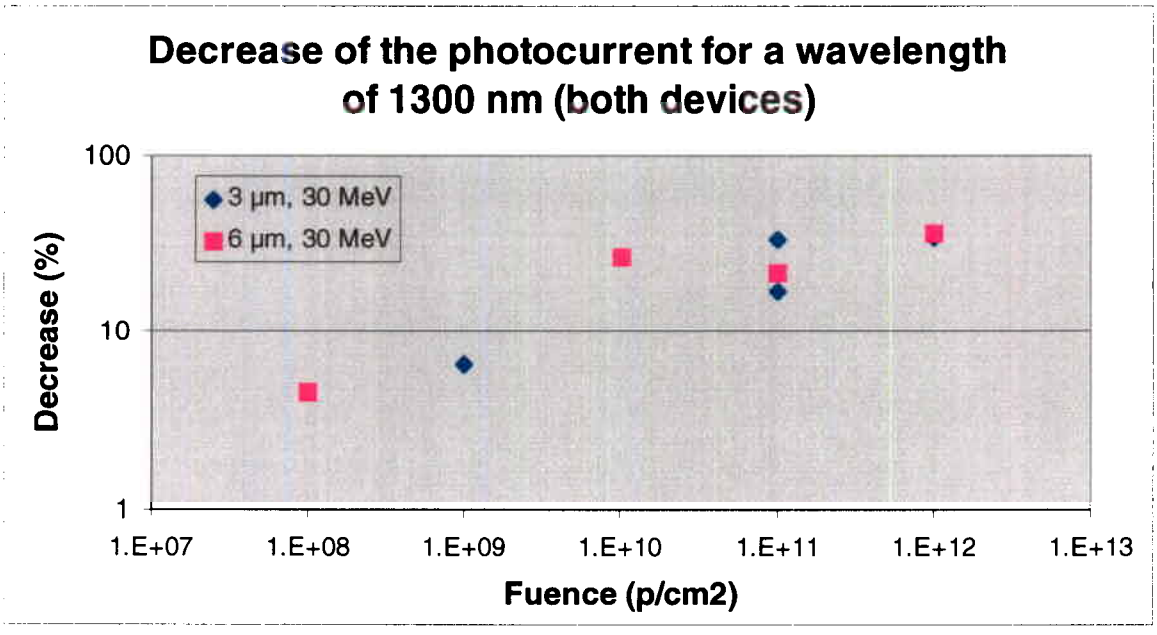

Figure 51: Photocurrent decrease for λ = 1300 nm, E = 30 MeV, for both devices as a function of fluence

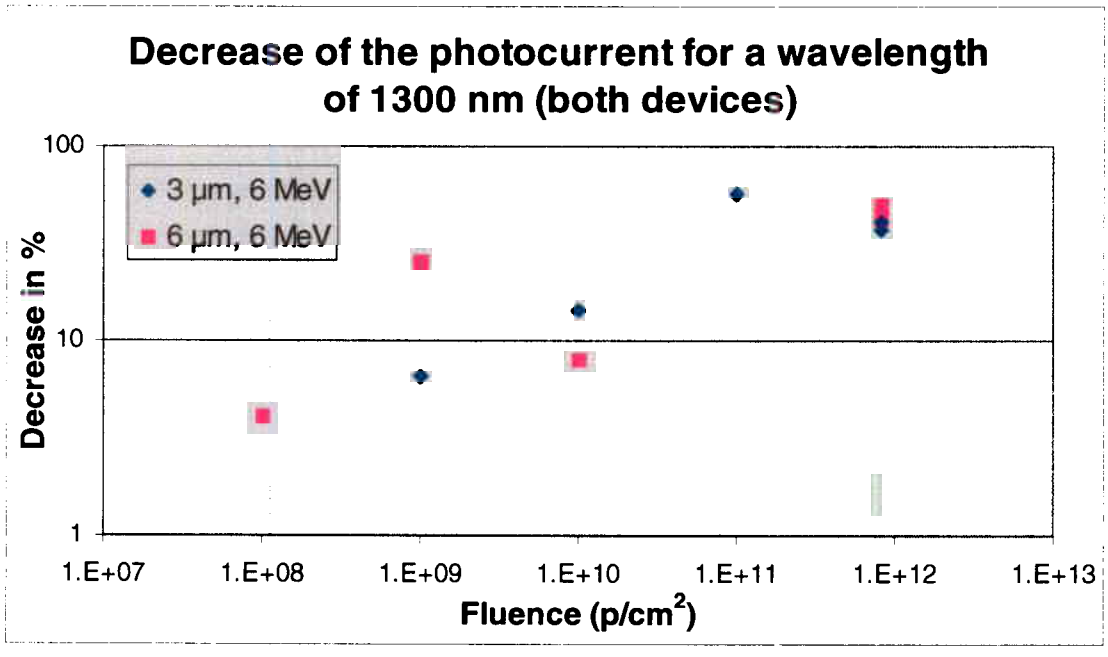

Figure 52: Photocurrent decrease for λ = 1300 nm, E = 6 MeV for both devices as a function of fluence

Figure 53 shows the photocurrent decrease for the two different InGaAs thickness devices, the two energies and for a wavelength of 1300 nm. As illustrated in this figure the photocurrent decrease more for 6 MeV proton irradiated devices. However, no real difference can be found between the 3 and 6 µm thick InGaAs layer devices.

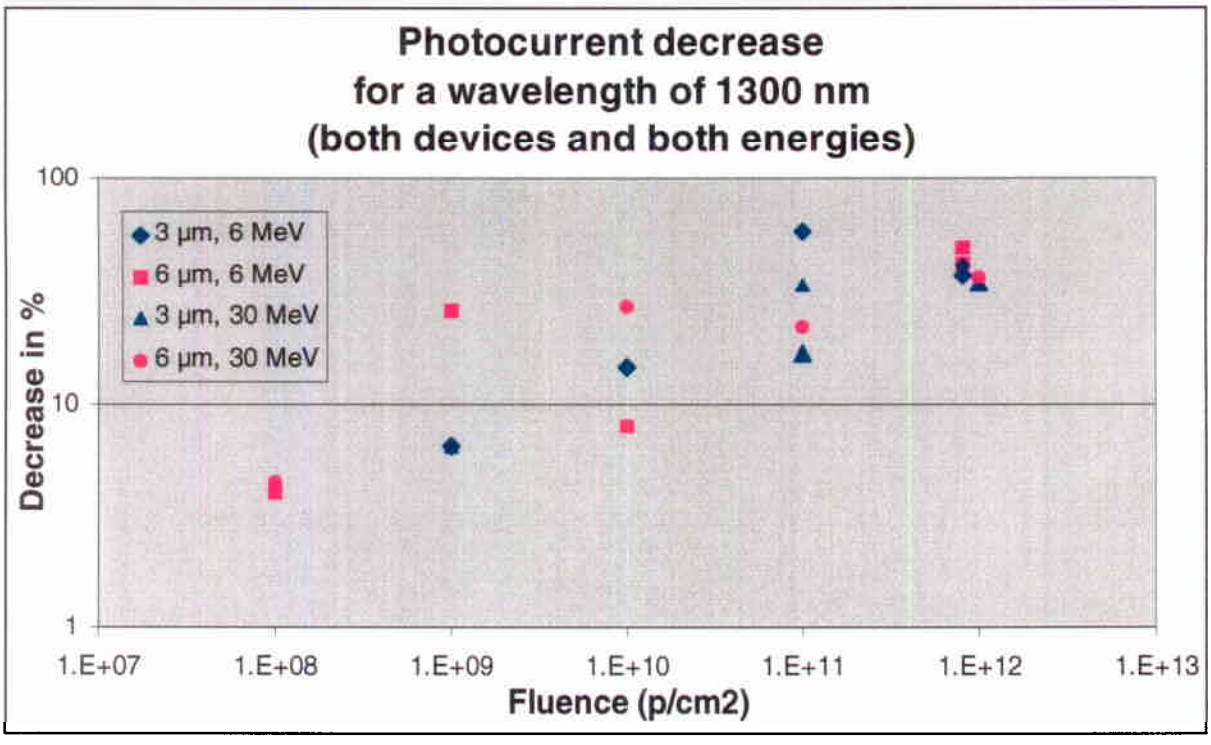

Figure 53: Photocurrent decrease for the two thickness layer devices, the two energies and for a wavelength of 1300 nm

Conclusion:

The photocurrent decreased with proton irradiation. The photocurrent decrease is higher for devices irradiated with 6 MeV protons than with 30 MeV protons. However, no differences were found between the two device types.

4. Summary of the results for THOMSON devices

Proton irradiation has an effect on the InGaAs THOMSON photodiodes tested here. The following effects were reported:

- Increase of the dark current
    - For MSG devices:

Increased dark current was observed only during the second irradiation run for fluence higher than 10^9 p/cm^2. The dark current increase is linear for fluence range 10^9p/ cm^2 and 10^{12}p/ cm^2.

- For 3 and 6 μm thick InGaAs layer devices:

Dark current increase is higher than for MSG devices and is linear in the fluence range 10^8 p/cm^2 and 10^{12} p/cm^2. Contrary to expectation, no clear difference was observed between the 6 and 30MeV post-irradiation measurements, also no measurable difference between the two InGaAs thickness layer was observed.

- Decrease of the threshold voltage and increase of the reverse current
    - MSG devices:

These parameter changes were observed only for samples exposed to > 10^{11} p/cm^2.

- 3 and 6 μm thick InGaAs layer devices:

These parameter changes were observed only for samples exposed to > 10^9 p/cm^2.

- Decrease of the photocurrent
    - MSG devices:

A photocurrent decrease in both samples was observed. However, the resulting high dark current in samples exposed to high proton fluence made it almost impossible to measure the correct photocurrent values.

- 3 and 6 μm thick InGaAs layer devices:

The photocurrent was observed to decrease with increasing fluence. No difference was observed between the two device types. Generally the photocurrent decrease was higher when the samples were irradiated to 6MeV protons.

5. Final conclusion

The following effects of radiation on the THOMSON InGaAs photodiodes were observed in agreement with results reported in the literature.

- Increase of the dark current
- Decrease of the threshold voltage in the forward part of the I-V characteristic
- Decrease of the photocurrent

However, following this study it appears that MSG devices are more resistant to proton radiation than the 3 and 6 µm thick InGaAs layer devices. Samples exposed to 6 MeV proton illustrate lower photocurrent than devices exposed to 30 MeV proton suggesting that protons of lower energies are more damaging (in agreement with NIEL as protons of lower energy deposit more of their energy in matter).

The proton radiation effects are due to the creation of traps in the forbidden bandgap of the semiconductor. Indeed, these defects:

- Increase the probability of transition of electrons from the valence band to the conduction band, thus increasing the leakage current.
- Trap electrons and holes, permitting their recombination with no contribution to the photocurrent, thus decreasing the value of the signal.

D. Heavy ion irradiation

In addition to proton irradiation, two THOMSON devices were also irradiated with heavy ions. The 3 µm thick InGaAs device was irradiated with Neon and the 6 µm thick device was irradiated with Argon.

1. Dark current results

Results of the dark current measurements are presented in figure 54.

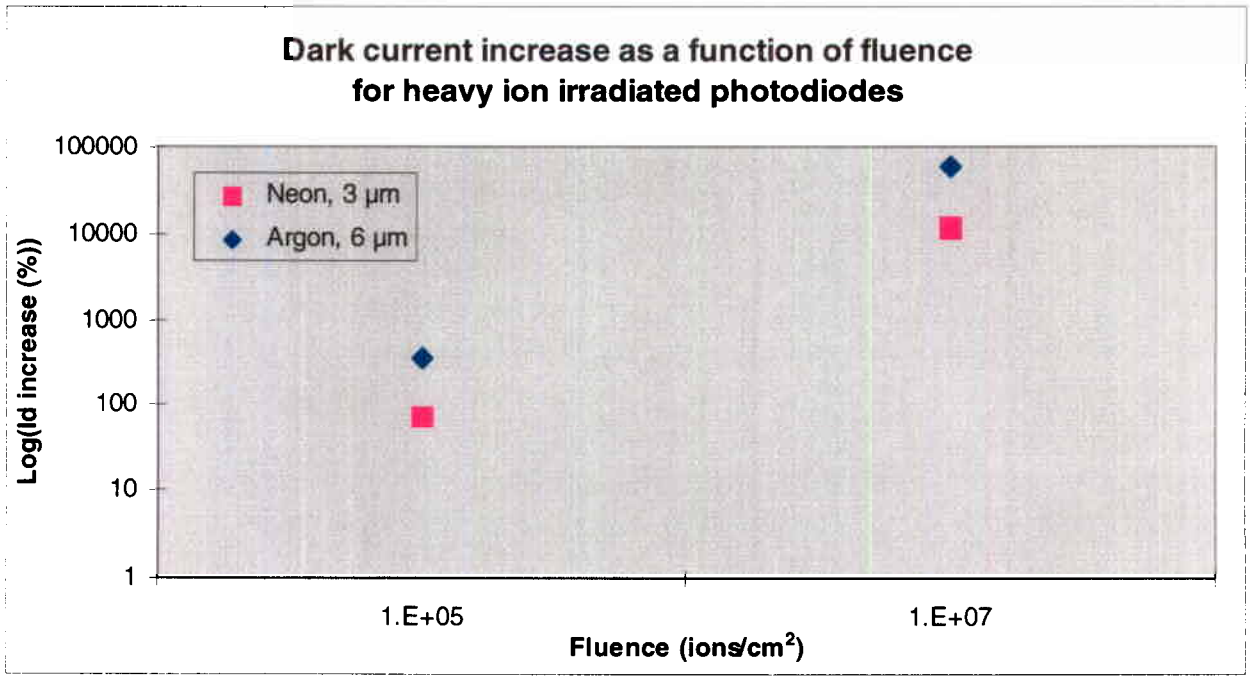

Figure 54: Dark current increase as a function of fluence
for heavy ion irradiated photodiodes

Figure 54 clearly shows that dark current increases already at fluences of 10^5 particles/cm^2 both for Argon and Neon irradiated devices.

Dark current increase for Neon irradiated device is 80% and about 11000% for fluences of 10^5 and 10^7 ions/cm^2 respectively. For Argon irradiated device, these numbers are about 300% and 56 000%. Argon irradiated device is thus 3-5 times more degraded than the Argon irradiated device. This result is expected, as Argon, due to its heavier atomic mass than Neon, should cause more displacement damage in matter. A thicker InGaAs layer may also be a contributing factor to the higher dark current values observed for the Argon irradiated device. The impact of Argon and

Neon irradiation in space on large area InGaAs photodiodes (as tested here) is low, as it takes 6 and 60 years to reach a fluence of 10^5 for Neon and Argon /cm^2 respectively. Results here show that each heavy ion particle is considerably more damaging than protons. There is therefore a possibility for heavy ions to create large lattice displacement damages.

2. I-V characteristic results

The following plots present the I-V characteristic for the two devices after irradiation.

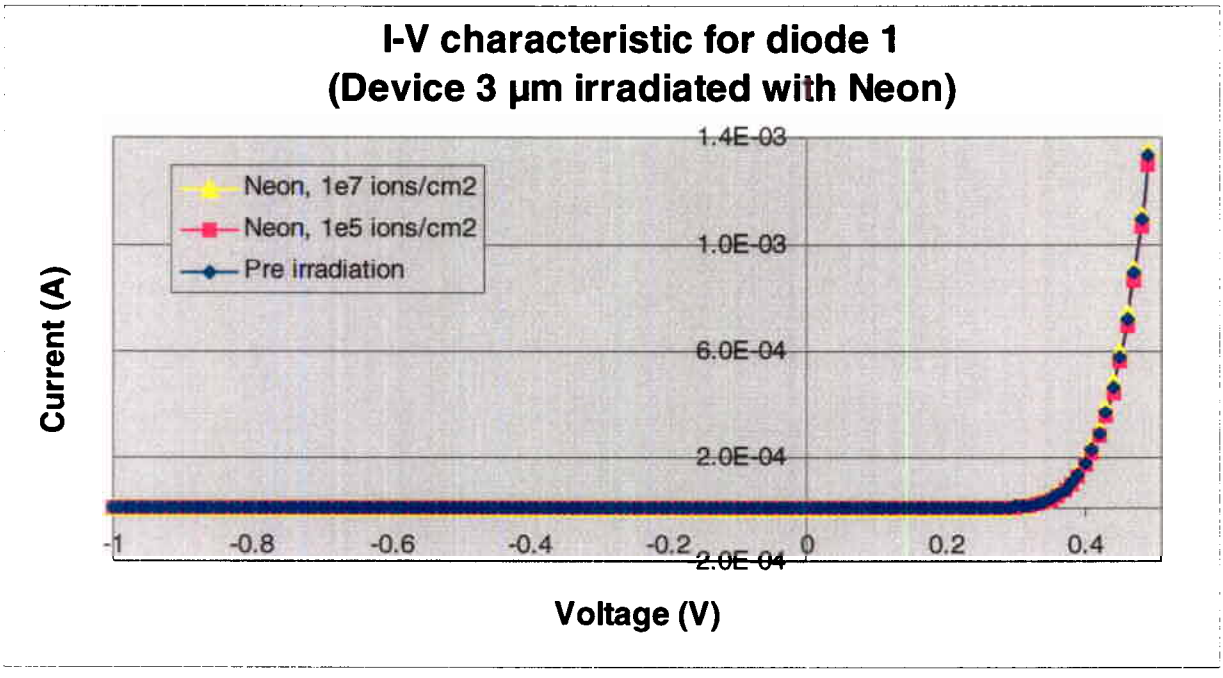

Figure 55: I-V characteristic for the 3 µm thick InGaAs layer device irradiated with Neon

Figure 55 shows that the I-V characteristic for the 3 µm thick layer device did not change after the two irradiation runs. However, in figure 56 (see next page), it can be seen that the threshold voltage in the forward part of the I-V characteristic decreases after the device was irradiated to a fluence of 10^7 Argon/cm^2. However, for the same device no changes were observed after irradiation to 10^5 Argon/cm^2.

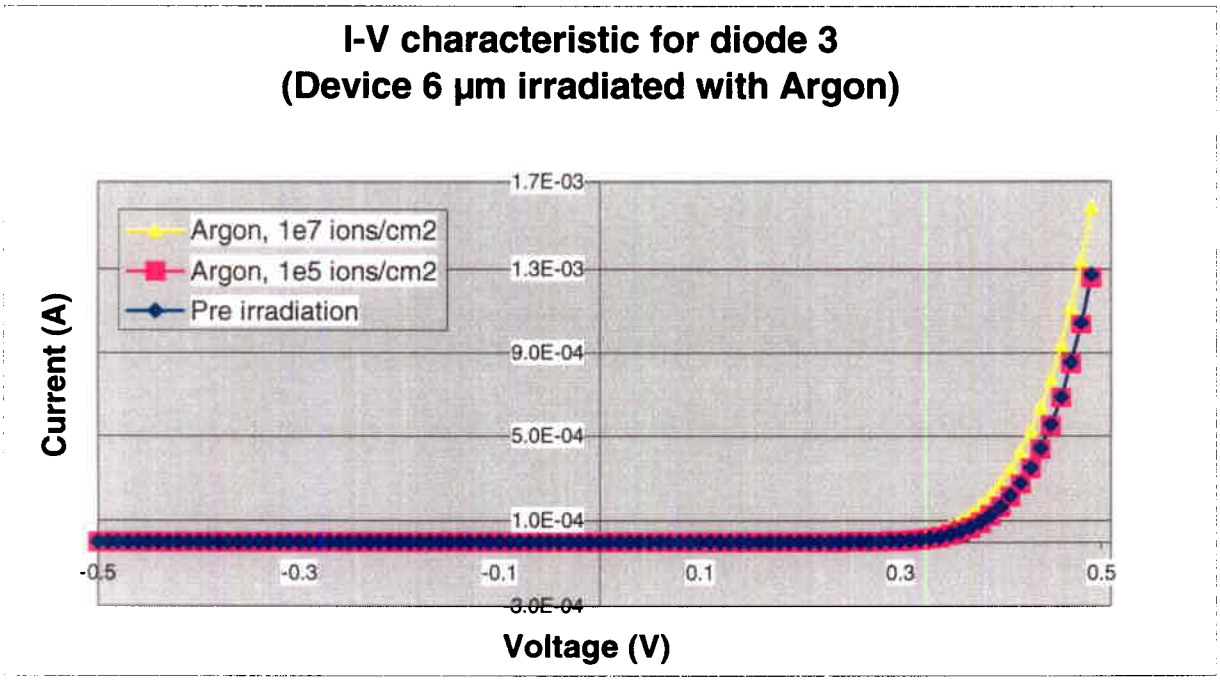

Figure 56: I-V characteristic for the 6 µm thick device irradiated with Argon

Figure 57 shows the reverse part of the I-V characteristic for Argon irradiation at high voltage.

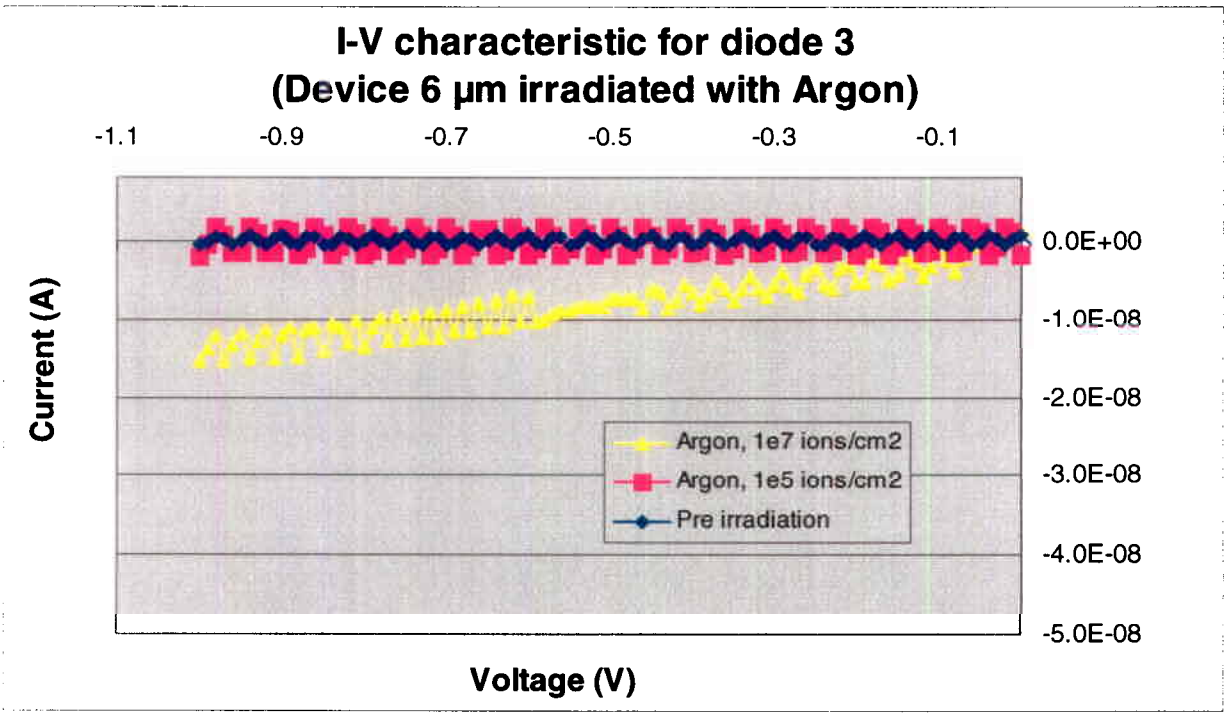

Figure 57: Detailed view of figure 55 for voltage < 0V

The reverse current increased after irradiation at 10^7 ions/cm^2 with Argon source.

3. Photocurrent results

The two following plots show the results of the photocurrent measurements.

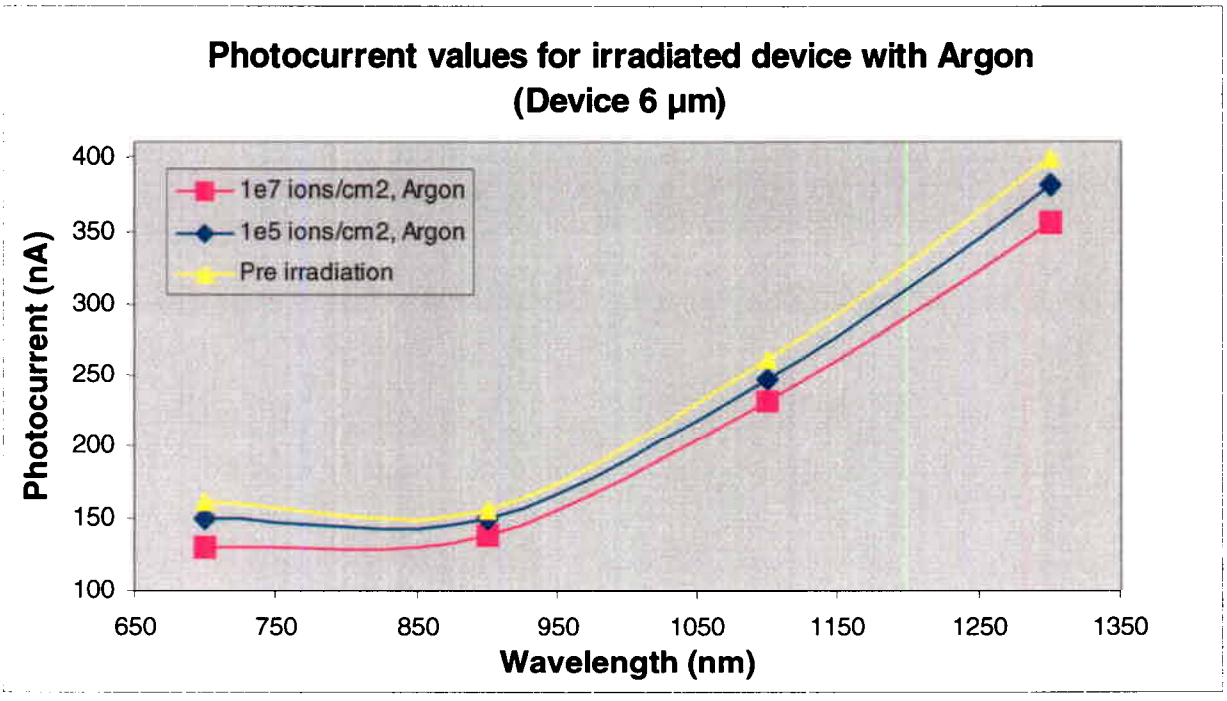

Figure 58: Photocurrent values as a function of wavelength
for the 6 µm thick device irradiated with Argon

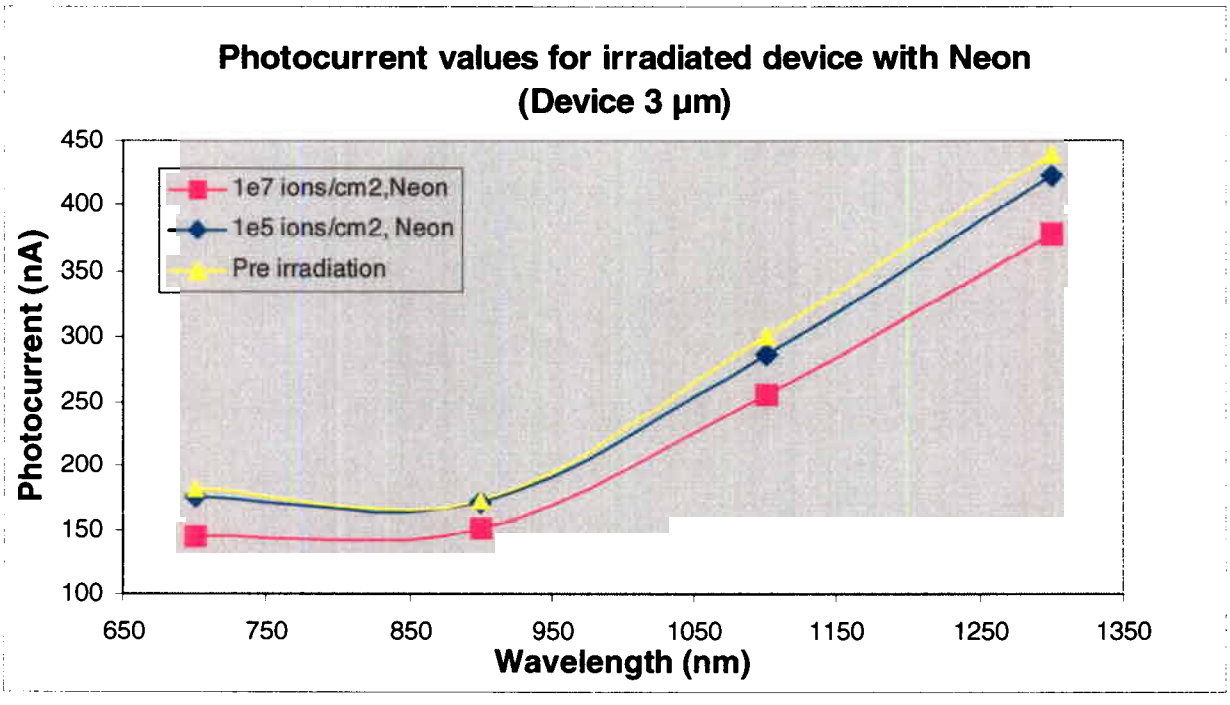

Figure 59: Photocurrent values as a function of wavelength
for the 3 µm thick device irradiated with Neon

The photocurrent for both devices decreased following Argon and Neon irradiations. The photocurrent decreases more with increasing fluence.

To compare both devices, a graph showing the decrease in percentage of the photocurrent for each wavelength was plotted.

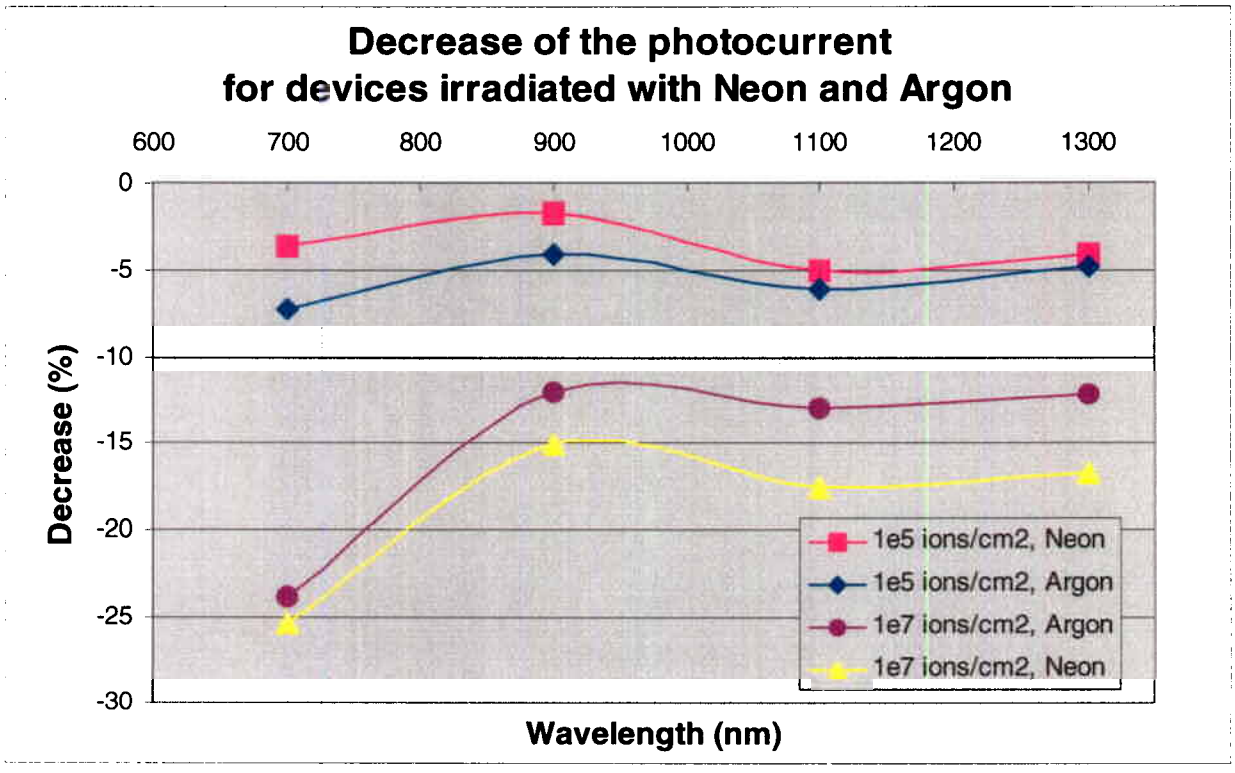

Figure 60: Decrease of the photocurrent (%)
for the two devices as a function of the wavelength

Figure 60 illustrates that the photocurrent for the Argon irradiated device degrades more than for the Neon irradiated device at 10^5 ion/cm^2. Contrary to assumption, the opposite is observed at 10^7 ions/cm^2.

Currently no explanation is found for this effect. More devices and irradiation tests are needed to obtain better statistical data. Figure 60 also shows that the photocurrent degradation is more pronounced for lower wavelengths (this device is optimised for 1600 nm).

4. Conclusion

Heavy ion irradiations on THOMSON devices show:

- A general increase of dark current with increasing fluence, Argon being more damaging than Neon
- A decrease of the threshold voltage in the forward part of the IV characteristic only for Argon irradiation and fluence of 10^7 ions/cm^2.
- The decrease of photocurrent: higher decrease for Argon than Neon irradiation at 10^5 ions/cm^2, but less at 10^7 ions/cm^2.
- Decrease of the photocurrent less important at 1300 nm than for longer wavelengths.

V. CONCLUSIONS OF THE STUDY

This study has shown that InGaAs photodiodes and laserdiodes can be affected by proton radiation with their electrical parameters degrading with increasing proton fluence. It has to be emphasised that only a few samples were available for some devices (i.e. one laserdiode, three photodiodes from MIPAS) providing poor statistical values.

- For MIPAS laserdiodes, the following effects were observed:

A decrease of the laserdiode output power and a small increase of the threshold current were observed following the first irradiation run (10^8 p/cm^2). Contrary to expectations, no output power or threshold current degradation was observed after a second irradiation run to a fluence of 10^{10} p/cm^2. However, a further decrease of the output power was observed post third irradiation run (10^{12} p/cm^2).

- For MIPAS photodiodes, the following effects were reported:
    - Increase of the dark current
    - Decrease of the threshold voltage and increase of the reverse current in the I-V characteristic measurements (for fluence higher than 10^{10} p/cm^2).
    - Decrease of the photocurrent

- For THOMSON photodiodes, the proton radiation gave the following results;
    - Increase of the dark current
    - Decrease of the forward threshold voltage and increase of the reverse current during I-V measurements
    - Decrease of the photocurrent

Following this study it appears that MSG devices are more tolerant to proton radiation than the 3 and 6 μm thick InGaAs layer devices.

According to NIEL lower energy protons are more damaging than higher energy protons. Thus, one would expect higher parameter degradation in test samples exposed to 6 MeV protons than those exposed to 30 MeV protons. However, this

effect was not unambiguously observed for dark current measurements and only observed for photocurrent measurements.

The radiation damage effects observed here may be explained by the radiation induced defects in the semiconductor material. These defects act as traps for electron and hole pairs, reducing their lifetime in the material. The exact nature of these defects is not known for the moment and will require a more detailed research on the physics of the material. Due to a lack of time, special laboratory instruments, and the number of available samples, this analysis could not be performed.

Heavy ion irradiations on two THOMSON devices show:

- A general increase of dark current with increasing fluence, Argon being more damaging than Neon
- A decrease of the threshold voltage in the forward part of the IV characteristic only for Argon irradiation and fluence of 10^7 ions/cm^2.
- The decrease of photocurrent: higher decrease for Argon than Neon irradiation at 10^5 ions/cm^2, but less at 10^7 ions/cm^2.
- Decrease of the photocurrent less important at 1300 nm than for longer wavelengths.

Recommendation:

The following improvements to the optical test bench set-up is proposed if additional tests are to be performed on the available devices.

1) Very high dark current values prevented photocurrent measurements of heavily irradiated devices. Photocurrent measurements may be improved by operating devices at lower temperatures, reducing the dark current, or by employing a stronger illumination source.

2) Improved wiring (i.e. use of coaxial cables) may improve measurements by reducing noise.

3) During this study, the photocurrent measurements were only performed for four wavelengths. A monochromator with more filters could have been used to obtain a better spectral resolution.

Final observation:

I have, during my YGT period, gained experience in the following areas:

- Radiation effects on electronics devices.
- Photodiode and laserdiode mechanisms / operation.
- Laboratory work, instrumentation and measurement methods including software development.
- Project planning and utilisation.

This 14 months working on this project will for sure help me in my future professional experience.

VI. BIBLIOGRAPHY

[1] Holmes-Siedle, L. Adams, "Handbook of Radiation Effects", Oxford Science Publications, 1993.

[2] "The Radiation Design Handbook", ESA PSS-01-609 Issue 1, ESTEC, ESA, 1993.

[3] Ali Mohammadzadeh, "Radiation Damage Evaluation of Space-Borne CCDs for the Cassini VIMS-V Instrument and the Microelectronics Photonics Test Bed", Thesis, Department of Physics, Brunel University, 1996.

[4] J. Wilson, J.F.B. Hawkes, "Optoelectronics: An Introduction", Prentice / Hall International, 1983.

[5] W. Nunley, J. S. Bechtel, "Infrared Optoelectronics: Devices and Applications", Optical Engineering Vol. 12, Marcel Dekker Inc., 1987.

[6] K. Gill, C. Aguilar and all, "Radiation Damage Studies of Optical Link Components for Applications in Future High Energy Physics Experiments", Part of the SPIE Conference on Photonics for Space Environment VI, SPIE Vol. 3440, July 1998.

[7] E. Barnes and J.J. Wiczer, "Radiation Effects in Optoelectronic Devices", Sandia Report SAND84-0771, 1984.

[8] S.M. Sze, "Physics of Semiconductor Devices", 2nd edition, John Wiley & Sons, 1981.

[9] H. Lischka et al., " Radiation Effects in Optoelectronic Devices", SPIE Vol. 2425, p. 43, 1994.

Other references:

- F.F. Mazda, "Electronics Engineer's Reference Book, 5th Edition, Butterworths, 1983.

- D. A. Bell, "Electronic Devices and Circuits", 2nd edition, Reston Publishing Company Inc., 1980.

- H. Lischka et al., "Radiation Sensitivity of Light Emitting Diodes (LED), Laser Diodes (LD) and Photodiodes (PD)", IEEE Trans. Nucl. Sci., Vol. NS39, pp.423-430, June 92.

- Y.F. Zhao, A.R. Patwary et al., " 200 MeV Proton Damage Effects on Multi-Quantum Well Laserdiodes", IEEE Trans. Nucl. Sci., Vol 44, Dec 1997.

- B.D. Evans, C.A. Gossett et al., "Effects of 5.5-MeV Proton Irradiation on Reliability of a Strained Quantum-well Laser Diode and a Multiple Quantum-well Broad-band Light-emitting Diode", SPIE Vol. 1791, Optical Materials Reliability and Testing, 1992.

- G. P. Summers, E.A. Burke et al., " Damage Correlations in Semiconductors Exposed to Gamma, Electron and Proton Radiations", IEEE Trans. Nucl. Sci. Vol 40, N°6, Dec. 1993.

- G.J. Shaw, S.R. Messenger et al., " Radiation-induced Reverse Dark Currents in $In_{0.53}Ga_{0.47}As$ Photodiodes"" J. Appl. Phys. 73 (11), June 1993.

- H. Ohyama, E. Simoen et al, " Radiation Source Dependence of Degradation and Recovery of Irradiated $In_{0.53}Ga_{0.47}As$ PIN Photodiodes", IEEE 1998.

VII. ANNEX 1

Annex 1 presents the source code of the visual basic "Dark_Current" program.

```
Public Sub Dark_Current()

Dim i As Integer

'*************************************************************************
**********************
'OPENING OF THE FILE IN COLUMNS

    Workbooks.OpenText filename:=UserForm1.txtPath.Value, Origin:=xlWindows _
        , StartRow:=1, DataType:=xlDelimited, TextQualifier:=xlDoubleQuote, _
        ConsecutiveDelimiter:=False, Tab:=True, Semicolon:=False, Comma:=True, _
        Space:=False, Other:=False, FieldInfo:=Array(Array(1, 1), Array(2, 1), Array( _
        3, 1), Array(4, 1), Array(5, 1))
'UserForm1.txtPat is the name of the button to select the data files to open

'*************************************************************************
**********************
If UserForm1.cbx1.Value Then  'if MIPAS box is selected then

    'Selection of the column of the dark current values
    Columns("C:C").Select
    Selection.Copy
    Columns("G:G").Select
    ActiveSheet.Paste


   'Deletion of the wrong figure
    Selection.Replace What:="""NDCA", Replacement:="", LookAt:=xlPart, _
        SearchOrder:=xlByColumns, MatchCase:=False
    Selection.Replace What:="""", Replacement:="", LookAt:=xlPart, _
```

```
    SearchOrder:=xlByColumns, MatchCase:=False

  ' Writing of average and dark current in a cell
  Range("C11").Select
  ActiveCell.FormulaR1C1 = "Average:"
  Range("D10").Select
  ActiveCell.FormulaR1C1 = "Dark current (A)"

  'Calcul of the average of the values
  Range("D11").Select
  ActiveCell.FormulaR1C1 = "=Average(R[-10]C[3]:R[-6]C[3])"
  Selection.Copy
  Selection.PasteSpecial Paste:=xlValues, Operation:=xlNone, SkipBlanks:= _
    False, Transpose:=False
  Selection.NumberFormat = "0.000E+00"   'Format of the average value


  'Positionning of the PD serial number and deletion of the incorrect symbol
  Range("B4").Select
  Selection.Copy
  Range("C10").Select
  ActiveSheet.Paste
  Range("C10").Select
  ActiveCell.Replace What:="""", """", Replacement:="", LookAt:=xlPart, _
    SearchOrder:=xlByRows, MatchCase:=False
  Range("C10").Select
  ActiveCell.Replace What:="""""", Replacement:="", LookAt:=xlPart, _
    SearchOrder:=xlByRows, MatchCase:=False

End If

'*****************************************************************
**********************
If UserForm1.cbx2.Value Then    'if THOMSON box is selected then
```

```
'Selection of the column of the dark current values
Columns("C:C").Select
Selection.Copy
Columns("G:G").Select
ActiveSheet.Paste

'Deletion of the incorrect symbol
Selection.Replace What:="""NDCA", Replacement:="", LookAt:=xlPart, _
   SearchOrder:=xlByColumns, MatchCase:=False
Selection.Replace What:="""", Replacement:="", LookAt:=xlPart, _
   SearchOrder:=xlByColumns, MatchCase:=False

'Insertion of rows to separate the diodes series
Rows("6:6").Select
Application.CutCopyMode = False
Selection.Insert Shift:=xlDown
Rows("12:12").Select
Selection.Insert Shift:=xlDown

'Writing of dark current in a cell
Range("B20").Select
ActiveCell.FormulaR1C1 = "Dark current (A)"

'Calcul of the average of the values
k = 23
   For j = 3 To 15 Step 6
      Cells(j, 9).FormulaR1C1 = "=average(R[-2]C[-2]:R[2]C[-2])"
      Cells(j, 9).Copy
      'The average value will be paste in a pre-defined place
      Cells(k, 2).Select
      Selection.PasteSpecial Paste:=xlValues, Operation:=xlNone, SkipBlanks:= _
         False, Transpose:=False
      k = k - 1
```

```
    Next

  'Change of format
  Range("B21:B23").Select
  Selection.NumberFormat = "0.000E+00"

  'Writing of the diode serial number in a column
  l = 23
    For i = 1 To 23 Step 8
      Cells(l, 1).Value = Cells(i, 2).Value
      l = l - 1
    Next

  ' Deletion of the wrong symbol in the serial number column
  Range("A21:A23").Select
  Selection.Replace What:="""", Replacement:="", LookAt:=xlPart, _
    SearchOrder:=xlByColumns, MatchCase:=False
  Range("A21:A23").Select
  Selection.Replace What:=", N", Replacement:="", LookAt:=xlPart, _
    SearchOrder:=xlByColumns, MatchCase:=False
  Range("A1").Select
 Range("D22").Select
  ActiveCell.FormulaR1C1 = "=AVERAGE(R[-1]C[-2]:R[1]C[-2])*1000000000"
  Range("D23").Select
End If
'*****************************************************************
*******************
'Deletion of the button view
UserForm1.Hide

End Sub
```

VIII. ANNEX 2

The planning of this 14 months study is presented in figure 61.

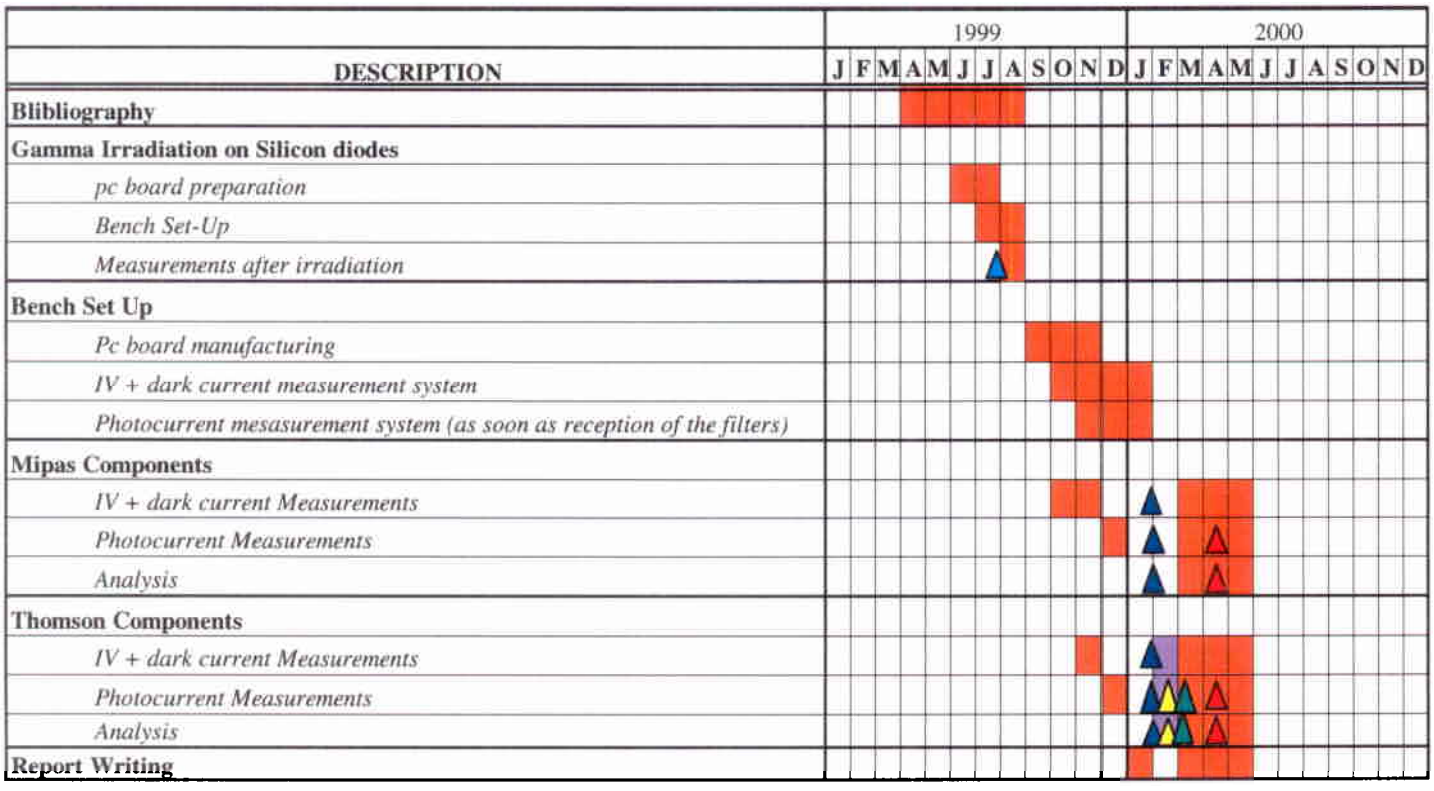

First proton irradiation run
Second proton irradiation run
First heavy ion irradiation run
Second heavy ion irradiation run
Gamma irradiation run
Due to a problem of transport, the samples were not received before the end of February after the first proton irradiation

Figure 61: Planning of the 14 months study

IX. ANNEX 3

The following pages present the two THOMSON and MIPAS irradiation test plans.

RADIATION TEST PLAN FOR INGAAS PHOTODIODES AND LASERDIODES

prepared by/*préparé par* C. Garden
TOS-QCA

reference/*réference* ESA_QCA_CG_001
issue/*édition* 3
revision/*révision* 0
date of issue/*date d'édition* 24 May 2000
status/*état* Draft
Document type/*type de document* Test Plan
Distribution/*distribution*

European Space Agency
Agence spatiale européenne

ESTEC
Keplerlaan 1 - 2201 AZ Noordwijk - The Netherlands
Tel. (31) 71 5656565 - Fax (31) 71 5656040

TABLE OF CONTENTS

1 INTRODUCTION

The following document describes a proton radiation test plan for InGaAs photodiodes and laserdiodes from MIPAS ODS project.

2 TEST PLAN

2.1 Reference number of test plan

ESA_QCA_CG_001

2.2 Reference

Issue: 3
Revision: 0
Date: 24/05/2000

2.3 Component designation

Photodetectors:

SCD 68031954-01-161-9536F
SCD 68031954-01-163-9536F
SCD 68031954-01-243-9536F
SCD 68031954-01-249-9536F

Laser modules:

NFT 680 24447-00 S/N 27
NFT 680 24447-00 S/N 36

2.4 Applicable ESA/SCC Generic and detail Specifications

The test plan is based on the ESA/SCC No.22900, "Total Dose Steady-State Irradiation Test Method".

2.5 Sample size and number of control devices:

The photodetector SCD 68031954-01-161-9536F was damaged during pre-irradiation characterisation. Thus, only two photodetectors will be irradiated whereas one will be used as a reference. The sample size can be found in Appendix A.
One laser module will be irradiated whereas the second one will be used as a reference. The sample size can be found in Appendix B.

2.6 Component family

Diode.

2.7 Component group

Laserdiode and photodiode.

2.8 Device package

Photodiode:

TO46 single nailhead package base, 3 legs.
TO18 window and lens cap

Laser Module:

Custom package

2.9 Manufacturer's name and address

Photodiode:

Front End:

Ortel

Back End:

Kongsberg Gruppen ASA
Aerospace
P.O. Box 1003
N-3600 Kongsberg
Norway

Laser Module:

Kongsberg Gruppen ASA
Aerospace
P.O. Box 1003
N-3600 Kongsberg
Norway

2.10 Test house

ESTEC, ESA, P.O. Box 299, 2200 AG Noordwijk, the Netherlands.

2.11 Originator of the test plan

Claire Garden, ESTEC-ESA, Tel: 071 565 5978

2.12 Facility name and type of radiation source

The proton irradiation will be performed at the Paul Scherrer Institute, Villigen, Switzerland.

2.13 Type of exposure

It will be a single exposure.
Samples will be irradiated with two different proton energies (6 MeV and 30 MeV) and submitted at three different irradiation runs as illustrated in table 1 to 5 (see next page).

MIPAS Photodiodes	Fluence (p/cm^2)	Device
30 MeV	10^8	SN 243
	10^{10}	SN 249
Reference		SN 163

Table 1: First irradiation run for MIPAS photodiodes

MIPAS Laser diodes	Fluence (p/cm^2)	Device
30 MeV	10^8	SN 36
Reference		SN 27

Table 2: First irradiation run for MIPAS laserdiodes

MIPAS Photodiodes	Fluence (p/cm^2)	Device
30 MeV	10^9	SN 243
	10^{12}	SN 249
Reference		SN 163

Table 3: Second irradiation run for MIPAS photodiodes

MIPAS Laser diodes	Fluence (p/cm^2)	Device
30 MeV	10^{10}	SN 36
Reference		SN 27

Table 4: Second irradiation run for MIPAS laserdiodes

MIPAS Laser diodes	Fluence (p/cm^2)	Device
30 MeV	10^{12}	SN 36
6 MeV	10^{12}	SN 27

Table 5: Third irradiation run for MIPAS laserdiodes

2.14 Irradiation conditions
All samples will be irradiated unbiased.

2.15 RT Anneal Conditions
Room temp (°C): 20
Anneal time (hr): 24

Accelerated ageing conditions:
Ageing temp (°c): 100
Ageing time (hr): 168

2.16 Flow chart for evaluating testing
See appendix C

2.17 List of electrical parameters
The following measurements will be performed on photodiodes:
- I-V characteristic
- Dark current
- Photocurrent

For laser modules, these electrical parameters will be studied:
- Optical power output
- Threshold current

Set-up and test conditions of the measurements are presented in appendix D.
Specifications of the laserdiodes and the photodiodes are presented in appendix E.

3 APPENDIX A

Figure 1 presents the physical dimension of the MIPAS photodiode.

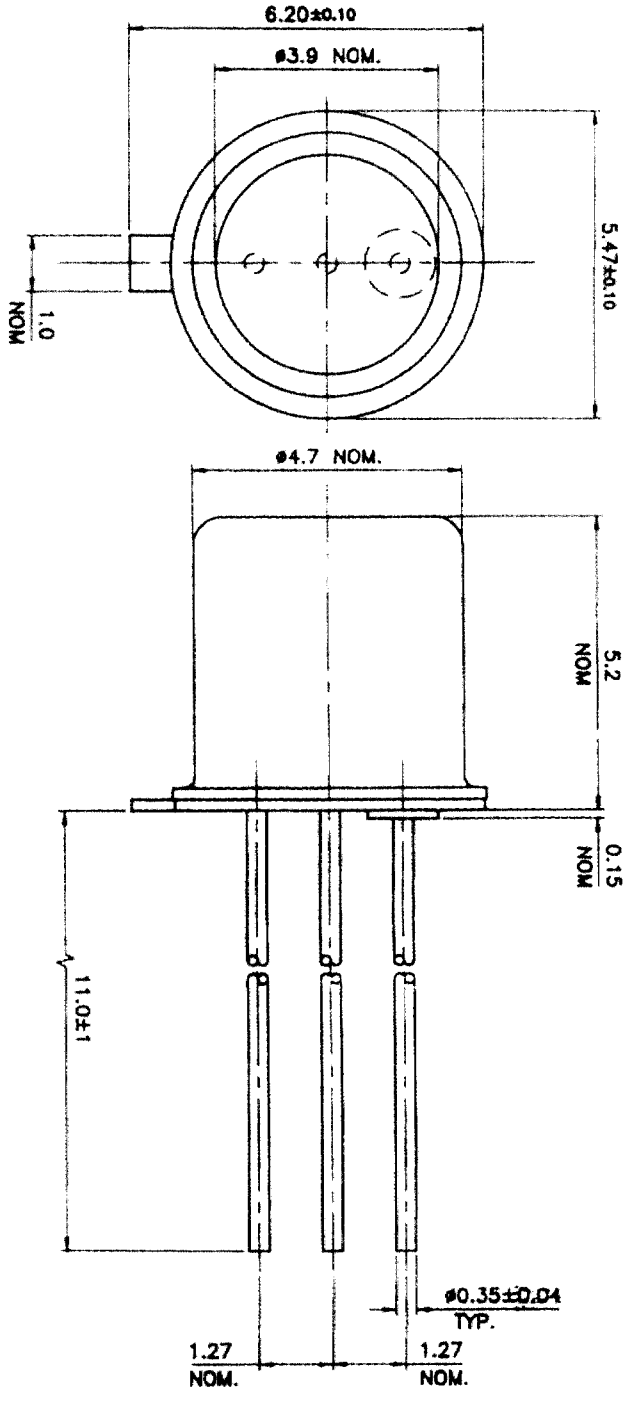

Figure 1: Physical dimension of the photodiode

4 APPENDIX B

Figure 2 shows the physical dimension of the MIPAS laserdiode.

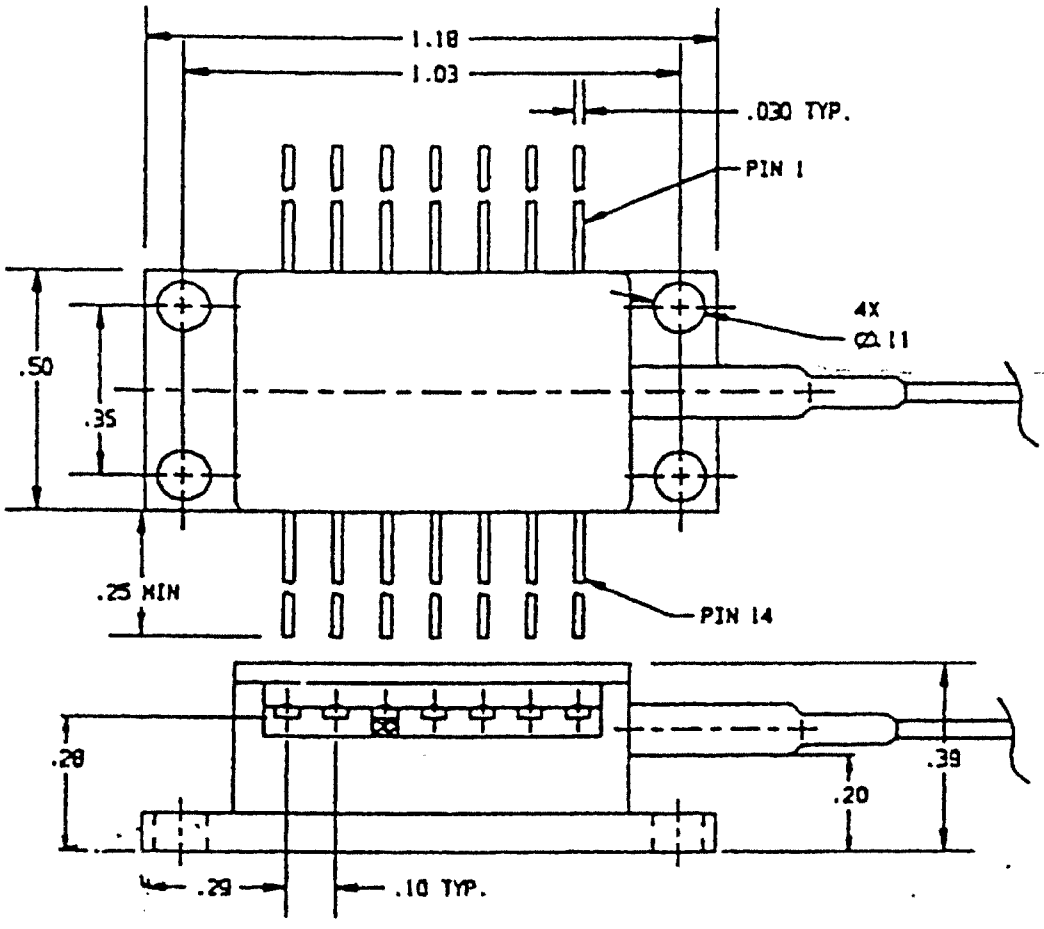

Figure 2: Physical dimension of the laser diode

5 APPENDIX C

Flow chart for evaluation testing.

The following flow diagram is used to perform technology evaluation tests.

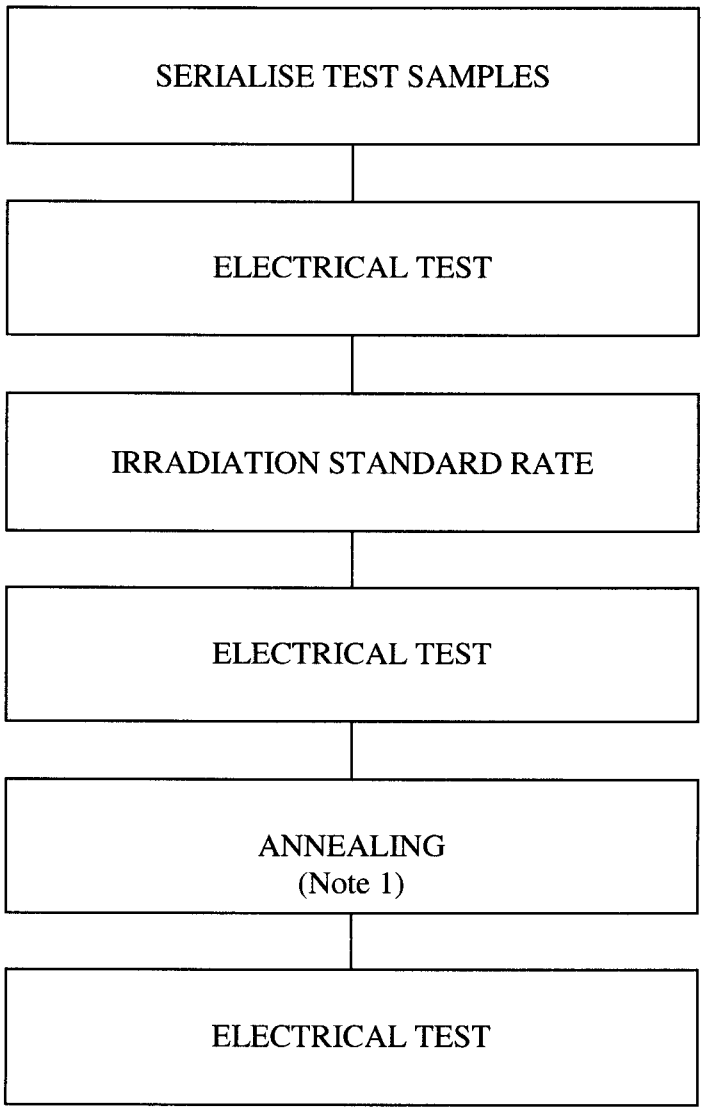

Figure 3: Flow chart for evaluating testing

Note1: A few samples will be subjected to the annealing and accelerated ageing procedure. If any effects are observed the remaining devices will also be annealed.

6 APPENDIX D

Set-up and test conditions for the measurements.

6.1 Laserdiodes

6.1.1 Optical power / threshold current

The test conditions are specified in table 5.

- Measured values: Output power
  Laser diode drive current

- Fixed Values: Set temperature of the laser diode at 20°C

Step	1	2	3	4	5	6	7	8	9	10	11	12
I [mA]	10	20	25	30	35	40	45	50	60	70	80	90

Table 5

Figure 4 illustrates the measurement set-up for electrical characterisation.

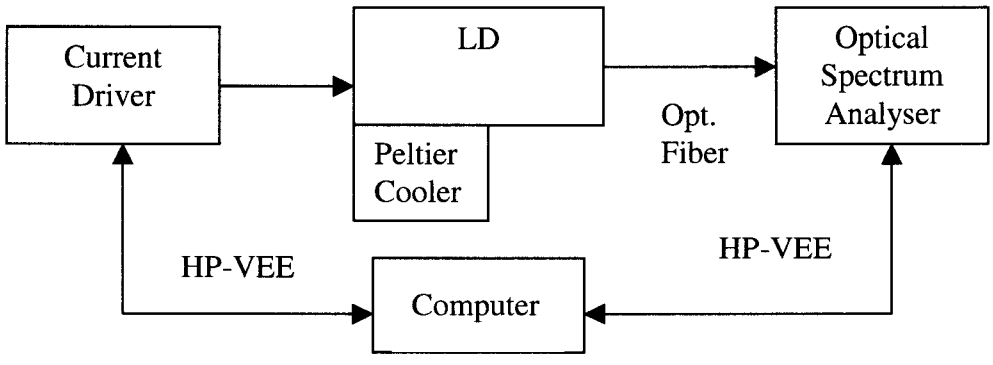

Figure 4: Measurement set-up for electrical characterisation for laserdiodes.

The laser diode driver current will be read directly from the display of the Diode Current Driver ILX LDC-3900.

The optical power will be deduced from the spectrum obtained by the Optical Spectrum Analyser Ando AQ 6310.

The driving current versus the optical power curve will give the characteristic of the laserdiode.

The threshold current defines the minimum driving current, where the laser diode starts to emit laser light.
It will be calculated by measuring the driver current to output power curve and calculating the linear fit. The point at which a straight-line fit to the linear portion of the curve intercepts the x-axis corresponding to the zero optical power define the threshold current of the diode (see figure 5).

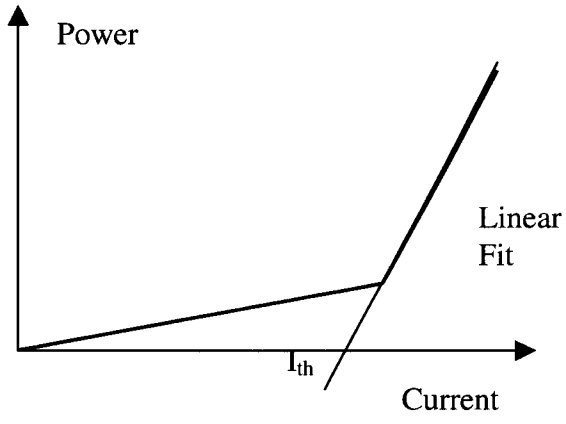

Figure 5: Determination of the threshold current.

6.2 Photodiodes

Four InGaAs photodiode samples (SN 161,163, 243 and 249) have been provided by MIPAS ODS project.
The SN 161 photodiode was degraded during pre-irradiation measurements. The SN 163 device will then be used as a reference.

6.2.1 I-V characteristic

The test conditions are listed below:

- Measured values: Current
  Voltage

- Fixed values: No source light
  Set the temperature of the photodiode at 20°C

Figure 6 (next page) illustrates the measurement set-up for I-V characterisation.

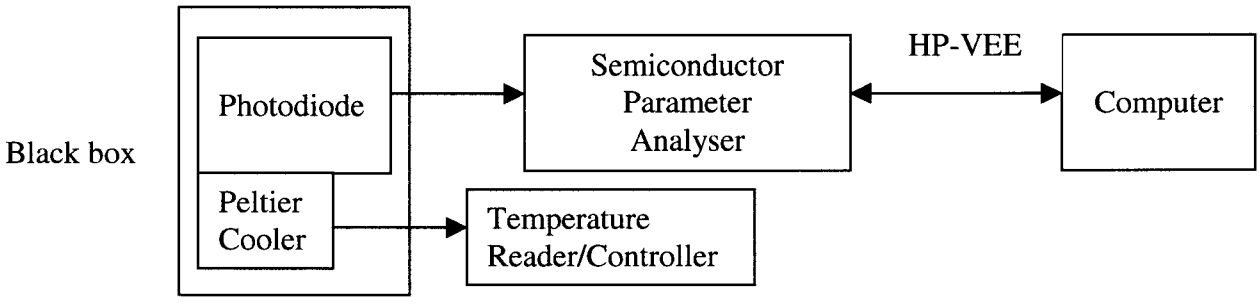

Figure 6: Measurement set-up for I-V characterisation.

The voltage will vary from –1V to 0.63V by steps of 10mV.
The I-V characteristic will be measured directly by the Semiconductor Parameter Analyser.

6.2.2 Dark current

The test conditions are listed below.

- Measured values: Dark current

- Fixed values: Reverse voltage at –5V
  Set the temperature of the photodiode at 20°C
  No light

Figure 7 illustrates the measurement set-up for the dark current characterisation.

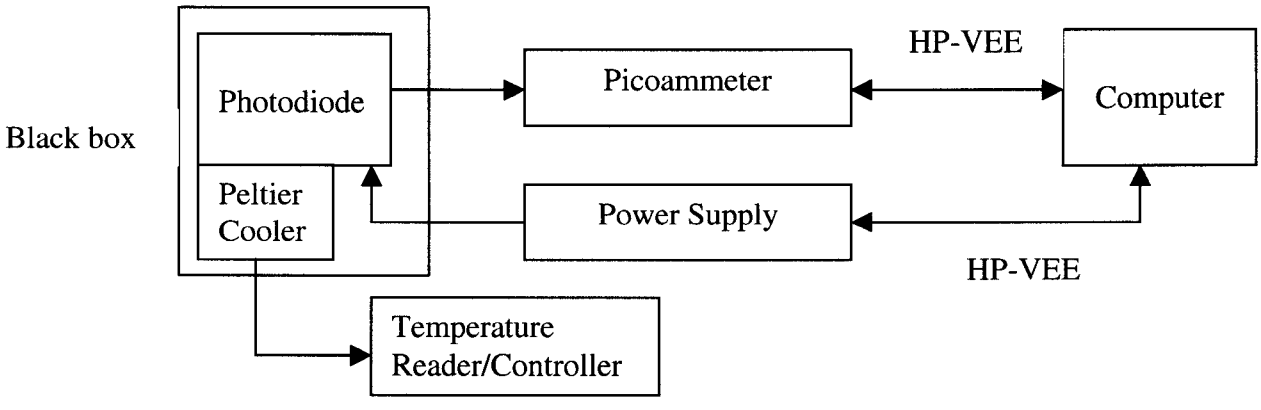

Figure 7: Measurement set-up for the dark current characterisation.

The dark current will be measured employing a Picoammeter.

6.2.3 Photocurrent

The test conditions are specified in table 6.

- Measured values: Photocurrent

- Fixed values: Reverse voltage at – 5V
Set the temperature of the photodiode at 20°C

Step	1	2	3	4
Bandpass Filters (nm)	700	900	1100	1300
Light Power ($\mu W/mm^2$)	1.960788899	0.904891344	0.364655806	0.667177521

Table 6

Two reference PDs were used to measure the light power (for each wavelength) at a fixed position from the light source. Each reference PD is optimised for a certain wavelength, 850 and 1300 nm for the two respectively. The light power, in table 6, thus reflects the Quantum Efficiency (QE) of the PDs.

Figure 8 illustrates the measurement set-up for the photocurrent characterisation.

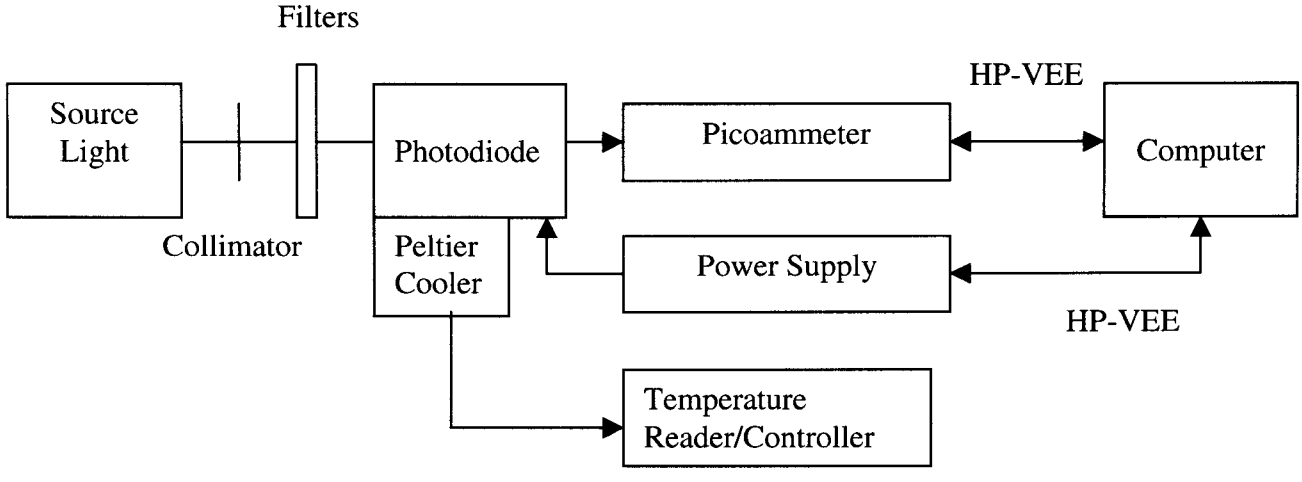

Figure 8: Measurement set-up for the photocurrent characterisation.

The photocurrent of the photodiodes when illuminated by monochromatic light (as defined in table 6) is measured employing a Picoammeter.

6.3 Instrumentation

The following instruments will be used in the electrical characterisation and measurements:

- Monochromatic Light Source
- Optical Spectrum Analyser Ando AQ 6310
- Semiconductor Parameter Analyser HP 4145B
- Diode Current Driver ILX LDC-3900 with module 39050 (for the laser diodes)
- System DC Power Supply 6634A HP (for the photodiodes)
- LDT-5910 Temperature Controller with cooler, ILX Lightwave

7 APPENDIX E

Specifications of the laserdiodes and the photodiodes.

7.1 Laserdiodes

Wavelength: 1310 ± 20 nm
Optical Output Power: > 3 mW
Laser Bias Threshold: < 40 mA
Operating Current: 65 mA (typ)
100 mA (max) at 2 V

7.2 Photodiodes

Maximum Reverse Voltage: 20 V
Max Forward Current: 20 mA
Dark Current (at V_R = 5 V): 10 nA
Photosensitivity (at V_R = 5 V and λ = 1300nm): 800 mA/W
Active Area: ϕ 500 μm

RADIATION TEST PLAN FOR

INGAAS PHOTODIODES

prepared by/*préparé par* C. Garden
TOS-QCA

reference/*réference* ESA_QCA_CG_002
issue/*édition* 3
revision/*révision* 0
date of issue/*date d'édition* 24 May 2000
status/*état* Draft
Document type/*type de document* Test Plan
Distribution/*distribution*

European Space Agency
Agence spatiale européenne

ESTEC
Keplerlaan 1 - 2201 AZ Noordwijk - The Netherlands
Tel. (31) 71 5656565 - Fax (31) 71 5656040

TABLE OF CONTENTS

1 INTRODUCTION

The following document describes a proton radiation test plan for InGaAs photodiodes provided by THOMSON-CSF.

2 TEST PLAN

2.1 Reference number of test plan

ESA_QCA_CG_002

2.2 Reference

Issue: 3
Revision: 0
Date: 24/05/2000

2.3 Component designation

Seven 3 µm epitaxy layer devices:

110B506-L3B5
110B506-L3B6
110B506-L3B7
110B506-L5B6
110B506-L6B10
110B506-L6B11
110B506-L6B12

Seven 6 µm epitaxy layer devices:

111B611-L3B7
111B611-L5B7
111B611-L5B8
111B611-L6B6
111B611-L6B7
111B611-L6B8
111B611-L6B9

Two MSG devices:

972-952-L6B5
972-952-L7B4

2.4 Applicable ESA/SCC Generic and detail Specifications

The test plan is based on the ESA/SCC No.22900, "Total Dose Steady-State Irradiation Test Method".

2.5 Sample size and number of control devices
Six photodiodes with 6 µm epitaxy layer, six photodiodes with 3 µm epitaxy layer and one MSG SEVIRI photodiode will be irradiated. Sample size can be found in Appendix A.

2.6 Component family
Diode.

2.7 Component group
Photodiode.

2.8 Device package
The photodiodes are assembled in standard DIL 24 pins package.

2.9 Manufacturer's name and address
THOMSON-CSF
Av. de Rochepleine BP 123
38521 Saint-Egrève Cedex
France

2.10 Test house
ESTEC, ESA, P.O. Box 299, 2200 AG Noordwijk, the Netherlands.

2.11 Originator of the test plan
Claire Garden, ESTEC-ESA, Tel: 071 565 5978

2.12 Facility name and type of radiation source
The proton irradiation will be performed at the Paul Scherrer Institute, Villigen, Switzerland.

2.13 Type of exposure
It will be a single exposure.
Samples will be irradiated with two different proton energies (~ 6 MeV and 30 MeV). Two irradiation runs are foreseen as illustrated in table 1 and 2 (see next page).

THOMSON Photodiodes	Fluence (p/cm^2)	3 µm epitaxy layer	6 µm epitaxy layer	MSG devices
30 MeV	10^8		111B611-L3B7	
	10^9	110B506-L3B5		972-952-L6B5
	10^{11}	110B506-L3B6	111B611-L5B7	
6 MeV	10^8		111B611-L5B8	972-952-L7B4
	10^9	110B506-L3B7		
	10^{10}	110B506-L5B6	111B611-L6B6	
	10^{12}	110B506-L6B10	111B611-L6B7	
Argon	10^5 ions/cm^2		111B611-L6B8	
Neon	10^5 ions/cm^2	110B506-L6B11		
Reference		110B506-L6B12	111B611-L6B9	

Table 1: First irradiation run

THOMSON Photodiodes	Fluence (p/cm^2)	3 µm epitaxy layer	6 µm epitaxy layer	MSG devices
30 MeV	10^{10}		111B611-L3B7	
	10^{11}	110B506-L3B5		972-952-L6B5
	10^{12}	110B506-L3B6	111B611-L5B7	
6 MeV	10^9		111B611-L5B8	
	10^{11}	110B506-L3B7		
	10^{12}	110B506-L5B6	111B611-L6B6	972-952-L7B4
Argon	10^7 ions/cm^2		111B611-L6B8	
Neon	10^7 ions/cm^2	110B506-L6B11		
Reference		110B506-L6B12	111B611-L6B9	

Table 2: Second irradiation run

2.14 Irradiation conditions

All samples will be irradiated unbiased.

2.15 RT Anneal Conditions

Room temp (°C): 20
Anneal time (hr): 24

Accelerated ageing conditions:
Ageing temp (°c): 100
Ageing time (hr): 168

2.16 Flow chart for evaluating testing

See appendix B

2.17 List of electrical parameters

The following measurements will be performed on InGaAs photodiodes:

- I-V characteristic
- Dark current
- Photocurrent

Set-up and test conditions of the measurements are presented in appendix C.
Device specifications are presented in appendix D.

Electrical parameters are still to be determined for the MSG photodiodes.
Specifications for MSG devices are still to be obtained.

3 APPENDIX A

Figure 1 presents the physical dimension of the photodiodes

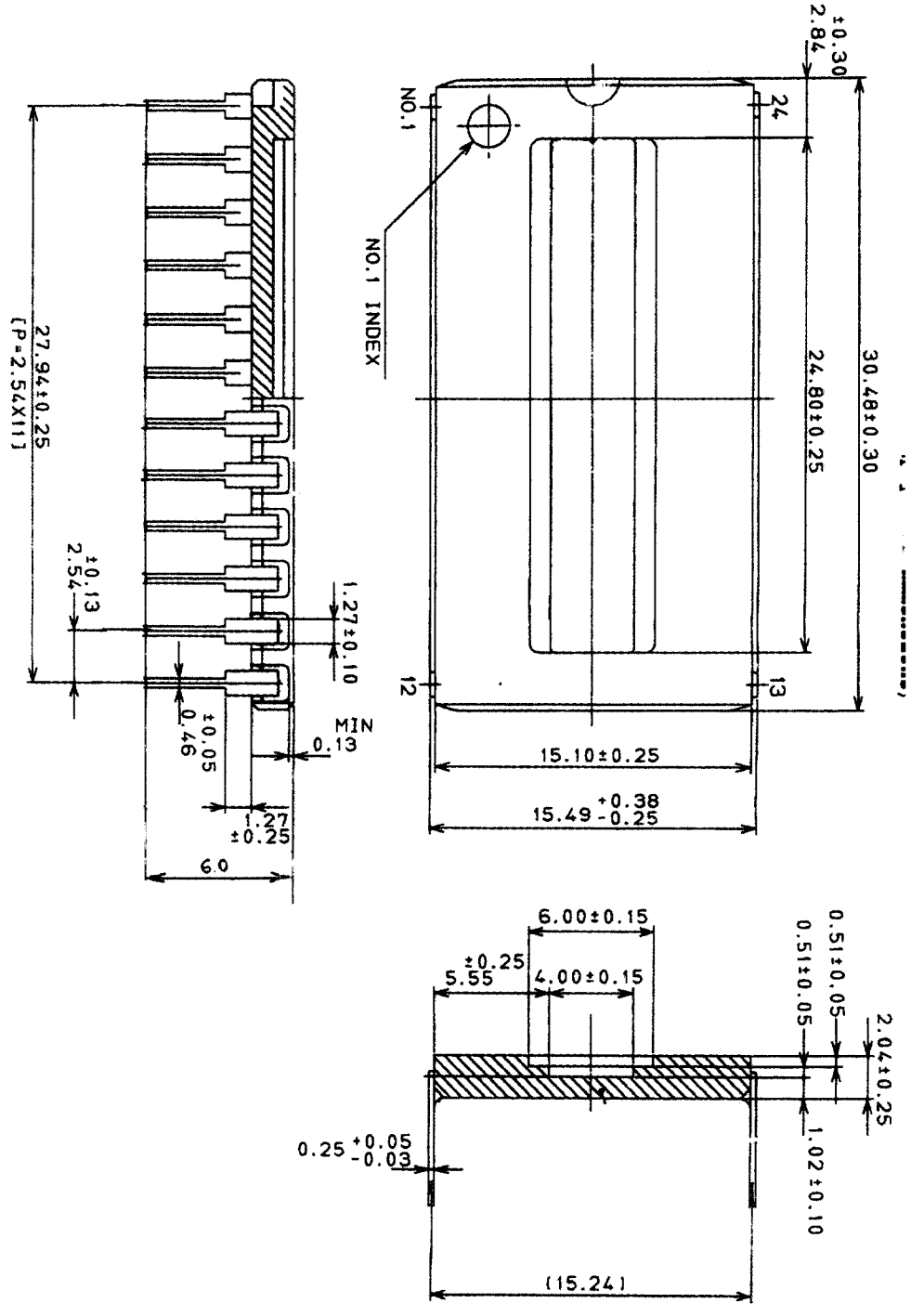

Figure 1: Physical dimension of the photodiode

4 APPENDIX B

Flow chart for evaluation testing

The following flow diagram is used to perform technology evaluation tests.

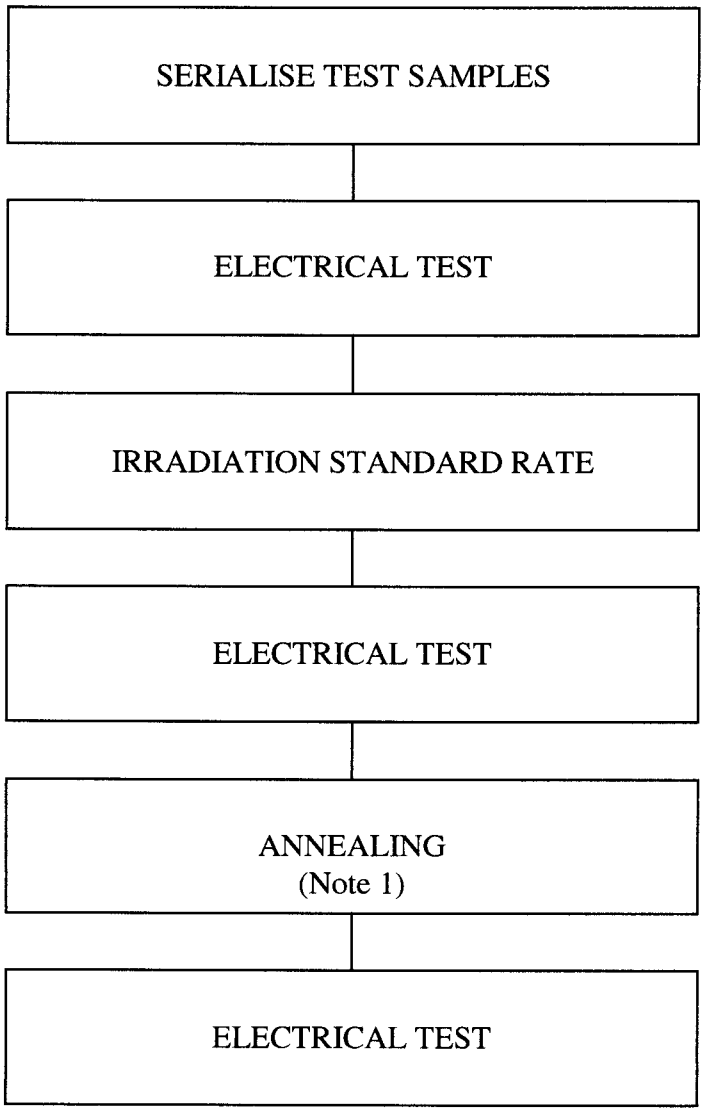

Figure 2: Flow chart for evaluating testing

Note1: A few samples will be subjected to the annealing and accelerated ageing procedure. If any effects are observed the remaining devices will also be annealed.

5 APPENDIX C

Set-up and test conditions for the measurements.

5.1 I-V characteristic

The test conditions are listed below:

- Measured values: Current
  Voltage

- Fixed values: No source light
  Set the temperature of the photodiode at 20°C

The voltage will vary from –1V to 0.49V by steps of 10mV.
The I-V characteristic will be measured directly by the Semiconductor Parameter Analyser.

Figure 3 illustrates the measurement set-up for I-V characterisation.

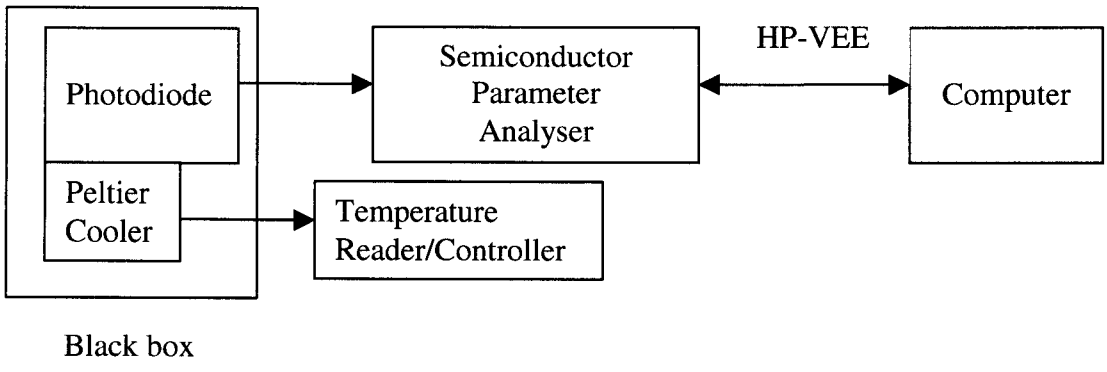

Figure 3: Measurement set-up for I-V characterisation.

5.2 Dark current

The test conditions are listed below.

- Measured values: Dark current

- Fixed values: Reverse voltage at –5V
  Set the temperature of the photodiode at 20°C
  No light

The reverse voltage will be set by the power supply and the dark current will be measured employing a Picoammeter.

Figure 4 illustrates the measurement set-up for the dark current characterisation.

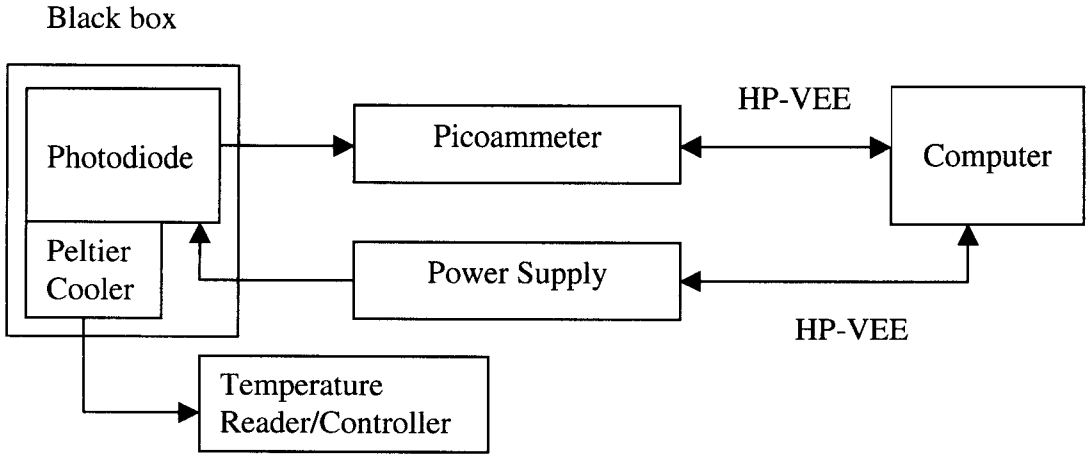

Figure 4: Measurement set-up for the dark current characterisation

5.3 Photocurrent

The test conditions are specified in table 3.

- Measured values: Photocurrent

- Fixed values: Reverse voltage at – 5V
Set the temperature of the photodiode at 20°C

Step	1	2	3	4
Bandpass Filters(nm)	700	900	1100	1300
Light Power ($\mu W/mm^2$)	1.960788899	0.904891344	0.364655806	0.667177521

Table 3

Two reference PDs were used to measure the light power (for each wavelength) at a fixed position from the light source. Each reference PD is optimised for a certain wavelength, 850 and 1300 nm for the two respectively. The light power, in table 3, thus reflects the Quantum Efficiency (QE) of the PDs.

The photocurrent of the photodiode when illuminated by monochromatic light (as defined in table 3) is measured employing a Picoammeter.

Figure 5 illustrates the measurement set-up for the photocurrent characterisation.

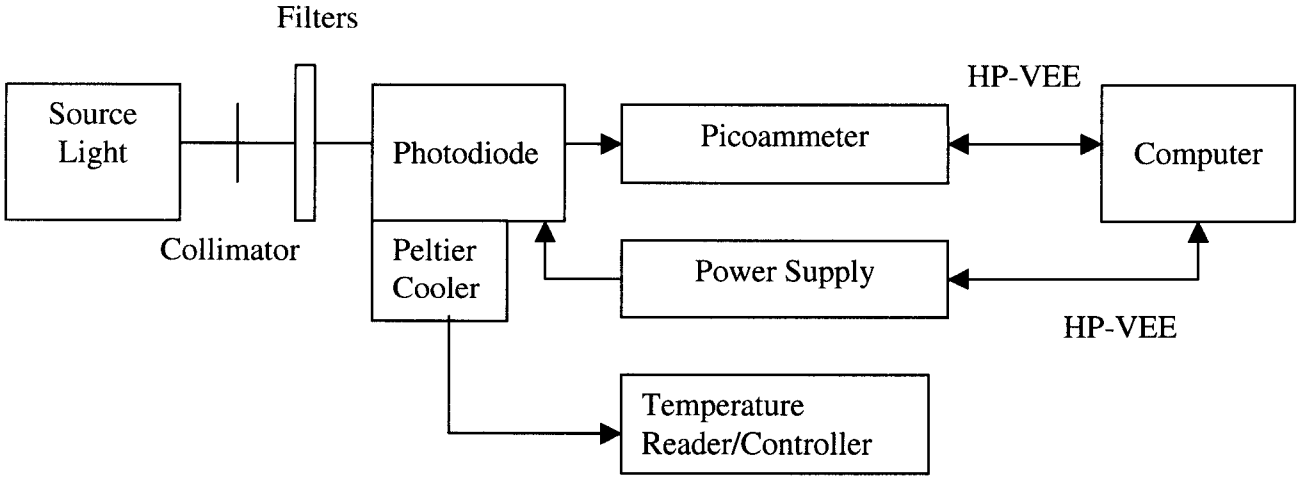

Figure 5: Measurement set-up for the photocurrent characterisation.

5.4 Instrumentation

The following instruments will be used in the electrical characterisations and measurements:

- Light Source
- Autoranging Picoammeter Keithley 485
- Semiconductor Parameter Analyser HP 4145B
- System DC Power Supply HP 6634A
- LDT-5910 Temperature Controller with cooler, ILX Lightwave

6 APPENDIX D

Specifications of the photodiodes.

Maximum rating:

- InGaAs forward current: 2 mA
- InGaAs reverse voltage : 12 V
- Illumination level: 2 mW
- Operating temperature range: 0 / 70 °C

Active area: 720 x 720 μm^2